Pattern Formation in Multi-component Membranes

Vorgelegt von
Tahereh Rouhiparkouhi, M. Sc
Iran, Sari

Von der Fakultät II - Mathematik und Naturwissenschaften
der Technischen Universität Berlin
zur
Erlangung des akademischen Grades

Doktor der Naturwissenschaften
(Dr.rer.nat)
genehmigte Dissertation

Vorsitzender: Prof. Holger Stark
Gutachter: Prof. Reinhard Lipowsky
Gutachter: Prof. Peter Hildebrandt

Tag der wissenschaftlichen Aussprache: 13.12.2012

Berlin 2013
D 83

Here I would like to thank to

Prof. Reinhard Lipowsky
Prof. Dennis Discher
my family
and all dear friends

who supported me during this PhD.

Zusammenfassung

Biologische Membranen bestehen aus einer Vielzahl von verschiedenen Komponenten und dienen als selektive Barrieren, die das Innere von Zellen vor Einflüssen aus der Umgebung schützen. Als einfache Modelle dieser sehr komplexen Biomembranen dienen Multi-Komponenten-Membranen aus einer kleinen Anzahl von Lipidsorten. Da die Dicke von Lipidmembranen sehr klein ist im Vergleich zu ihrer Fläche, können wir sie als zweidimensionale Systeme behandeln, die sich in verschiedene thermodynamischen Phasen befinden. Ändert sich die Zusammensetzung einer Multi-Komponenten-Membran, treten Phasenseparationen und intramembrane Domänen auf . Sind diese Domänen ausreichend groß, können sie im Fluoreszenzmikroskop auf sehr großen Lipidvesikeln supported lipid bilayers (Lipidmembranen auf ebenen Trägerstoffen) , hole-spanning or black lipid membranes und pore-spanning membranes (über Löcher in einem Trägermaterial gespannte Lipidmembranen) beobachtet werden.

In Gegenwart eines adhäsiven Substrats zeigen die verschiedenen Komponenten einer Membran im Allgemeinen unterschiedliche starke Oberflächenaffinitäten. Die generische Wechselwirkung zwischen den Lipidmolekülen und der Substratoberfläche wird bestimmt durch Hydrations-, van-der-Waals- und elektrostatische Kräfte, die von der molekularen Architektur der Lipide abhängen und mit der Entfernung zur Oberfläche abnehmen. Der Affinitätskontrast zwischen Substrat und Komponenten führt zu einer Änderung der Lipidzusammensetzung in der Kontaktfläche und somit zur Bildung von Mustern im ungebundenen und im haftenden Membransegment. In dieser Doktorarbeit wird das Phasenverhalten von Multi-Komponenten-Membranen in Kontakt mit adhäsiven Substratoberflächen mit Methoden der Thermodynamik und Statistischen Physik untersucht. Durch Kombination der Binodalen von freien Vesikelmembranen allgemeinen Relationen für die Partitionierung das Lipid moleküle und das chemische Gleichgewicht innerhalb der Membrane von adhärierenden vesikeln erhalten wir zwei Koexistenzregionen im Phasendiagramm des adhärierenden Membransystems. Ausserdem verwenden wir Ising modelle und binäre Gittermischungen als einfache Modell systeme. Dabei nutzen wir Molekularfeldnäherungen und exakte Lösungen des Ising-Modelle um das Phasenverhalten der adhärierenden Vesikel zu zeigen. Es stellt sich heraus, dass der Oberflächenaffinitätskontrast einen großen Einfluss auf das Phasenverhalten und die Erzeugung von zwei verschiedenen Phasenübergängen in großen Membransegmenten hat. Unsere Ergebnisse lassen sich von der Adhäsion von Vesikeln auf pore-spanning membranes und auf Membranen auf chemisch gemusterten Oberflächen übertragen und

in allen Fällen experimentell überprüfen.

Contents

1 Introduction

1.1 Biological membranes

Membranes are essential part of cells which define boundaries between cells and their environments, maintaining the difference between cell content and outside world. They can also act as active selective gates for interaction with the external world controlling the incoming and outgoing nutrient and wastes. [1]. They can be permeable to some water soluble molecules while impermeable to some other specific macromolecules [1, 2]. Membrane can also act as sensors to the external signals allowing the cells response to these signals.

All membrane are multicomponent and are composed of lipids and proteins [1, 3], see Fig. 1.1. Some membrane proteins ensure the stability of the cell structure by attaching to the cytoskeleton, whereas others are involved in transportation of the ions and polar molecules, as well as cell adhesion via receptor proteins. Lipid molecules are structured in the form of lipid bilayer in cells membrane and makes up 50% of the mass of most animal cell membranes. The density of the bilayer in animal cell is 5×10^6 lipid molecules per $1\mu m^2$, [1]. Lipid molecules in lipid bilayer are mostly phospholipids, cholesterols and glycolipids. Lipids typically have a hydrophilic head on one side and a hydrophobic head on the other side. The world of these molecules is governed by hydrophobic and hydrophilic effects. The same way that oil molecules assemble in to a droplet when we pore them into water, lipid molecules in aqueous solution assemble in such a way that the hydrophilic heads face the water while hydrophobic heads avoid the water as much as possible. The thickness of the lipid bilayer is about $4 - 5nm$ [1]. A phospholipid for example has a hydrophobic head and two hydrophilic tails. The arrangement of phospholipids in membrane forms two layers in which hydrophobic tails face each other in the internal side of two layer in order to avoid contact to water molecules as much as possible while hydrophilic heads face water molecules. The lipid bilayer prefer to close itself in order to keep avoiding water molecules in open edges and resist gaining additional energy. Cholesterols, proteins and other macromolecules exist among lipid bilayer. The bilayer structure is a fluid so the lipid molecules are mostly allowed to move and diffuse within the membrane freely. Biomembranes are significant part of every cells life and biological process, therefore the role and structure of biomembranes are the focus of many experimental and theoretical researches [5]. One simple way to study the cell's membrane is to look at a biomimetic membrane which has fewer components

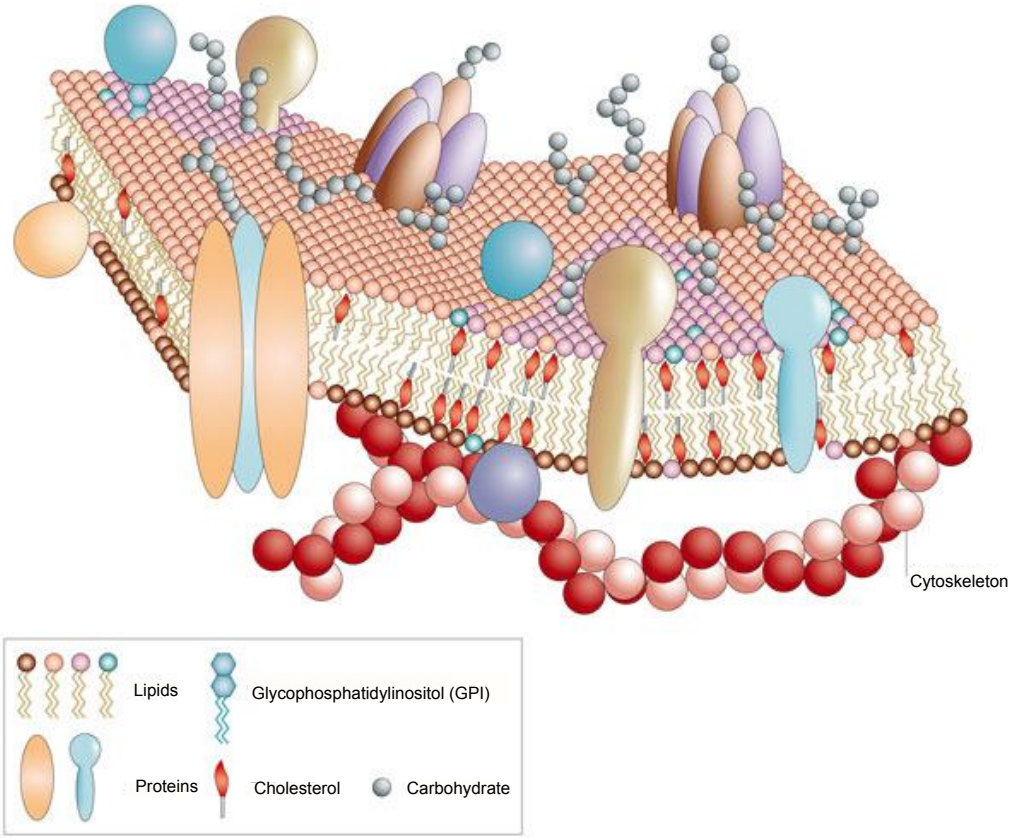

Figure 1.1 : *Cartoon of a cell membrane with its components [4]. A biomembrane typically composed of protein and lipids such as phospholipids cholesterol and glycoglycolipids. The lipid molecules form lipid bilayer in order to gain optimum energy. Proteins have different functions in membrane; they have strong effect on importing and exporting ions and molecules as well as attaching to cytoskeleton to support the stability of the cell.*

in comparison and mimics the basic biological properties of such membrane. As an example, the mixture of cholesterol and phospholipid is a biomimetic membrane which is a simple model for biological membrane. Therefore instead of a complicated system with more than hundreds of different components we focus on a simple two component membrane [6].

1.2 Domain formation in biomembranes

Multi-component membranes consisting of a small number of lipids provide simple model systems for biological membranes, which contain hundreds of different molecular components. The thickness of lipid bilayer in this system is few nanometer while its lateral extension is up to tens of micrometers, therefore this bilayer can be considered as a 2-dimensional sheet.

Biomimetic membranes can attain different thermodynamic phases and undergo transitions between these phases. When the membrane composition is altered, each phase transition leads to a miscibility gap, in which the membrane undergoes phase separation and forms intra-membrane domains. For freely suspended vesicles, these domains have a strong influence on the vesicle morphology [6, 7]as well as significant effect on signaling, budding or adhesion [1, 2]. Domains can arise from segregation of embedded or adsorbed macromolecules or can be driven by[6] lipid molecules de-mixing in membrane bilayer [6]. Lipid molecules have high affinity toward each other thus their distribution is not homogeneous and they can form some domains or lateral assemblies. The domain formation and two phase coexistence in ternary mixture of cholesterol and unsaturated phospholipid plus sphingomyelin or other saturated phospholipids, is called lipid raft [8, 9, 10, 11]. Lipid rafts organize the membrane proteins interaction during signal transduction or transportation via membrane. Domain can also be the result of anchored macromolecules aggregation. The Protein-membrane and protein-protein interactions lead to phase segregation in biomembranes [12, 13, 14].

There are large number of literature with the focus on membrane domain driven by protein aggregation, but in this research we are more interested in the formation of domains arising from lipid separation. In the next section, we introduce phase separation in biomembrane induced by adhesion to a substrate surface and then focus specifically on lipid phase separation in adhering multicomponent membrane.

1.3 Adhesion Induced phase separation in multicomponent membrane

Consider a multicmponent membrane with two different components; for example two type of protein or lipid. If one brings this membrane in contact to a substrate surface,

the surface attracts one of the components stronger than the other one. Hence, the concentration of two components in contact area and non-contact membrane change; those components which are attracted by the substrate surface enrich in the contact area while other components will be repelled from this area. This means the substrate surface has non ignorable effect on the membrane composition and the formation of domains in adhering membrane.

The generic interactions between the lipid molecules and the substrate surface arise from hydration, van der Waals, and electrostatic forces that depend on the molecular architecture of the lipids and decrease with increasing separation from the surface [15, 16]. In addition, some specific interactions may be involved such as the lipopolymers used in [17] or noncovalent bonds between membrane-anchored receptors and ligands [18].

Adhesion induced phase separation in biomembrane have been observed experimentally both in membrane proteins and lipids. In Fig. 1.2(a) optical microscopy picture of lipid domain during vesicle adhesion and in Fig. 1.2(b) the protein aggregation during T-cell adhesion to a cancer cell are illustrated. In this research we are interested in direct

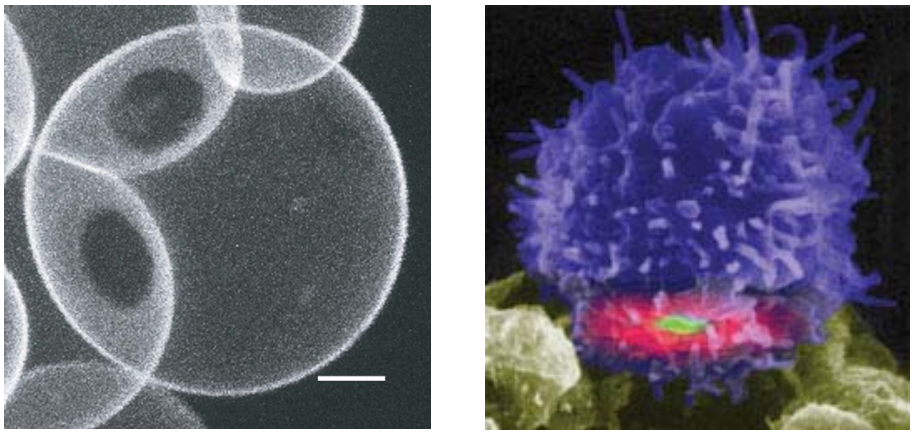

(a) (b)

Figure 1.2 : *Lipid domain during vesicle adhesion to another vesicle, (a) [19]. Protein Domain during T-cell adhesion, (b) [20]. Biomembranes exhibit phase separation and patterns of intra-membrane domains for a certain range of component composition and temperature. Domains can either arise from protein aggregation as shown in (b) or can be driven by lipid molecules separation. Scale bar in (a): 5 μm.*

interaction between a multicmponent membrane and a substrate which leads to patterns of intra-membrane lipid domains. Using thermodynamics considerations and explicit calculations based on the lattice binary mixture, it was shown that the surface has a rather strong effect on the phase behavior for a variety of membrane systems including adhering vesicles, hole-spanning membranes, also known as black lipid membranes, pore-spanning membranes, and membranes adhering to a chemically patterned substrate surface. In all of these cases, the interaction of the membrane with the adhesive surface leads to a decomposition of the membrane into an adhering and an unbound segment.

Adhesion of vesicles. In biological system cells are never isolated but always in adhesion to other cells, cytoskeletons, extra-cellular matrix or simply their substrates. Considering the importance of the adhesion in cells ' biology and biophysics, adhering vesicle has been studied theoretically and experimentally, see, e.g., [21, 22] for one-component membranes and [19] for multi-component membranes.

The morphology of a bound vesicle change with respect to the adhesion energy [21]. For strong adhesion, the vesicle shape becomes a spherical cap as shown in Fig. 3.2. Thus, the membrane bounding the vesicle is divided up into two segments, an adhering segment in close contact with the substrate surface and an unbound segment far away from the surface. The corresponding surface areas will be denoted by $\mathcal{A}^{\rm ad}$ and $\mathcal{A}^{\rm ub}$, see Fig. 1.3, and the total membrane area by $\mathcal{A}$ with $\mathcal{A} = \mathcal{A}^{\rm ad} + \mathcal{A}^{\rm ub}$.

The spherical cap shape is determined by two parameters, the total area $\mathcal{A}$ of the vesicle membrane and the volume $\mathcal{V}$ of the vesicle's volume. The total area $\mathcal{A}$ plays the role of a basic scale for surface area. Using this scale, one can define the reduced volume v in such a way that $v = 0$ corresponds to a flat pancake and $v = 1$ to a complete sphere touching the substrate in a single point. The vesicle shape is then uniquely defined, up to an overall scale, by the reduced volume v. The reduced volume also determines the area fraction

$$q \equiv \mathcal{A}^{\rm ub}/(\mathcal{A}^{\rm ad} + \mathcal{A}^{\rm ub}) = \mathcal{A}^{\rm ub}/\mathcal{A}\,. \tag{1.1}$$

For an adhering vesicle, the area fraction q can vary within the range

$$\tfrac{1}{2} \le q \le 1 \quad \text{(vesicles)}\,, \tag{1.2}$$

where $q = 1/2$ corresponds to a flat pancake and $q = 1$ to a complete sphere touching the substrate in a single point.

Partially supported membranes. Two examples for partially supported membranes are provided by hole-spanning membranes, also known as black lipid membranes, see, e.g., [23], as well as by pore-spanning membranes as in [24]. Here, a 'hole' corresponds to a channel through a relatively thin rigid plate whereas a 'pore' refers to a groove in a relatively thick substrate. If the hole and the pore have the same cross-section, both

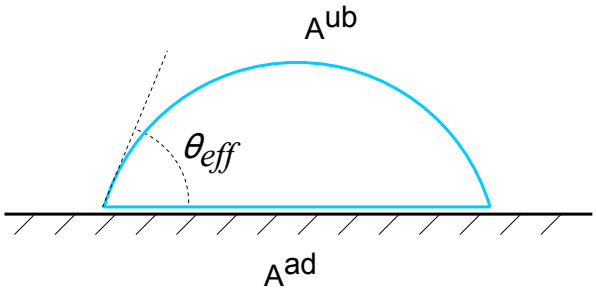

Figure 1.3 : *Side view of a vesicle that strongly adheres to a planar substrate surface. The adhering membrane segment with contact area A^{ad} and the un-bound segment with area A^{ub} meet along the contact line. The effective contact angle is denoted by θ_{eff}. Adhesion induce phase separation in the multicomponent membrane by shifting the composition in contact area and unbound membrane segment.*

systems lead to the same adhesion geometry as shown in the left panel of Fig. 1.4for a circular cross-section.

The membrane is again divided up into an adhering segment in close contact with the supporting surface and an unbound segment spanning the hole or pore. In this case, the area $\mathcal{A}_{\rm ad}$ of the adhering segment is typically larger than the area $\mathcal{A}_{\rm ub}$ of the unbound segment and the area ratio $q = \mathcal{A}^{\rm ub}/\mathcal{A}$ now varies within the range

$$0 \leq q \lesssim \tfrac{1}{2} \quad \text{(supported membranes)}\,. \tag{1.3}$$

If the membrane spans several holes or pores, it contains several unbound segments, and the area $\mathcal{A}^{\rm ub}$ is now given by the total area of all of these unbound membrane segments.

Membranes supported by structured surfaces. Another adhesion geometry of interest are membranes adhering to a chemically patterned surface as depicted in the right panel of Fig. 1.4. A variety of patterning techniques have been used to produce such systems [25, 26]. Here, we consider substrate surfaces that contain two types of surface domains, both of which attract the membrane. The simple example shown in Fig. 1.4 corresponds to a single, circular domain embedded in a larger surface matrix. In general, the surface may contain several domains and these domains may have non-circular shapes.

When a multi-component membrane adheres to such a patterned surface, the different

molecular components of the membrane will experience different interactions with the surface domains and with the surface matrix. As a result of these affinity contrasts, a supported membrane of total area $\mathcal{A}$ will form two segments that differ in their composition and have the areas $\mathcal{A}^{\rm do}$ and $\mathcal{A} - \mathcal{A}^{\rm do}$, respectively. The area fraction q is now defined by

$$q \equiv \mathcal{A}^{\rm do}/\mathcal{A} \quad \text{with} \quad 0 \leq q \leq 1\,. \tag{1.4}$$

The two limiting cases $q = 0$ and $q = 1$ correspond to membranes supported by uniform substrate surfaces. Furthermore, in the limit, in which the attraction between the membrane and the surface domains vanishes, the adhesion geometry in the right panel of Fig. 1.4becomes equivalent to the one for a hole- or pore-spanning membrane as depicted in the left panel of this figure.

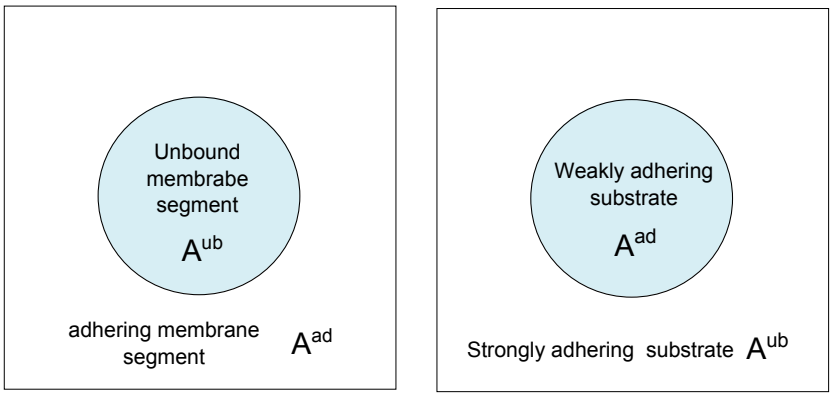

Figure 1.4 : *(Left) Top view of a partially supported membrane spanning a single circular hole or pore within the rigid support. The membrane consists of an adhering segment in close contact with the supporting surface and an unbound segment spanning the hole or pore. In this case, the area $\mathcal{A}^{\rm ad}$ of the adhering segment is typically larger than the area $\mathcal{A}^{\rm ub}$ of the unbound segment; and (Right) Membrane supported by a chemically patterned surface with a single, circular surface domain with area $\mathcal{A}^{\rm do}$. Because of their different chemical compositions, the surface domain and the surrounding surface matrix differ in their interactions with the membrane molecules. As a result of these affinity contrasts, a supported membrane of total area $\mathcal{A}$ will form two segments that differ in their composition and have the areas $\mathcal{A}^{\rm do}$ and $\mathcal{A} - \mathcal{A}^{\rm do}$, respectively.*

1.4 Outline of the thesis

This Thesis has the following order.

Chapter 2 provides an introduction to phase diagram of free membranes. In this chapter a general view of phase separation in phospholipid/cholesterol binary mixture is presented. The corresponding phase diagram reached by experiment is an essential material for further calculations in chapter 4.

Chapter 3 gives the background knowledge on strong adhesion regime in which the shape of an adhering vesicle membrane attains spherical cap. Within this regime, one can neglect the effect of boundaries and treat the adhered vesicle as a flat surface composed of the adhering *ad* and unbound *ub* segments.

Chapter 4 discuss the phase behavior of a vesicle in contact to a substrate surface from the thermodynamic point of view. Using the experimental phase diagram introduced in chapter 2 and performing calculations based on chemical potential equilibrium, we obtained the phase diagram of the adhering membrane. The results are extended to the limit of small and large affinity contrast of the membrane components to the substrate surface.

Chapter 5 introduces the Lattice model as an applicable model to describe order-disorder phenomena in binary mixtures. The exact solution for the component concentrations are available since lattice model corresponds the Ising model. Thus the binodals for two phase separation for an adhering lattice system is reached in the limit of strong and week affinity contrast. Furthermore, mean filed approximation is used as helpful tool to reach the coexistence regions of the same adhering lattice.

In summery, the results from three different methods confirm that adding the substrate surface to the free membrane, duplicate the phase diagram in to two regions of coexisting phases belong to the unbound and adhering membrane segments, respectively.

2 Phase diagrams of two-component membranes

2.1 Liquid order-disorder phase separation in biological membranes

Biological membranes with several molecular components exhibit phase separation and patterns of domains. As an example, consider a membrane vesicle that consists of phospholipid and cholesterol molecules. Phase separation in this mixture has been studied experimentally with different methods, see [27, 28, 29, 30, 31, 32, 33, 34]. All of these studies agree on phase coexistence regions for certain ranges of composition and temperature.

Phospholipid and cholesterol are two important lipids in the membrane composition. A phospholipid molecule consists of two long hydrophobic hydrocarbon chains connected to a hydrophilic head group. Cholesterol is composed of a rigid sterol with a hydroxyl group in one end and a highly flexible hydrocarbon chain on the other end.

In the absence of cholesterol, phospholipid exists in two distinct forms in thermodynamic equilibrium: The gel phase and the liquid disordered (L_d) phase. The gel, or solid, phase occurs at low temperature and within increasing the temperature, the liquid disordered (L_d) or liquid crystalline occurs, see compare as depicted in Fig. 2.1.

In each of the gel or L_d phases, the properties of the lipid bilayer are different. In gel phase, the phospholipid hydrocarbon chains are in the fully extended all-trans conformation. In this phase, the phospholipid molecules have the minimal cross-sectional area and the bilayer's thickness is maximum. Also in gel phase the intra- and intermolecular movements are extremely limited [36]. In liquid disordered state L_d, the phospholipid hydrocarbon chains have flexible rotational conformation. In contrast to the gel phase, the cross sections of the lipid molecules in the L_d phase is larger and the bilayer's is thicker. The rates of both intra- and intermolecular movement increase in the L_d state compared to the gel phase.

Cholesterol has some significance for in the lipid bilayer's properties. Cholesterol partly acts as a regulator of the fluidity in the membrane bilayer. It also increases the thickness of the gel phase and decreases the thickness of the L_d phase. Cholesterol increases the rigidity of the L_d state, whereas it gives the gel phase more fluidity. There

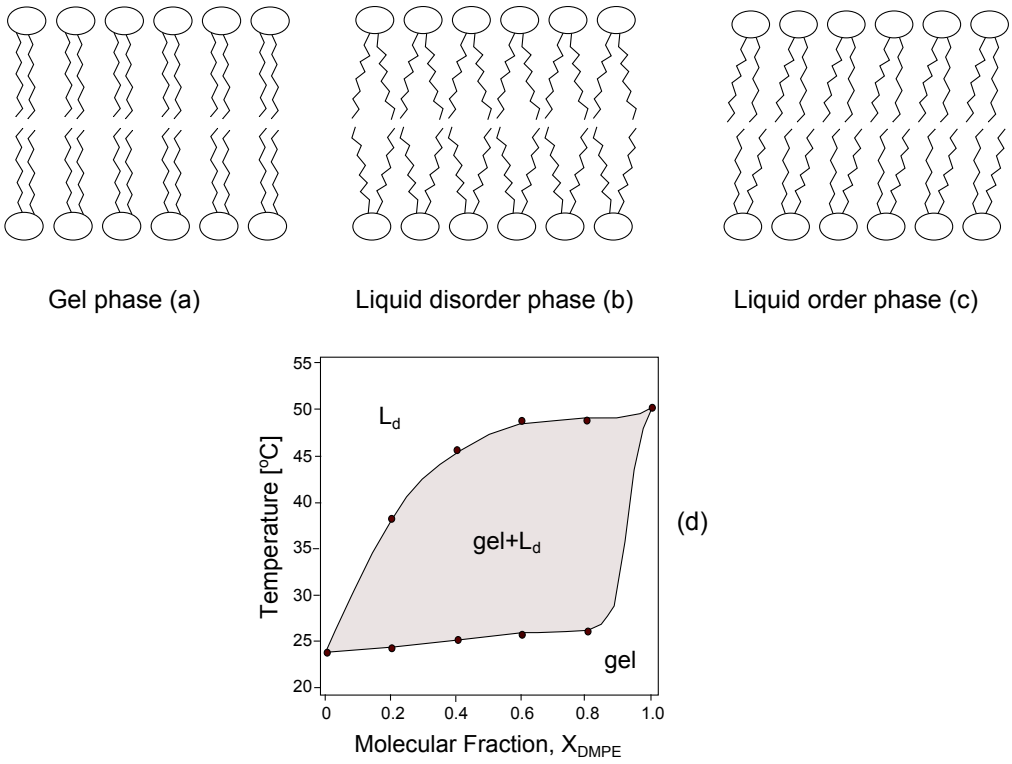

Figure 2.1 : *Phospholipid can be found in the liquid disorder phase or in the gel phase in the absence of cholesterol. In the gel phase, the phospholipid hydrocarbon chains are in the fully extended all-trans conformation(a). In liquid disordered state L_d, the hydrocarbon chains loose their order and have clumsy rotational conformation(b). Liquid ordered L_o phase is a state between the gel phase and the L_d phase(c). The gel-L_d phase diagram in the absence of cholesterol is shown in (d). The phospholipid used for this experimental phase diagram is DMPE, [35]. The coexistence region of the gel and L_d phase is shown in gray in this figure.*

is another functional role referred to cholesterol in bilayer membranes. Cholesterol can induce a separate phase called liquid ordered phase (L_o), which is distinct from gel phase and L_d.

In L_o, phase the properties of the phospholipid is different from other phase. The hydrocarbon chains are all extended and in the ordered phase. The L_o phase shows the characteristic of liquids, for example rotational mobility and lateral diffusion. Short-range orientational order and long-range translational disorder are also further specific

properties of the L_o phase.

Phase diagrams are a standard way to document the different states of the multicomponent membranes at thermodynamic equilibrium. The phase diagram of the cholesterol and phospholipid is illustrated in Fig. 2.2. In this diagram, one can find the gel and L_o coexisting phase at low temperatures, whereas L_d and L_o coexistence region is found at higher temperatures. A mixture of dipalmitoylphosphatidylcholine (DPPC) and cholesterol is used to plot this phase diagram [27]. For fix concentration of cholesterol, L_o-L_d coexisting region occurs in $T_m < T < T_c$ in which T_m is triple point temperature

2.2 Two-phase coexistence regions of mixed membranes

We consider biomimetic membranes that consist a a- and b-molecules and focus on such binary systems that undergo phase separation into two fluid phases. Therefore, these systems exhibit fluid-fluid two-phase coexistence regions in their phase diagrams. The a and b-molecules can represent any binary system, eg. cholesterol and phospholipid, Fig. 2.2.

The number of a- and b-molecules within the membrane will be denoted by $\mathcal{N}_a$ and $\mathcal{N}_b$. The mole fraction of the a-molecules is defined by

$$X_a \equiv \frac{\mathcal{N}_a}{\mathcal{N}}, \tag{2.1}$$

where the total number of molecules $\mathcal{N}$ is equal to

$$\mathcal{N} = \mathcal{N}_a + \mathcal{N}_b. \tag{2.2}$$

As one varies the temperature T and the mole fraction X_a of cholesterol or a-molecules, these systems typically exhibit coexistence regions of liquid-ordered and liquid-disordered phases, as illustrated in Fig. 2.2. One can define the fluid-fluid coexistence regions by the two binodal lines

$$X_a = X_{a,\alpha}(T) \quad \text{and} \quad X_a = X_{a,\beta}(T)\,, \tag{2.3}$$

which represent the boundaries of the coexistence regions with the α- and β-phases, see Fig. 2.2. These two binodals meet at the critical point with $T = T_c$. Thus, fluid-fluid coexistence occurs for mole fractions X_a that satisfy

$$X_{a,\beta}(T) < X_a < X_{a,\alpha}(T) \quad \text{for} \quad T_t < T < T_c\,. \tag{2.4}$$

The phase diagram depicted in Fig. 2.2 contains the coexistence region for any binary system, for example Ising spins or lattice model with different order parameters. This

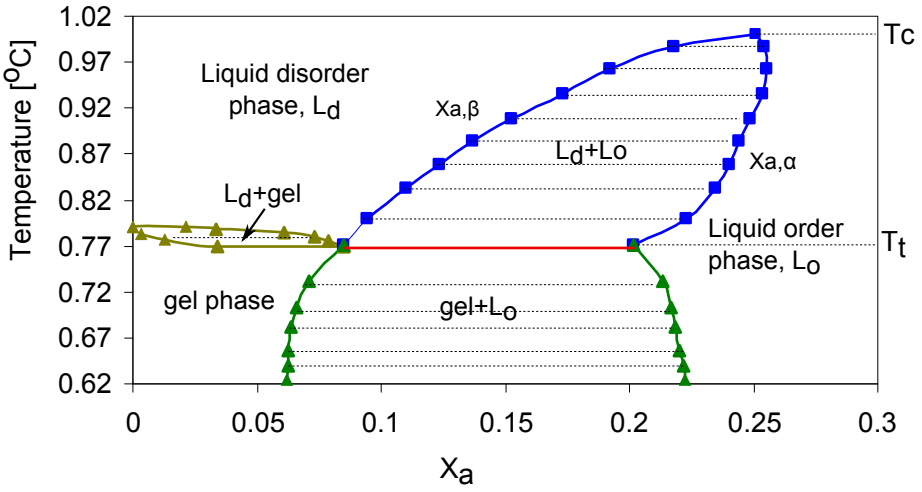

Figure 2.2 : *Generic phase diagram for mixed membranes consisting of cholesterol and phospholipid. The variable X_a represents the mole fraction of cholesterol; the phase boundaries correspond to those measured for the phospholipid DPPC. The fluid-fluid coexistence region between the liquid-ordered phase α on the right and the liquid-disordered phase on the left β is bounded by the two binodal lines $X_a = X_{a,\beta}(T)$ and $X_a = X_{a,\alpha}(T)$, which meet at the critical point with $T = T_c$ is shown in blue. For fix concentration of cholesterol, L_o-L_d coexisting region occurs in $T_m < T < T_c$ in which T_m is triple point temperature. The horizontal dashed lines represent tie lines within the two-phase coexistence region. The phase coexistence of the gel and the liquid ordered phase is the lower side which is shown in green. Furthermore the gel phase and the liquid disorder phase have a narrow coexistence region on the left side of the diagram, [27].*

phase diagram also fits the mixture of cholesterol and phospholipid molecules which is comparable to the experimental phase diagram illustrated in Fig. 2.2.

If we prepared a vesicle with a mole fraction X_a within the range described by (2.4), the phase separation within the membrane would lead to the formation of α and β domains. After the separation process has been completed, the membrane will be subdivided into one large α- and one large β-domain. The combined number $\mathcal{N}_\alpha$ of a- and b-molecules

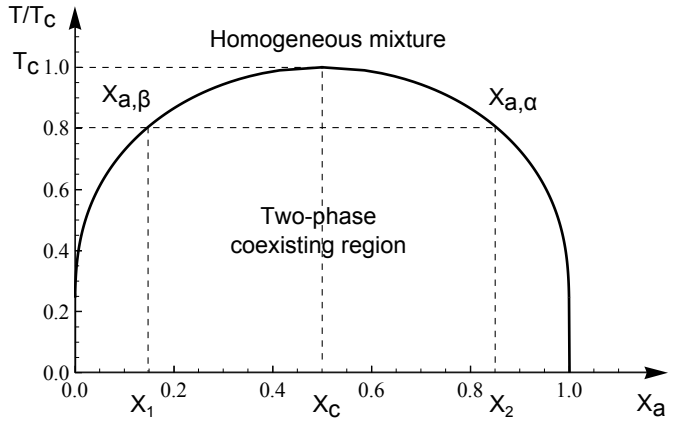

Figure 2.3 : *The theoretical binary mixture phase diagram in the (X_a, T)-plane. The two binodal branches are denoted by $X_{a,\beta}(T)$ and $X_{a,\alpha}(T)$ corresponding to the b-rich and the a-rich phase, respectively. The two branches meet in the critical point at $(X_a, T) = (X_c, T_c)$.*

within the α domain is given by

$$\frac{\mathcal{N}_\alpha}{\mathcal{N}} = \frac{X_a - X_{a,\beta}}{X_{a,\alpha} - X_{a,\beta}}\,, \tag{2.5}$$

with $\mathcal{N} \equiv \mathcal{N}_a + \mathcal{N}_b$ being the total number of membrane molecules. The combined number $\mathcal{N}_\beta$ of a- and b- molecules within the β domain then follows from $\mathcal{N}_\beta/\mathcal{N} = 1 - \mathcal{N}_\alpha/\mathcal{N}$.

By definition, all molecular fractions X attain values within the range $0 \leq X \leq 1$. For example, $X_a^{\rm ad} = 0$ means there are no a-molecules in the adhering segment. Similarly, $X_a^{\rm ad} = 1$ means that the adhering segment is full of a molecules. Therefore the value of the $X_a^{\rm ad}$ varies between 0 and 1.

In this project, we are focusing on the phase separation in adhering multi-component membranes. Thus we are interested in the L_o-L_d (fluid-fluid) phase coexistence in phospholipid-cholesterol mixture as seen in Fig. 2.2. So, with neglecting the L_o-gel phase coexistence part in the phase diagram (2.2), we only focus on the blue coexistence line on the same figure. In the next section, we give a suitable physical interpretation for phase coexistence regions in binary systems.

3 Strong adhesion regime

3.1 Strong adhesion regime

The shape of a vesicle which sticks to a flat substrate surface can be characterized by the membrane bending rigidity κ and the adhesion free energy. The contact mean curvature of such vesicle is given by [21]

$$M = (2|W|/\kappa)^{1/2} \tag{3.1}$$

where W is the adhesion free energy per unit area. For a flat substrate, the curvature tangential to the contact line is equal to zero therefore the curvature normal to the contact line is M. For a vesicle with the total area $\mathcal{A}$ the linear vesicle size R_{ve} is defined as

$$R_{\mathrm{ve}} = (\mathcal{A}/4\pi)^{1/2}, \tag{3.2}$$

also the contact curvature can be characterized by its radius

$$R_{\mathrm{co}} = (\kappa/2|W|)^{1/2}. \tag{3.3}$$

By minimization of the free energy of an adhering vesicle combined with the boundary condition of the contact curvature one can obtain many different shapes for adhering vesicle. Fig. 3.1 shows some of the different shapes obtained by varying the adhesion energy while holding the overall membrane area constant [21]. For small bending rigidity the shape of adhering vesicle evolves into a spherical cap (shown in Fig. 3.1) which fits to the strong adhesion regime requirement. The strong adhesion regime is defined by the condition that the contact curvature radius R_{co} is much smaller than the vesicle size R_{ve}

$$R_{\mathrm{co}} \ll R_{\mathrm{ve}}. \tag{3.4}$$

Combining the inequality in Eq. (3.4) with (3.3) one can obtain the limit of adhesion energy required by strong adhesion regime;

$$|W|^{1/2} \gg (2\pi\kappa/\mathcal{A})^{1/2} \tag{3.5}$$

where the quantity $\kappa/\mathcal{A}$ may be regarded as the membrane tension arising from the closure of the vesicle membrane.

Let us now focus on giant vesicles that are conveniently studied by optical microscopy.

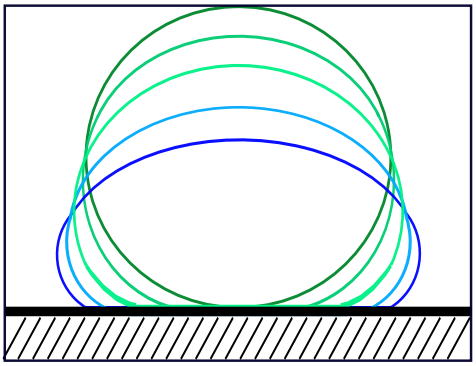

Figure 3.1 : *Schematic shapes of adhering vesicles with the similar overall vesicle area for various adhesion energies, [21]. The contact area of the vesicle increases with increasing adhesion energy.*

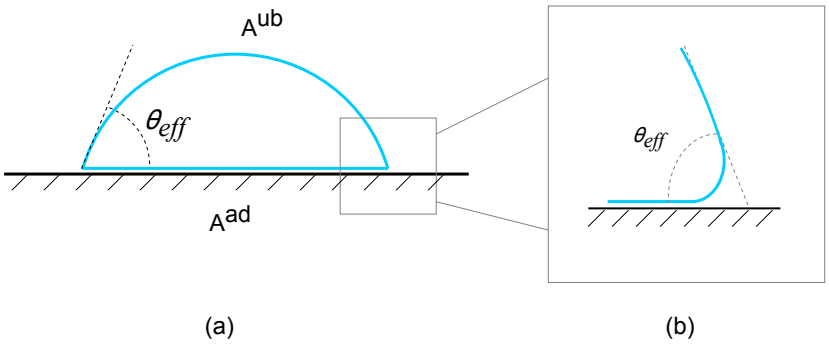

Figure 3.2 : *(a) Spherical cap shape of adhering vesicle in the strong adhesion regime. The adhering membrane segment with contact area $\mathcal{A}^{\rm ad}$ and the unbound segment with area $\mathcal{A}^{\rm ub}$ meet along the contact line. The effective contact angle is denoted by $\theta_{\rm eff}$; (b) When viewed with increased resolution, the membrane segment close to the contact line is smoothly curved.*

The size $R_{\rm ve}$ of such vesicles usually exceeds $20\,\mu$m. Therefore, these vesicles are in the strong adhesion regime as soon as the contact curvature radius is below optical resolution, i,e., $R_{\rm co} < L_* \simeq 0.5\,\mu$m or

$$|W| > |W|_* \equiv \frac{\kappa}{2L_*^2} \simeq \frac{\kappa}{0.5\,\mu{\rm m}^2}\,. \tag{3.6}$$

For a lipid bilayer, the bending rigidity κ is of the order of 10^{-19} J or $24\,k_BT_o$ at room temperature $T_o = 25^\circ$ C, which implies $|W|_* \simeq 2\times10^{-4}\,\mathrm{mJ/m^2}$ or $|W|_* \simeq 0.5\,k_BT/(100\,\mathrm{nm})^2$. Thus, the strong adhesion regime should typically apply as long as the adhesion is mediated by a large number of molecular interactions. In this regime, the vesicle spreads onto the surface as much as possible.

For fixed vesicle volume $\mathcal{V}$ and fixed membrane area $\mathcal{A}$, the shape with the largest contact area is provided by a spherical cap, which can be characterized by an effective contact angle θ_{eff} as shown in Fig. 3.2. In this figure, we have assumed that we can ignore the excess area stored in the bending undulations of the vesicle membrane. Thus the strong adhesion regime occurs when:
(*i*) the bending rigidity κ is not larger than 10^{-19} J,
(*ii*) the vesicle size R_{ve} is much larger than the contact curvature radius R_{co} so not smaller than couple of micrometers and also
(*iii*) the number of interacting molecules the adhesion area should be sufficiently large.

3.2 Two membrane segments of adhering vesicle

In general, a vesicle that sticks to a planar substrate surface can be divided into two membrane segments: an adhering segment that forms the contact area and an unbound segment that is not in contact with the substrate surface. The surface areas of the adhering and unbound membrane segments will be denoted by $\mathcal{A}^{\mathrm{ad}}$ and $\mathcal{A}^{\mathrm{ub}}$, respectively Fig. 3.2. The overall area $\mathcal{A}$ of the membrane is then given by

$$\mathcal{A} = \mathcal{A}^{\mathrm{ad}} + \mathcal{A}^{\mathrm{ub}}\,. \tag{3.7}$$

The adhering and unbound segments meet at the contact line of the vesicle. Along this line, the unbound membrane segment has the contact curvature radius R_{co}.

To parametrize the spherical cap in terms of contact angle, we need to start from the geometry of the cap in terms of the overall membrane area $\mathcal{A}$ and the cap height h Fig. 3.3. All geometric quantities like the segment area or volume can be expressed in terms of these two parameters as follow the adhering segment area:

$$\mathcal{A}^{ad} = (1/2)(\mathcal{A} - h^2), \tag{3.8}$$

curvature radius of spherical segment R_{co}:

$$R_{\mathrm{co}} = (\mathcal{A} + \pi h^2)(4\pi h), \tag{3.9}$$

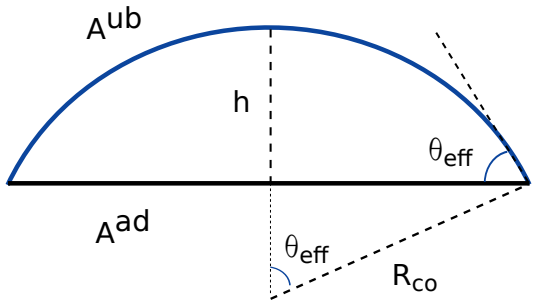

Figure 3.3 : *Spherical cap geometry of an adhering vesicle in the strong adhesion regime . The adhering membrane segment with contact area $\mathcal{A}^{\rm ad}$ and the unbound segment with area $\mathcal{A}^{\rm ub}$ meet along the contact line with the curvature radius $R_{\rm co}$. The effective contact angle is denoted by $\theta_{\rm eff}$ and the height of the cap is denoted by h. All geometric quantities can be expressed in terms of $\theta_{\rm eff}$ and overall area $\mathcal{A} = \mathcal{A}^{\rm ad} + \mathcal{A}^{\rm ub}$.*

effective contact angle $\theta_{\rm eff}$:

$$cos(\theta_{\rm eff}) = (\mathcal{A} - 3\pi h^2)/(\mathcal{A} + \pi h^2), \tag{3.10}$$

and the vesicle volume $\mathcal{V}$:

$$\mathcal{V} = (h/12)(3\mathcal{A} - \pi h^2). \tag{3.11}$$

We can solve Eq. (3.10) for cap height as a function of effective contact angle $\theta_{\rm eff}$ and overall membrane area $\mathcal{A}$.

$$h = \left(\frac{\mathcal{A}(1 - cos(\theta_{\rm eff}))}{\pi(3 + cos(\theta_{\rm eff}))}\right)^{\frac{1}{2}}. \tag{3.12}$$

By substituting relation (3.12) into equations (3.8, 3.9 and 3.11) we can express $\mathcal{A}^{ad}$, $R_{\rm co}$ and $\mathcal{V}$ in terms of $\theta_{\rm eff}$ and $\mathcal{A}$.

3.2.1 Area of adhering membrane segment

For the spherical cap shape shown in Fig. 3.3, the area ratios $\mathcal{A}^{\rm ub}/\mathcal{A}$ and $\mathcal{A}^{\rm ad}/\mathcal{A}$ can be expressed in terms of the effective contact angle $\theta_{\rm eff}$:

$$\frac{\mathcal{A}^{\rm ub}}{\mathcal{A}} = \frac{2}{3 + \cos(\theta_{\rm eff})} \tag{3.13}$$

and

$$\frac{\mathcal{A}^{\mathrm{ad}}}{\mathcal{A}} = \frac{1+\cos(\theta_{\mathrm{eff}})}{3+\cos(\theta_{\mathrm{eff}})}\,. \tag{3.14}$$

Likewise, the reduced volume of the vesicle as defined by

$$v \equiv \frac{3\mathcal{V}/4\pi}{(\mathcal{A}/4\pi)^{3/2}} \tag{3.15}$$

satisfies the relation

$$v = 2\,\frac{[1-\cos(\theta_{\mathrm{eff}})]^{1/2}\,[2+\cos(\theta_{\mathrm{eff}})]}{[3+\cos(\theta_{\mathrm{eff}})]^{3/2}}\,. \tag{3.16}$$

Inverting this latter relation numerically, one obtains

$$\cos(\theta_{\mathrm{eff}}) = f(v) \tag{3.17}$$

as shown in Fig. 3.4(a). Substituting (3.17) into (3.14), the area ratios can be written as

$$\frac{\mathcal{A}^{\mathrm{ad}}}{\mathcal{A}} = 1 - \frac{\mathcal{A}^{\mathrm{ub}}}{\mathcal{A}} \quad \text{and} \quad \frac{\mathcal{A}^{\mathrm{ub}}}{\mathcal{A}} = \frac{2}{3+f(v)} \tag{3.18}$$

for $0 \le v \le 1$ as displayed in Fig. 3.4(b). For $v = 0$, the vesicle is a pancake shaped with contact angle $\theta_{\mathrm{eff}} = 0$ and contact area $\mathcal{A}^{\mathrm{ad}} = \frac{1}{2}\,\mathcal{A}$. For $v = 1$, it is a spherical with $\theta_{\mathrm{eff}} = \pi$ and $\mathcal{A}^{\mathrm{ad}} = 0$.

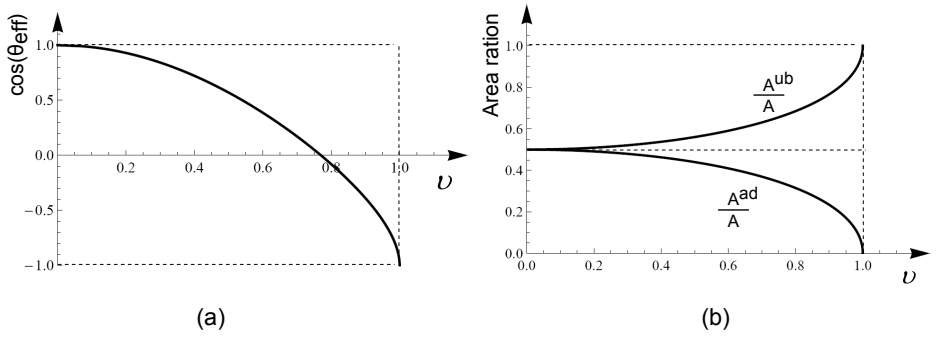

Figure 3.4 : *Spherical cap geometry: (a) Cosine of the effective contact angle θ_{eff} and (b) Area ratios $\mathcal{A}^{\mathrm{ad}}/\mathcal{A}$ and $\mathcal{A}^{\mathrm{ub}}/\mathcal{A}$ of the adhering and unbound membrane segment as a function of reduced vesicle volume v.*

Therefore, for constant area $\mathcal{A}$ and volume $\mathcal{V}$, both the contact area $\mathcal{A}^{\mathrm{ad}}$ and the area $\mathcal{A}^{\mathrm{ub}}$ of the unbound membrane segment are fixed. On the other hand, if the volume

of the adhering vesicle is changed by osmotic inflation or deflation, its contact area will decrease and increase, respectively, as described by relation (3.18) and shown in Fig. 3.4(b). Therefore, the vesicle volume provides an experimentally accessible control parameter that can be used to change the area $\mathcal{A}^{\mathrm{ad}}$ of the adhering membrane segment.

4 Phase behaviour of adhering vesicles

A membrane exposed to a substrate surface is composed of two separate segments, an adhering segment (denoted by ad) that forms the vesicle's contact area and an unbound segment (denoted by ub) that is not in contact with the substrate surface, see Fig. 3.2. For constant temperature, the surface areas of these two membrane segments are essentially controlled by the reduced vesicle volume and are, thus, fixed for fixed volume. Furthermore, when the two membrane segments exchange a- and b-molecules, they actually exchange molecular areas in such a way that their surface areas remain, on average, unchanged.

The a- and b-components have the molecular areas A_a and A_b within the mixed membranes. Since the molecules in the membrane bilayer are densely packed, the number of a and b-molecules ($\mathcal{N}_a$ and $\mathcal{N}_b$) are not independent but satisfy the constraint

$$\mathcal{N}_a A_a + \mathcal{N}_b A_b = 2\mathcal{A}. \tag{4.1}$$

Now we couple the membrane to two chemical potential reservoirs μ_a and μ_b for a and b-molecules, respectively. Since the total number of molecules is fixed and satisfies the constraint in (4.1), the exchange of the molecules between two reservoirs have to be simultaneously. If one moves m molecules from the a-reservoir into the membrane, then $n = mA_a/A_b$ number of b-molecules move back to the reservoir. In close analogy to semi-grand canonical ensembles [37, 38], the corresponding change in membrane's Gibbs free energy is given by $m\Delta\mu = m\mu_a - n\mu_b$ which is equivalent to relative chemical potential

$$\Delta\mu \equiv A_a \left[\frac{\mu_a}{A_a} - \frac{\mu_b}{A_b} \right] . \tag{4.2}$$

To continue the calculation, we need to have the two molecular areas A_a and A_b. Since these molecular areas are not easy to determine and may also depend on membrane composition [39], it is instructive to assume that a- and b-molecules have the same area

$$A_a = A_b. \tag{4.3}$$

The expression (4.2) for the relative chemical potential then simplifies and becomes

$$\Delta\mu \equiv \mu_a - \mu_b. \tag{4.4}$$

In order to get a clear definition of parameters involved in the membrane adhesion, we need to distinguish between parameters in the adhering and in the unbound membrane segments. Starting from the number of the a- and b-molecules which are now partitioned into these two segments. We define the number of a and b molecules within the adhering segment as $\mathcal{N}_a^{\rm ad}$ and $\mathcal{N}_b^{\rm ad}$ as well as the number of molecules $\mathcal{N}_a^{\rm ub}$ and $\mathcal{N}_b^{\rm ub}$ of the a- and b-molecules within the unbound membrane segment. Each leaflet of the bilayer membranes contains half of these numbers.

The total area of the membrane is $\mathcal{A}$, while the adhering segment has the surface area $\mathcal{A}^{\rm ad}$ and the unbound segment's total area is $\mathcal{A}^{\rm ub}$. Using again the molecular areas A_a and A_b of the a- and b-molecules, one can decompose the areas of the two membrane segments into

$$\mathcal{A}^{\rm ad} = \tfrac{1}{2}\,\mathcal{N}_a^{\rm ad}\,A_a + \tfrac{1}{2}\,\mathcal{N}_b^{\rm ad}A_b \tag{4.5}$$

and

$$\mathcal{A}^{\rm ub} = \tfrac{1}{2}\,\mathcal{N}_a^{\rm ub}\,A_a + \tfrac{1}{2}\,\mathcal{N}_b^{\rm ub}A_b. \tag{4.6}$$

4.1 Chemical potentials for the two membrane segments and affinity contrast

Chemical potentials for unbound membrane segment

In this section, we focus on the unbound membrane segment of the vesicle and try to derive the chemical potential of this segment. The total number of particles in unbound membrane segment is equal to

$$\mathcal{N}^{\rm ub} = \mathcal{N}_a^{\rm ub} + \mathcal{N}_b^{\rm ub}, \tag{4.7}$$

and the surface area of this segment is

$$\mathcal{A}^{\rm ub} = \mathcal{N}_a^{\rm ub}A_a + \mathcal{N}_b^{\rm ub}A_b. \tag{4.8}$$

Since the vesicle is in contact with an aqueous solution, the a- and b-molecules have diffusive motion within the fluid membrane. Because of this lateral diffusion , the a- and b-molecules can attain many molecular configurations (or patterns) at temperature T. We denote these molecular configurations by $\mathcal{C}$. The energies of these configurations have the general form:

$$\mathcal{E}_{\mathcal{C}}^{\rm ub} \equiv \mathcal{E}^{\rm ub}(\mathcal{C}\,|\,\mathcal{N}_a^{\rm ub}, \mathcal{N}_b^{\rm ub}). \tag{4.9}$$

The energy introduced above depends on the molecule numbers $\mathcal{N}_a^{\rm ub}$ and $\mathcal{N}_b^{\rm ub}$ as well as on the intermolecular interactions. The most effective interactions which play a role in the molecular configuration are hydrophobic, van der Waals, and electrostatic

interactions. In Sec. 5.1 we will describe these interactions within some lattice models. For now, we skips the explicit description of the energy and continue with the general discussion, since this representation will be sufficient.

The Helmholtz free energy of the molecules within the unbound membrane segment is then given by

$$\mathcal{F}^{\rm ub}(\mathcal{N}_a^{\rm ub},\mathcal{N}_b^{\rm ub},\mathcal{A}^{\rm ub},T) = -k_BT\ln\left(\sum_{\mathcal{C}}\exp[-\mathcal{E}_{\mathcal{C}}^{\rm ub}/k_BT]\right)\,. \tag{4.10}$$

Since this free energy is an extensive quantity, it must be proportional to another extensive quantity which we choose to be the rescaled surface area of the unbound membrane segment

$$\bar{\mathcal{A}}^{\rm ub} \equiv \mathcal{A}^{\rm ub}/A_a. \tag{4.11}$$

The rescaled surface area $\bar{\mathcal{A}}^{\rm ub}$ also represents the maximum number of a-molecules that can be accommodated within the unbound membrane segment. In the limit of large area $\mathcal{A}^{\rm ub}$, the free energy then is equivalent to

$$\mathcal{F}^{\rm ub}(\mathcal{N}_a^{\rm ub},\mathcal{N}_b^{\rm ub},\mathcal{A}^{\rm ub},T) \approx \bar{\mathcal{A}}^{\rm ub}\,F(X_a^{\rm ub},A_a/A_b,T)\,, \tag{4.12}$$

which for the condition $A_b = A_a$ attains the final form

$$\mathcal{F}^{\rm ub} \approx \bar{\mathcal{A}}^{\rm ub}\,F(X_a^{\rm ub},T)\,. \tag{4.13}$$

One can derive the chemical potential of the a- and b- molecules from the Helmholtz free energy (4.10). Therefore, the chemical potentials $\mu_a^{\rm ub}$ and $\mu_b^{\rm ub}$ of the two molecular components within the unbound membrane segment are defined by

$$\mu_a^{\rm ub} \equiv \partial\mathcal{F}^{\rm ub}/\partial\mathcal{N}_a^{\rm ub} \quad \text{and} \quad \mu_b^{\rm ub} \equiv \partial\mathcal{F}^{\rm ub}/\partial\mathcal{N}_b^{\rm ub}\,, \tag{4.14}$$

where these derivatives are taken for fixed surface area $\mathcal{A}^{\rm ub}$ of the unbound membrane segment. The relation $\mathcal{A}^{\rm ub} = \frac{1}{2}\mathcal{N}_a^{\rm ub}\,A_a + \frac{1}{2}\mathcal{N}_b^{\rm ub}\,A_b$ implies that, for fixed surface area $\mathcal{A}^{\rm ub}$, we have to remove b-molecules when we insert a-molecules and vice versa.

From the expressions (4.13) and (4.14) for the free energy $\mathcal{F}^{\rm ub}$, one can extract the chemical potential as a function of area fraction in both membrane segments, which have the form

$$\mu_a^{\rm ub} = \partial F/\partial X_a^{\rm ub} \equiv F'(X_a^{\rm ub}) \tag{4.15}$$

and

$$\mu_b^{\rm ub} = \frac{\partial F}{\partial X_b^{\rm ub}} = -\,\mu_a^{\rm ub} \quad \text{for} \quad A_b = A_a, \tag{4.16}$$

where $X_b^{\rm ub} = 1 - X_a^{\rm ub}$ has been used in the last equality.

In these calculations, we have implicitly assumed that the molecular areas A_a and A_b are essentially independent of the membrane composition. The simulation of the cholesterol/DPPC mixture shows that up to a certain amount of cholesterol concentration ($X_a = 0.4$), the molecular areas do not change, which confirms that the molecular areas are independent of the component's concentrations. [39].

The generic form of the chemical potential $\mu_a^{\rm ub} = F'(X_a^{\rm ub})$ as a function of mole fraction $X_a^{\rm ub}$ can be deduced from thermodynamics. When the two system are not in chemical equilibrium and allowed to exchange molecules or molecular area, they will approach a state of chemical equilibrium. In this state, both of the systems have the same chemical potential. Furthermore, for the two system which have initially different chemical potentials, the equilibrium state is approached via an overall flux of molecules from the system with the higher chemical potential to the system with the lower one.

From thermodynamic stability, i.e., the stability of the equilibrium state, one can conclude that the derivative of the chemical potential with respect to molecular number or mole fraction cannot be negative. Therefore the function $\mu_a^{\rm ub} = F'(X_a^{\rm ub})$ is, in general, characterized by

$$\partial \mu_a^{\rm ub}/\partial X_a^{\rm ub} = \partial F'(X_a^{\rm ub})/\partial X_a^{\rm ub} \geq 0, \tag{4.17}$$

i.e., by a derivative or local slope that cannot be negative.

Now it is important to distinguish between two different cases as shown in Fig. 4.1. The first case occurs when the $\partial \mu_a^{\rm ub}/\partial X_a^{\rm ub} > 0$ increases with increasing $X_a^{\rm ub}$ in a strictly monotonic manner, for all values of mole fraction $X_a^{\rm ub}$ and the chemical potential $\mu_a^{\rm ub}$. In this case, the unbound membrane segment remains in the one-phase region for all values of the area fraction $X_a^{\rm ub}$. It means that the unbound segment is a homogeneous mixture of the a- and b-molecules. For cholesterol/phospholipid mixtures, this behavior is observed for high temperatures $T > T_c$, i.e., above the critical temperature in Fig. 2.2.

On the other hand, the chemical potential attains a constant value when

$$\partial \mu_a^{\rm ub}/\partial X_a^{\rm ub} = 0 \quad \text{and} \quad \mu_a^{\rm ub} = \mu_{\alpha\beta}\,. \tag{4.18}$$

In this case, the mole fraction X_a varies in the certain range

$$X_{a,\beta}(T) < X_a^{\rm ub} < X_{a,\alpha}(T), \tag{4.19}$$

which implies a coexistence region in the unbound membrane composition. For the case of cholesterol/phospholipid mixtures, a two-phase coexistence region is observed for $T < T_c$ that is shown by two binodal lines Fig. 2.2

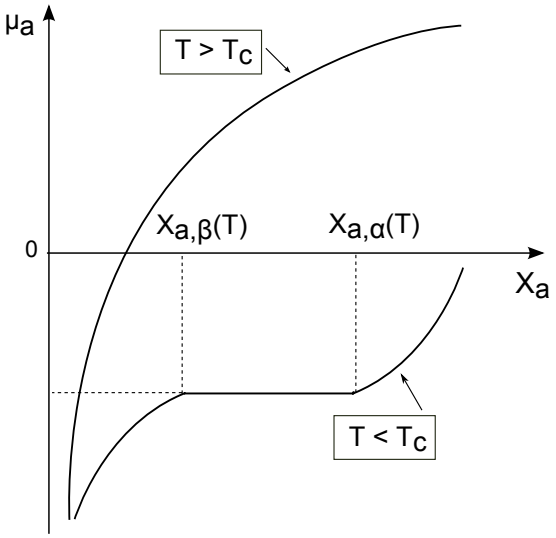

Figure 4.1 : *Chemical potential $\mu = \mu_a^{\rm ub}$ as a function of area fraction $X = X_a^{\rm ub}$ of the unbound membrane segment for cholesterol/phospholipid mixtures. Thermodynamic stability implies that $\partial\mu_a/\partial X_a \geq 0$. For temperatures $T > T_c$, the membrane segment remains in the one-phase region and the slope $\partial\mu_a^{\rm ub}/\partial X_a^{\rm ub} > 0$ is positive for all area fractions $X_a^{\rm ub}$ as illustrated by the upper curve. In contrast, for temperatures $T < T_c$, the chemical potential has the constant value $\mu_a^{\rm ub} = \mu_{\alpha\beta}$, as the molecular area fraction $X_a^{\rm ub}$ varies within the range $X_{a,\beta} \leq X_a^{\rm ub} \leq X_{a,\alpha}$. In the latter case, the membrane segment undergoes phase separation and forms β domains with area fraction $X_{a,\beta}$ as well as α domains with area fraction $X_{a,\alpha}$.*

Chemical potentials for adhering membrane segment and affinity contrast

Next, similar to the unbound membrane segments, we consider the adhering membrane segment of the vesicle, which contains

$$\mathcal{N}^{\rm ad} = \mathcal{N}_a^{\rm ad} + \mathcal{N}_b^{\rm ad} \tag{4.20}$$

molecules and has the surface area

$$\mathcal{A}^{\rm ad} = \tfrac{1}{2}\,\mathcal{N}_a^{\rm ad} A_a + \tfrac{1}{2}\,\mathcal{N}_b^{\rm ad} A_b. \tag{4.21}$$

When the membrane is in contact to a substrate, there are some molecular interactions between the membrane molecules and the substrate surface. This interaction is described by the adhesion (or binding) energies

$$U_a \leq 0 \quad \text{and} \quad U_b \leq 0 \tag{4.22}$$

for the a- and b-molecules, respectively. The negative adhesion energy represent the attractive interaction between molecules and the substrate surface. One has to notice that the substrate surface has different affinities to the a- and b-molecules, $U_a \neq U_b$.

The configuration energies of the molecules within the adhering membrane segment can be written in the form

$$\mathcal{E}_{\mathcal{C}}^{\mathrm{ad}} \equiv \mathcal{E}^{\mathrm{ub}}(\mathcal{C}\,|\,\mathcal{N}_a^{\mathrm{ub}}, \mathcal{N}_b^{\mathrm{ub}}) + U_a\,\mathcal{N}_a^{\mathrm{ad}} + U_b\,\mathcal{N}_b^{\mathrm{ad}} \tag{4.23}$$

The first term in relation above has the same functional form as the configuration energy of the unbound segment in (4.9). The additional part on the right side is standing for the adhesion energy imposed by the substrate surface on the a- and b-molecules. Following the same line of arguments as for the unbound segment, the free energy of the adhering segment is now found to behave as

$$\mathcal{F}^{\mathrm{ad}}(\mathcal{N}_a^{\mathrm{ad}}, \mathcal{N}_b^{\mathrm{ad}}, \mathcal{A}^{\mathrm{ad}}, T) \approx \bar{\mathcal{A}}^{\mathrm{ad}}\ \left[F(X_a^{\mathrm{ad}}, T) + U_a\,X_a^{\mathrm{ad}} + U_b\ X_b^{\mathrm{ad}}\right] \tag{4.24}$$

in the limit of large area

$$\bar{\mathcal{A}}^{\mathrm{ad}} \equiv \mathcal{A}^{\mathrm{ad}}/A_a \tag{4.25}$$

with $X_b^{\mathrm{ad}} = 1 - X_a^{\mathrm{ad}}$ and $A_a = A_b$.

The chemical potential μ_a^{ad} of the a-molecules within the adhering membrane segment now has an additional part, which is equivalent to the adhesion energy and is given by

$$\mu_a^{\mathrm{ad}} = F'(X_a^{\mathrm{ad}}) + \Delta U, \tag{4.26}$$

with $F'(X) = \partial F(X)/\partial X$ as before.

The affinity contrast between the two membrane components can be characterized by the definition of the parameter ΔU:

$$\Delta U \equiv A_a \left(\frac{U_a}{A_a} - \frac{U_b}{A_b}\right) = U_a - U_b. \tag{4.27}$$

From the chemical equilibrium of the a- and b-molecules, we again obtain the simple relation for the chemical potential of this particles as

$$\mu_b^{\mathrm{ad}} = -\mu_a^{\mathrm{ad}}\,. \tag{4.28}$$

Since we use the convention that the attractive substrate surface is characterized by negative values of U_a and U_b, the affinity contrast ΔU as defined by (4.27) is positive if the b-molecules are attracted more strongly to the surface, i.e., if $U_b < U_a$.

For two-component membranes consisting of cholesterol and a single phospholipid, the cholesterol is 'buried' within the bilayer membrane. Therefore it is plausible to assume that cholesterol hardly interacts with the surface and the attraction to the surface is primarily mediated via the phospholipids. Since we chose the phospholipids of cholesterol/phospholipid bilayers to represent the b-molecules, these membranes should be characterized by a positive affinity contrast $\Delta U > 0$. This affinity contrast implies that the phospholipid is enriched whereas cholesterol is depleted in the adhering membrane segment. The consequences for the phase behavior will be explained further below.

4.2 Chemical equilibrium between membrane segments

The adhering and the unbound membrane segments can exchange molecules via diffusion over the contact line. In chemical equilibrium, the chemical potentials in the unbound segment must be equal to the chemical potentials in the adhering segment. Thus, for the a-molecules, we have the equilibrium condition

$$\mu_a^{\rm ad} = \mu_a^{\rm ub} \equiv \mu_a^{\rm eq} \,. \tag{4.29}$$

Because the chemical potentials for the b-molecules are proportional to those of the a-molecules, see (4.28) and (4.16), chemical equilibrium for the a-molecules implies chemical equilibrium for the b-molecules, i.e.,

$$\mu_b^{\rm ad} = \mu_b^{\rm ub} = -\mu_a^{\rm eq}. \tag{4.30}$$

The relation (4.29) represents the equilibrium condition in the canonical ensemble. The thermodynamic control parameters in the canonical ensemble are the molecule numbers. To interpret this condition from a grand-canonical point of view, we need to couple the vesicle to a reservoir for a- and b-molecules. Also we need to choose the chemical potentials of these reservoirs to be equal to $\mu_a^{\rm eq}$ and $-\mu_a^{\rm eq}$, respectively.

Using the explicit expressions (4.26) and (4.15) for the chemical potentials of the a-molecules, the chemical equilibrium relation (4.29) can be rewritten in the form

$$\mu_a^{\rm eq} = F'(X_a^{\rm ad}) + \Delta U = F'(X_a^{\rm ub}) \tag{4.31}$$

with $F'(X) = \partial F/\partial X$ and the affinity contrast ΔU as defined in (4.27).

4.3 Partitioning of molecules between membrane segments

The main goal in this chapter is to calculate the adhering membrane generic phase diagram in terms of the mole fraction and chemical potential. To this aim, we need to have a clear relation between these parameters.

The two mole fractions $X_a^{\rm ad}$ and $X_{\rm ad}^{\rm ub}$ describe the partitioning of the molecules in the adhering and in the unbound membrane segments. In order to calculate these two quantities, we need two equations. The first equation is provided by the implicit equation

$$F'(X_a^{\rm ub}) = F'(X_a^{\rm ad}) + \Delta U\,, \tag{4.32}$$

which describes the chemical equilibrium between the two segments, see the second equality in (4.31). The second equation follows directly from the definitions of the mole fractions $X_a^{\rm ad}$ and $X_a^{\rm ub}$ that imply the linear relation

$$q\,X_a^{\rm ub} + (1-q)\,X_a^{\rm ad} = X_a \quad \text{with} \quad q \equiv \mathcal{A}^{\rm ub}/\mathcal{A} \tag{4.33}$$

between $X_a^{\rm ub}$, $X_a^{\rm ad}$ and the overall mole fraction X_a of the whole membrane as defined in (2.1). Thus, the mole fractions $X_a^{\rm ad}$ and $X_a^{\rm ub}$ are obtained from the solution of the two equations (4.32) and (4.33).

These two equations depend on three parameters each of which can in principle be varied and controlled experimentally: (i) the overall mole fraction X_a of the a-molecules within the vesicle membrane, which represents the overall membrane composition; (ii) the area ratio $q = \mathcal{A}^{\rm ub}/\mathcal{A}$ of the adhering vesicle, which is a purely geometric parameter; and (iii) the affinity contrast ΔU arising from the interactions of the a- and b-molecules with the substrate surface. In addition, equation (4.32) involves the chemical potential

$$\mu_a = F'(X_a) = \partial F(X_a)/\partial X_a \tag{4.34}$$

of the a-molecules as a function of the mole fraction X_a of these molecules within a large membrane segment.

The generic functional forms of the chemical potentials $\mu_a^{\rm ub} = F'(X_a^{\rm ub})$ and $\mu_a^{\rm ad} = F'(X_a^{\rm ad}) + \Delta U$ are depicted in Fig. 4.2 for positive affinity contrast $\Delta U > 0$ and two different temperatures. The two mole fractions $X_a^{\rm ub}$ and $X_a^{\rm ad}$ in the unbound and in the adhering membrane segments are obtained from the intersections of the chemical potentials $\mu = \mu_a^{\rm ub}(X_a^{\rm ub})$ and $\mu = \mu_a^{\rm ad}(X_a^{\rm ad})$ with the horizontal line $\mu = \mu_a^{\rm eq}$ as indicated by the two examples in Fig. 4.2. Inspection of this figure reveals that the inequality $X_a^{\rm ad} < X_a^{\rm ub}$ is valid both for $T > T_c$ and for $T < T_c$. This fact implies that the a-molecules are depleted from the adhering membrane segment and enriched in the unbound segment for all temperatures. As we discussed in final paragraph of the section

4.1, for the cholesterol/phospholipid mixture, the phospholipid (b-molecule) is enriched in the adhering membrane segment, whereas cholesterol is depleted in the same membrane segment.

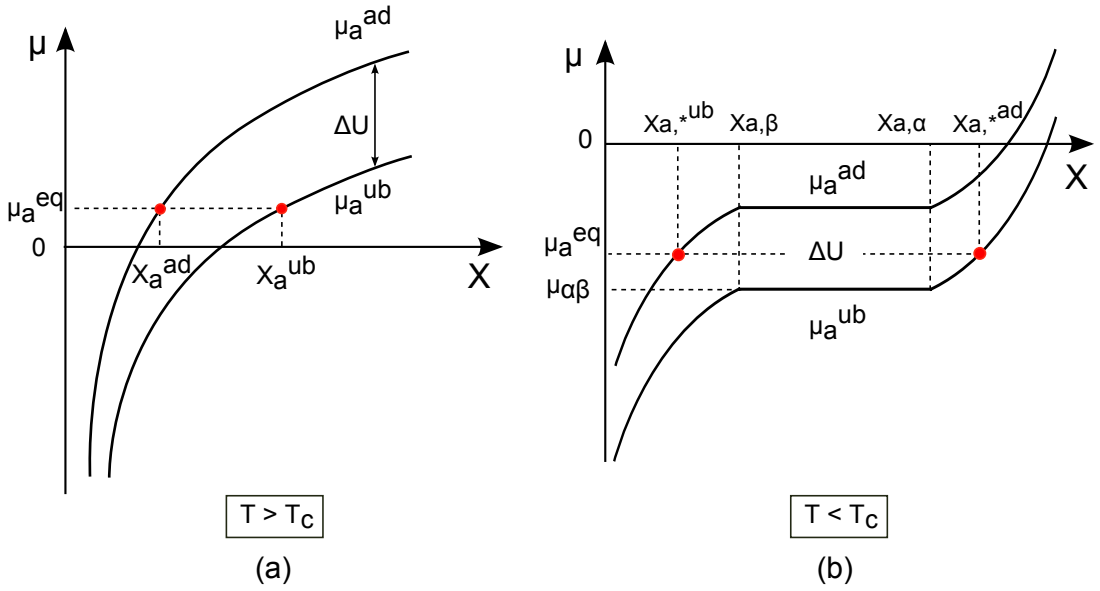

Figure 4.2 : *Chemical potentials μ versus area fractions X of the a-molecules for affinity contrast $\Delta U > 0$: (Bottom) Chemical potential $\mu = \mu_a^{\rm ub}$ of the unbound membrane segment as function of $X = X_a^{\rm ub}$; (Top) Chemical potential $\mu = \mu_a^{\rm ad} = \mu_a^{\rm ub} + \Delta U$ of the adhering membrane segment as function of $X = X_a^{\rm ad}$. The functional forms in (a) and (b) correspond to $T > T_c$ and $T < T_c$, respectively, compare Fig. 4.1. The intersection points (red) of these chemical potentials with the horizontal broken lines corresponding to the equilibrium values $\mu = \mu_a^{\rm eq}$ determine the mole fractions $X_a^{\rm ub}$ and $X_a^{\rm ad}$ in chemical equilibrium. For the example in (a), the equilibrium chemical potential $\mu_a^{\rm eq}$ is taken to be positive; for the one in (b), it is chosen to lie within the range $\mu_{\alpha,\beta} < \mu_a^{\rm eq} < \mu_{\alpha,\beta} + \Delta U$. In the latter example, the unbound segment is in the α phase, whereas the adhering segment is in the β phase. The unbound and the adhering segments undergo phase separation into α and β domains for $\mu_a^{\rm eq} = \mu_{\alpha,\beta}$ and $\mu_a^{\rm eq} = \mu_{\alpha,\beta} + \Delta U$, respectively. The two coexisting phases are characterized by mole fractions $X_{a,\alpha}$ and $X_{a,\beta}$.*

Another consequence of the graphical solution described in Fig. 4.2 is that both $X_a^{\rm ad}$ and $X_a^{\rm ub}$ increase with increasing chemical potential $\mu_a^{\rm eq}$. From the relation (4.33) one

can conclude that the overall mole fraction X_a also increases with increasing $\mu_a^{\rm eq}$, as expected. In this way, we obtain a unique decomposition of the overall fraction X_a into the two fractions $X_a^{\rm ad}$ and $X_a^{\rm ub}$. Later within the lattice model we will see that increasing chemical potential also adds to values of the two component's concentrations as well.

In Fig. 4.2, different values of the equilibrium chemical potential $\mu_a^{\rm eq}$ define different horizontal lines. Thus, the composition trajectory starts with a horizontal line being located at the bottom of Fig. 4.2, and this line moves upwards with increasing overall area fraction X_a. One can obtain the phase behavior in the two membrane segments from the corresponding evolution of the two intersection points in Fig. 4.2. The two intersection points are located at small values of $X_a^{\rm ub}$ and $X_a^{\rm ad}$ for the limit of large negative $\mu_a^{\rm eq}$. As we moves the horizontal line $\mu_a = \mu_a^{\rm eq}$ upwards, these intersection points evolve smoothly towards larger values of $X_a^{\rm ub}$ and $X_a^{\rm ad}$.

At the range of temperature above the critical value $T > T_c$ as shown in Fig. 4.2(a), such a smooth evolution is found for all values of $\mu_a^{\rm eq}$. Thus, for $T > T_c$, the area fractions $X_a^{\rm ub}$ and $X_a^{\rm ad}$ increase smoothly with increasing $\mu_a^{\rm eq}$. This monotonic increasing area fraction functions imply that both the unbound and the adhering membrane segment remain in the one-phase region but differ in their compositions. We can determine the corresponding overall fraction X_a via relation (4.33) for each solution $X_a^{\rm ad}$ and $X_a^{\rm ub}$ with

$$\mu_a^{\rm ad}(X_a^{\rm ad}) = \mu_a^{\rm ub}(X_a^{\rm ub}). \tag{4.35}$$

For $T < T_c$ as shown in Fig. 4.2(b), on the other hand, the smooth evolution of the mole fractions $X_a^{\rm ub}$ and $X_a^{\rm ad}$ is interrupted as soon as the fraction $X_a^{\rm ub}$ reaches the value $X_{a,\beta}$. When the overall area fraction X_a is further increased, the unbound membrane segment undergoes phase separation and its area fraction $X_a^{\rm ub}$ evolves from $X_{a,\beta}$ to $X_{a,\alpha}$. At the same point, the area fraction $X_a^{\rm ad}$ of the adhering segment attains a constant value within the β phase, which we denote by $X_{a,*}^{\rm ad}$, see Fig. 4.3(a). Therefore the composition of the adhering membrane segment is fixed along the transition line of the unbound membrane and described by

$$X_a^{\rm ad} = X_{a,*}^{\rm ad} < X_{a,\beta} \quad \text{for} \quad X_{a,\beta} \le X_a^{\rm ub} \le X_{a,\alpha}\,. \tag{4.36}$$

In this composition range, the adhering membrane segment plays the role of a spectator phase for the phase separation within the unbound segment.

The two membrane segments change their role when the equilibrium chemical potential increases more and reaches the value $\mu_a^{\rm eq} = \mu_{\alpha\beta} + \Delta U$. In this case, the adhering membrane segment undergoes phase separation and its area fraction $X_a^{\rm ad}$ evolves from $X_{a,\beta}$ to $X_{a,\alpha}$. Similarly, the area fraction $X_a^{\rm ub}$ of the unbound segment attains a constant value within the α phase, which we denote by $X_{a,*}^{\rm ub}$, see Fig. 4.3(a). In this case the

composition of the unbound membrane segment is fixed and described by

$$X_a^{\rm ub} = X_{a,*}^{\rm ub} > X_{a,\alpha} \quad \text{for} \quad X_{a,\beta} \leq X_a^{\rm ad} \leq X_{a,\alpha}\,. \tag{4.37}$$

Now, the unbound membrane segment plays the role of a spectator phase for the phase separation within the adhering segment.

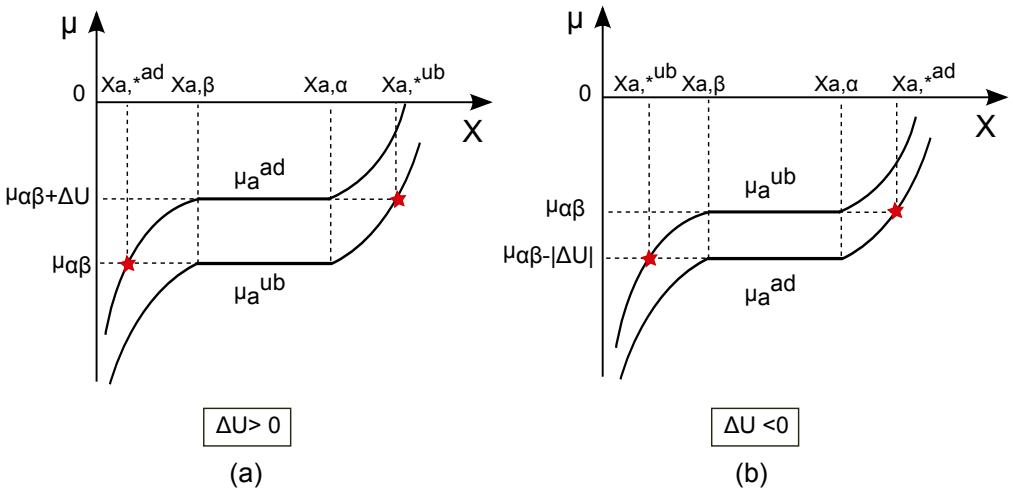

Figure 4.3 : *Spectator phases (red stars) for temperature $T < T_c$: (a) Affinity contrast $\Delta U > 0$ as in Fig. 4.2(b) corresponding to a depletion of a-molecules within the contact area. For $\mu = \mu_{\alpha,\beta}$, the unbound membrane segment undergoes phase separation whereas the adhering segment plays the role of a spectator phase with constant composition described by $X = X_{a,*}^{\rm ad} < X_{a,\beta}$. In contrast, for $\mu = \mu_{\alpha,\beta} + \Delta U$, the adhering membrane segment undergoes phase separation whereas the unbound segment plays the role of a spectator phase with constant composition described by $X = X_{a,*}^{\rm ub} > X_{a,\alpha}$; and (b) Affinity contrast $\Delta U < 0$ corresponding to an enrichment of a-molecules within the contact area. Now, the adhering membrane segment undergoes phase separation for $\mu = \mu_{\alpha,\beta} - |\Delta U|$ while the phase separation of the unbound segment still occurs at $\mu = \mu_{\alpha,\beta}$.*

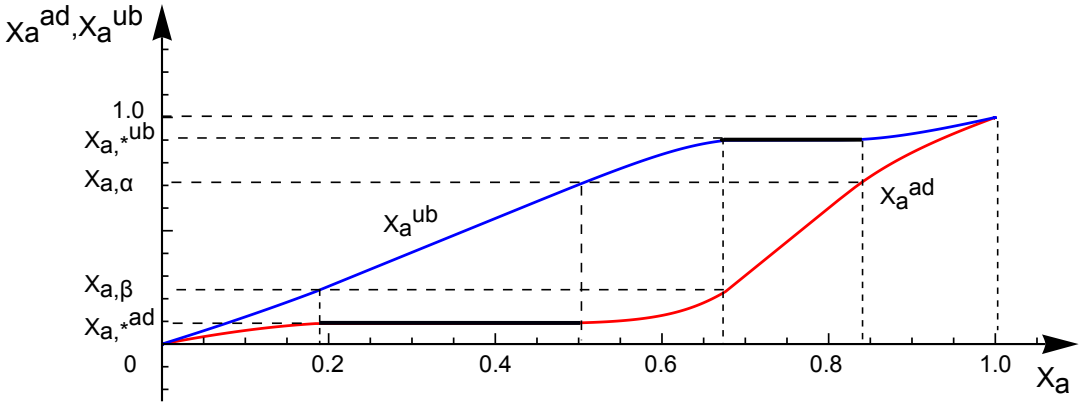

Figure 4.4 : *Mole fractions* $X_a^{\rm ub}$ *and* $X_a^{\rm ad}$ *within the unbound and adhering membrane segments as functions of the overall fraction* X_a *of the a-molecules. In this example, the adhering vesicle has the shape of a half sphere with area ratio* $q = \frac{2}{3}$ *and the constant composition variables* $X_{a,*}^{\rm ad} = \frac{4}{5}X_{a,\beta}$ *and* $X_{a,*}^{\rm ub} = \frac{5}{4}X_{a,\alpha}$.

4.4 Phase diagram for vanishing affinity contrast

When the affinity contrast is equal to zero, $\Delta U = 0$ the membrane is considered untouched by the substrate surface. In this case intermolecular interactions between the membrane components remain unchanged in both membrane segments. Thus the mole fractions $X_a^{\rm un}$ and $X_a^{\rm ad}$ are equal to

$$X_a^{\rm un} = X_a^{\rm ad} = X \quad \text{for} \quad \Delta U = 0\,, \tag{4.38}$$

which $X_a^{\rm un} = X_a^{\rm ad}$ is solution of the two equations (4.32) and (4.33).

Therefore, for zero affinity contrast the phase behavior of the adhering membrane is identical to the free vesicle membrane which is described by the two binodal lines $X_a = X_{a,\beta}(T)$ and $X_a = X_{a,\alpha}(T)$ in relation (2.3). The phase diagram of a freely suspended membrane consists of cholesterol and a single phospholipid is shown in Fig. 2.2. This phase diagram also fits the adhering vesicle provided $\Delta U = 0$ and independent of the overall area fraction q. In contrast, small nonzero values of affinity contrast strongly affect the phase behavior as will be shown in the next section.

4.5 Phase diagrams for non-vanishing affinity contrast

The phase diagram of an adhering vesicle membrane is much different to non adhering vesicle since the non zero value of ΔU duplicate the two-phase coexistence region in phase diagram in Fig. 2.2. Therefore, when $\Delta U \neq 0$ the adhering membrane undergoes phase separation in two segments; one in the adhering membrane segment and another one in the unbound segment. One has to notice that the negative or positive affinity contrast have strong effect on the relative locations of these two coexistence regions.

The phase diagram of non vanishing affinity contrast $\Delta U \neq 0$, depends on four parameters , temperature T, mole fraction X_a of the a-molecules which is a representative for membrane composition, overall area fraction q, and finally affinity contrast ΔU. Thus, this diagram can be illustrated in the four-dimensional parameter space. To visualize the binodals hyper-surfaces we consider two-dimensional slices through this four-dimensional space. For example, (X, T)-slices for constant q and ΔU is convenient selection and also comparable to the (X, T)- plane as obtained in the absence of the adhesive substrate surface.

According to the Sec. 4.3, phase separation in unbound membrane segment occurs when the mole fraction $X_a^{\rm un}$ in in the range $X_{a,\beta} \leq X_a^{\rm un} \leq X_{a,\alpha}$. As shown in Fig. 4.2(b) in this interval the unbound chemical potential remains unchanged and equal to $\mu_{\alpha\beta}$. The mole fraction in the adhering membrane segment attains the value $X_{a,*}^{\rm ad}$ which can be determined by chemical potential $\mu_a^{\rm ad} = \mu_{\alpha\beta}$. The adhering membrane attains uniform composition at the coexistence region of the unbound segment and plays the role of a spectator phase, see Fig.4.2. Combining the coexisting interval of the unbound membrane and the corresponding value of the adhering segment,

$$X_{a,\beta}(T) \leq X_a^{\rm un} \leq X_{a,\alpha}(T) \quad \text{and} \quad X_a^{\rm ad} = X_{a,*}^{\rm ad}(T, \Delta U) \tag{4.39}$$

with the repartitioning relation (4.33) leads to

$$X_{a,\beta}^{\rm un}(T, q, \Delta U) \leq X_a \leq X_{a,\alpha}^{\rm un}(T, q, \Delta U) \tag{4.40}$$

where the two binodals are:

$$X_{a,\beta}^{\rm un}(T, q, \Delta U) \equiv q\, X_{a,\beta}(T) + (1-q)\, X_{a,*}^{\rm ad}(T, \Delta U) \tag{4.41}$$

and

$$X_{a,\alpha}^{\rm un}(T, q, \Delta U) \equiv q\, X_{a,\alpha}(T) + (1-q)\, X_{a,*}^{\rm ad}(T, \Delta U)\,. \tag{4.42}$$

The derivation of two relations (4.41) and (4.42) show that these binodals have q-functionality which is coming from the repartitioning (4.33) whereas their ΔU-dependency is determined by chemical equilibrium condition (4.32).

When the unbound membrane segment is in the coexistence region, the corresponding

chemical potential $\mu_a^{\rm un}$ stays constant denoted by $\mu_{\alpha\beta}$, see Fig. 4.2. At the same value of chemical potential, the adhering membrane segment is the spectator phase with mole fraction $X_a^{\rm ad} = X_{a,*}^{\rm ad}$ which fits the equilibrium condition (4.32).

Similar to unbound membrane the adhering membrane segment undergoes phase separation when $X_a^{\rm ad}$ satisfies the condition $X_{a,\beta} \leq X_a^{\rm ad} \leq X_{a,\alpha}$. In this case, the unbound mole fraction $X_{a,*}^{\rm un}$ remains constant and the unbound segment plays the role of a spectator phase. Combining the condition

$$X_{a,\beta}(T) \leq X_a^{\rm ad} \leq X_{a,\alpha}(T) \quad \text{and} \quad X_a^{\rm un} = X_{a,*}^{\rm un}(T, \Delta U) \tag{4.43}$$

and the repartitioning relation (4.33), the coexistence region for the adhering segment attains the form

$$X_{a,\beta}^{\rm ad}(T, q, \Delta U) \leq X_a \leq X_{a,\alpha}^{\rm ad}(T, q, \Delta U) \tag{4.44}$$

with the two binodals

$$X_{a,\beta}^{\rm ad}(T, q, \Delta U) \equiv q\, X_{a,*}^{\rm un}(T, \Delta U) + (1-q)\, X_{a,\beta}(T) \tag{4.45}$$

and

$$X_{a,\alpha}^{\rm ad}(T, q, \Delta U) \equiv q\, X_{a,*}^{\rm un}(T, \Delta U) + (1-q)\, X_{a,\alpha}(T)\,. \tag{4.46}$$

Likewise, at phase separation of the adhering membrane segment the corresponding chemical potential $\mu_a^{\rm ad}$ has the the constant value $\mu_{\alpha\beta} + \Delta U$, see Fig. 4.2. The mole fraction $X_a^{\rm un} = X_{a,*}^{\rm un}$ of the spectator phase within the unbound membrane segment satisfies the chemical equilibrium condition (4.32).

Parameter dependence of binodals

To build the adhering membrane phase diagram it is necessary to know that on which parameters the binodals for the unbound segment as in (4.41) and (4.42) as well as those for adhering membrane segment in (4.45) and (4.46) depend on. These binodals are function of (i) the binodals $X_{a,\beta}(T)$ and $X_{a,\alpha}(T)$ for non adhering membranes, (ii) the overall area fraction q, and (iii) the mole fractions $X_{a,*}^{\rm ad}(T, \Delta U)$ and $X_{a,*}^{\rm un}(T, \Delta U)$ of the adhering and unbound spectator phases. We can determine the binodals $X_{a,\beta}(T)$ and $X_{a,\alpha}(T)$ using the experimental phase diagram as in Fig. 2.2 by mathematical fitting and interpolation technics. Also the overall area fraction $q = \mathcal{A}^{\rm un}/\mathcal{A}$ for a giant vesicle can be easily obtained by optical microscopy. Thus, we need to specify the adhering and unbound spectator phases ($X_{a,*}^{\rm ad}(T, \Delta U)$ and $X_{a,*}^{\rm un}(T, \Delta U)$) to reach the phase boundaries for adhering vesicle.

4.6 phase diagrams for small positive and small negative affinity contrasts

We have shown that the graphical solution of chemical potential equilibrium condition (4.32) leads to obtain the mole fractions $X^{\mathrm{ad}}_{a,*}(T,\Delta U)$ and $X^{\mathrm{un}}_{a,*}(T,\Delta U)$ of the two spectator phases. The chemical potential corresponds to coexistence region of membrane segment is equal to $\mu_{\alpha\beta}$. from the same graphical solution one can conclude that the mole fractions $X^{\mathrm{ad}}_{a,*}(T,\Delta U)$ and $X^{\mathrm{un}}_{a,*}(T,\Delta U)$ exhibit a discontinuity at $\Delta U = 0$. Now we are able to determine the phase diagram of an adhering membrane. In following sections, we separate the two case of small positive and negative affinity contrast and obtain the adhering membrane phase diagram for each case.

4.6.1 Small positive affinity contrasts

As mentioned before, even a small adhesion energy has an strong effect on the phase diagram and cause duplication and shift in free membrane phase diagram. To avoid unrelevant solution, we focus on relatively small adhesion energy and chose small value for ΔU. If one expands the relative chemical potential in powers of $X - X_{a,\beta}$ for two membrane segments and inserting the results into (4.31) and (4.32), then the spectator phases mole fractions obtain as

$$X^{\mathrm{ad}}_{a,*} \approx X_{a,\beta} - \frac{\Delta U}{(\partial \Delta\mu^{\mathrm{ad}}_a / \partial X^{\mathrm{ad}}_a)_{X_{a,\beta}}} \tag{4.47}$$

and

$$X^{\mathrm{un}}_{a,*} \approx X_{a,\alpha} + \frac{\Delta U}{(\partial \Delta\mu^{\mathrm{un}}_a / \partial X^{\mathrm{un}}_a)_{X_{a,\alpha}}} \tag{4.48}$$

up to first order in ΔU.

In the expressions (4.47) and (4.48) the mole fractions $X^{\mathrm{ad}}_{a,*}$ and $X^{\mathrm{un}}_{a,*}$ depend on temperature via $X_a = X_{a,\beta}(T)$ and $X_{a,\alpha} = X_{a,\alpha}(T)$ as well as partial derivatives $\partial\Delta\mu_a/\partial X_a$.

One can bring the latter derivatives into a more explicit form by using the Gibbs-Duhem relation

$$X_a \frac{\partial \mu_a}{\partial X_a} + X_b \frac{\partial \mu_b}{\partial X_a} = 0 \tag{4.49}$$

In order to fit the above relation to cholesterol/phospholipid binary mixture we replace $X_b = 1 - X_a$, therefore the partial derivatives $\partial\Delta\mu_a/\partial X_a$ term in (4.47) and (4.48) obtain as following

$$\frac{\partial \Delta\mu_a}{\partial X_a} = \frac{\partial \mu_a}{\partial X_a}\left(1 + \frac{A_a}{A_b}\frac{X_a}{1 - X_a}\right) \tag{4.50}$$

which can be reduced to the simpler form

$$\frac{\partial \Delta\mu_a}{\partial X_a} = \frac{1}{1-X_a}\,\frac{\partial \mu_a}{\partial X_a} \quad \text{for} \quad A_a = A_b\,. \tag{4.51}$$

As shown in Fig. 2.2 the liquid-liquid coexistence regions for phospholipid/cholesterol binary mixtures occurs at mole fractions $X_a \lesssim 0.25$, Thus from ideal solution theory it is possible to estimate the quantity $\partial\mu_a/\partial X_a$ at $X_a = X_{a,\beta}$ and $X = X_{a,\alpha}$, the relation

$$\mu_a \simeq \mu_a^o + k_B T \ln(X_a)\,, \tag{4.52}$$

leads to

$$\left(\frac{\partial \mu_a}{\partial X a}\right)_{X_{a,\beta}} \simeq \frac{k_B T}{X_{a,\beta}} \quad \text{and} \quad \left(\frac{\partial \mu_a}{\partial X_a}\right)_{X_{a,\alpha}} \simeq \frac{k_B T}{X_{a,\alpha}}\,. \tag{4.53}$$

To make the calculations simpler we define the dimensionless affinity contrast as follow

$$\Delta u \equiv \Delta U/(k_B T) \tag{4.54}$$

which has similar sign as ΔU. Combining the approximate expressions in (4.53) with relation (4.51) the relations (4.47) and (4.48) for mole fractions of the spectator phases change into the new form

$$X_{a,*}^{\rm ad} \;\approx\; X_{a,\beta} - X_{a,\beta}(1-X_{a,\beta})\,\Delta u \quad \text{for small } \Delta u > 0 \tag{4.55}$$

and

$$X_{a,*}^{\rm un} \;\approx\; X_{a,\alpha} + X_{a,\alpha}(1-X_{a,\alpha})\,\Delta u \quad \text{for small } \Delta u > 0 \tag{4.56}$$

Binodals for positive affinity contrast

Positive affinity contrast $\Delta U > 0$ for the binary mixture of cholesterol/ phospholipid is defined the condition in which the substrate surface strongly attract the b-molecules (phospholipids) and thus the a-molecules (cholesterol) are depleted from the contact area. To get the coexistence region of the unbound segment we insert the expression in (4.55) for the mole fraction into the binodals (4.41) and (4.42), then we have

$$X_{a,\beta}^{\rm un} \approx X_{a,\beta} - (1-q)\,X_{a,\beta}(1-X_{a,\beta})\,\Delta u \quad (\Delta u > 0) \tag{4.57}$$

and

$$X_{a,\alpha}^{\rm un} \approx X_{a,\beta} + q(X_{a,\alpha} - X_{a,\beta}) - (1-q)\,X_{a,\beta}(1-X_{a,\beta})\,\Delta u. \quad (\Delta u > 0) \tag{4.58}$$

As we mentioned before, since $X_{a,\beta}(T)$ and $X_{a,\alpha}(T)$ for free membrane are function of temperature, therefore the T-dependence of the $X^{\rm un}_{a,\beta}$ and $X^{\rm un}_{a,\alpha}$ is provided, see Fig. 2.2.

To reach the coexistence regions of the adhering membrane segment we combine the relation (4.56) with the binodals reached in (4.45) and (4.46) which leads to (4.45) and (4.46) which leads to

$$X^{\rm ad}_{a,\beta} \approx X_{a,\beta} + q(X_{a,\alpha} - X_{a,\beta}) + qX_{a,\alpha}(1 - X_{a,\alpha})\,\Delta u \quad (\Delta u > 0) \tag{4.59}$$

and

$$X^{\rm ad}_{a,\alpha} \approx X_{a,\alpha} + qX_{a,\alpha}(1 - X_{a,\alpha})\,\Delta u\,. \quad (\Delta u > 0) \tag{4.60}$$

In Fig. 4.5 the coexistence regions for unbound and adhering segment of a vesicle in adhesion is depicted as blue and red area, respectively. This phase diagram is reached for overall area fraction $q = 2/3$and for different value of $\Delta u = 0^+, 0.1, 0.2$, and 0.4. For $\Delta U > 0$ when we increase the mole fraction X_a starting from $X_a = 0$ first we hit the coexistence region for unbound membrane because the a-molecules (cholesterol) prefer to enrich in unbound membrane segment. By increasing the mole fraction X_a more, we hit the coexisting area for adhering membrane segment which is shown in red. This implies that adding more a-molecules to the system after unbound membrane segment full, brings the adhering segment into two phase coexistence area, see Fig. 4.6.

Physical range of cholesterol mole fraction.

From experiments we know that for binary phospholipid/cholesterol mixtures, the bilayer membrane forms at the cholesterol mole fraction $X_a \lesssim 0.5$. For adhering membrane with positive affinity contrast $\Delta U > 0$ the largest mole fraction is is provided by $X^{\rm un}_{a,*}$ of the unbound membrane segment. Thus the spectator phase fits the constrain imposed by the bilayer formation

$$X^{\rm un}_{a,*} \approx X_{a,\alpha} + X_{a,\alpha}(1 - X_{a,\alpha})\,\Delta U/(k_BT) \lesssim 0.5\,. \tag{4.61}$$

Refer to the experimental phase diagram of a free vesicle in Fig. 2.2 the mole fraction $X_{a,\alpha}$ has the maximum value about 0.25. Using the bilayer constraint (4.61) the relative affinity contrast can be deduced as

$$\Delta U/(k_BT) < 1\,. \tag{4.62}$$

In the phase diagrams for positive affinity contrast in Fig. 4.5 as well as negative contrast in Fig. 4.7 we have applied relatively small values of ΔU.

It is interesting to compare the pattern formation in the free and adhering vesicle membrane for the same value of mole fraction. In Fig. 4.5(c) there are four stars each of which represents a composition of adhering or free vesicle. The corresponding domain

pattern to each star is represented in one row in Fig. 4.6. The first star with the very low mole fraction X_a is in the coexistence region of unbound membrane in an adhering membrane while it is in β phase of free vesicle, see Fig. 4.6(a) and (b). By increasing the mole fraction the star moves into the two coexistence region of the free vesicle as well as unbound segment of adhering membrane, as in Fig. 4.6(c) and (d). The third star from the left side in Fig. 4.5(c) is in the two phase coexistence of free vesicle while with the same mole fraction the adhering membrane exhibit no domains in the adhering and unbound segments, ass seen in Fig. 4.6(e) and (f). Finally for sufficiently large value of mole fraction, the adhering segment of adhering membrane undergoes phase separation but the free vesicle is in the α-phase, as depicted in Fig. 4.6(g) and (h).

4.6.2 Symmetry relations

As it shown in Fig. 4.2, the symmetry between the two condition on positive and negative affinity contrast let us derive corresponding symmetry between the adhering and unbound mole fractions. When the affinity contrast is negative $\Delta U < 0$ see Fig. 4.2(b), the bound chemical potential $\mu_a^{\rm ad}$ is located below the curve $\mu_a^{\rm un}$. Therefore the mole fractions $X_{a,*}^{\rm ad}$ and $X_{a,*}^{\rm un}$ fit the symmetric relation

$$X_{a,*}^{\rm ad}(T,-\Delta U) = X_{a,*}^{\rm un}(T,\Delta U)\,, \tag{4.63}$$

or the equivalent relation

$$X_{*}^{\rm un}(T,-\Delta U) = X_{*}^{\rm ad}(T,\Delta U)\,, \tag{4.64}$$

for all values of T and ΔU. The relations above are independent of the function $G(X)$.

Also from the two binodals of the unbound membrane segment, see (4.41) and (4.42) and adhering membrane segment in (4.45) and (4.46) one can conclude the relation between $X_{a,\beta}$ and $X_{a,\alpha}$ for bound and unbound segments in different sing of affinity contrast:

$$X_{a,\beta}^{\rm ad}(T,q,-\Delta U) = X_{a,\beta}^{\rm un}(T,1-q,\Delta U) \tag{4.65}$$

and by

$$X_{a,\alpha}^{\rm ad}(T,q,-\Delta U) = X_{a,\alpha}^{\rm un}(T,1-q,\Delta U)\,. \tag{4.66}$$

Thus, by knowing the binodals for positive values of ΔU, we have those for negative values of ΔU only by replacing q by $1-q$.

Small negative affinity contrasts

The symmetry between membrane segments mole fraction in positive and negative affinity contrast let us to derive the spectator phases mole fractions for negative affinity. By combining the (4.63) and (4.56) one can reach the spectator mole fractions in adhering membrane segment

$$X_{a,*}^{\rm ad} \approx X_{a,\alpha} + X_{a,\alpha}(1-X_{a,\alpha})\,|\Delta U|/(k_BT) \quad (\Delta U<0) \tag{4.67}$$

as well as unbound membrane

$$X_{a,*}^{\rm un} \approx X_{a,\beta} - X_{a,\beta}(1-X_{a,\beta})\,|\Delta U|/(k_BT) \quad (\Delta U<0) \tag{4.68}$$

by using relations (4.65) and (4.55) up to first order in ΔU.

Binodals for negative affinity contrast

Similar to positive affinity contrast, we can obtain the phase diagram for negative affinity contrast $\Delta U < 0$ by determining the binodals of the two membrane segments.

Using the symmetry relations (4.65) and (4.66) the coexistence region for the adhering membrane segment is described as

$$X_{a,\beta}^{\mathrm{ad}} \approx X_{a,\beta} - qX_{a,\beta}(1 - X_{a,\beta})\,|\Delta u| \quad (\Delta u < 0) \tag{4.69}$$

and

$$X_{a,\alpha}^{\mathrm{ad}} \approx X_{a,\alpha} - q(X_{a,\alpha} - X_{a,\beta}) - qX_{a,\beta}(1 - X_{a,\beta})\,|\Delta u| \quad (\Delta u < 0) \tag{4.70}$$

Similarly the two binodals for the unbound membrane segment coexistence region is located in

$$X_{a,\beta}^{\mathrm{un}} \approx X_{a,\alpha} - q(X_{a,\alpha} - X_{a,\beta}) + (1 - q)X_{a,\alpha}(1 - X_{a,\alpha})\,|\Delta u| \quad (\Delta u < 0) \tag{4.71}$$

and

$$X_{a,\alpha}^{\mathrm{un}} \approx X_{a,\alpha} + (1 - q)X_{a,\alpha}(1 - X_{a,\alpha})\,|\Delta u| \quad (\Delta u < 0)\,. \tag{4.72}$$

Similar to the Fig. 4.5 the phase diagram for different values of negative affinity contrast $\Delta u < 0$ is shown in Fig. 4.7. The first diagram belong to the free vesicle in Fig. 2.2 and the overall area fraction in these diagrams are chosen equal to $q = 2/3$. In the case of negative affinity contrast the substrate surface attracts the a-molecules more strongly and thus the a-molecules enriched in the adhering membrane segments. When we increase the mole fraction X_a from $X_a = 0$ first we enter the coexistence region for the adhering segment which has the red color code and then the unbound membrane which is shown in blue.

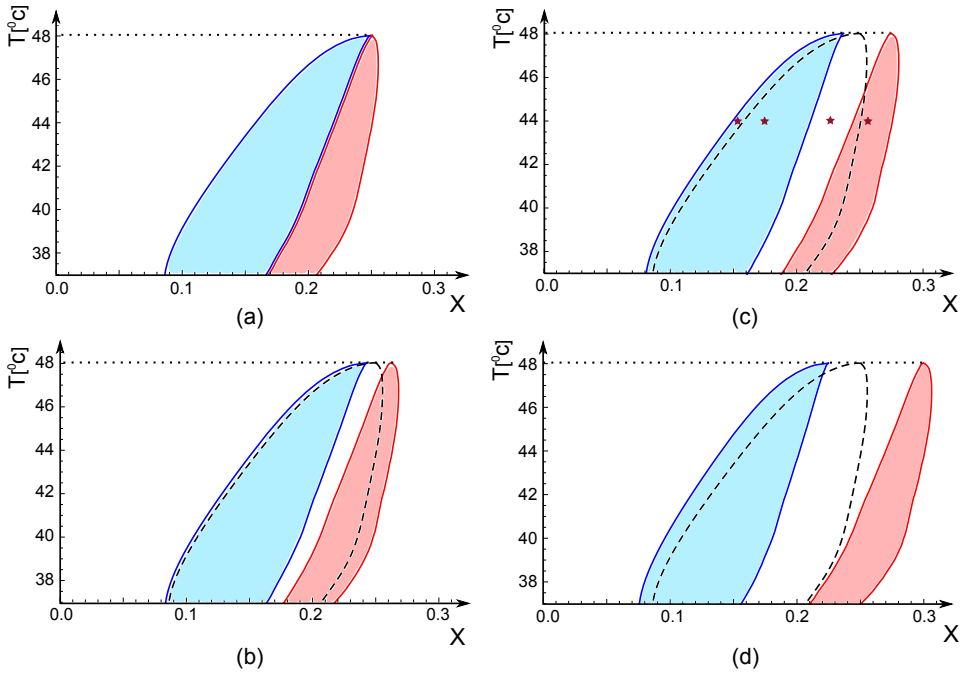

Figure 4.5 : *Phase diagram of a multi-component membrane in the presence of adhesive substrate with* $\Delta u = \Delta U/(k_B T) > 0$. *The corresponding phase diagram for free membrane is shown in Fig. 2.2. In this figure, the phase diagram for different value of affinity contrast is depicted, (a)* $\Delta u = 0^+$, *(b)* $\Delta u = 0.05$, *(c)* $\Delta u = 0.1$, *and (d)* $\Delta u = 0.2$. *The color code are as follow, blue and red region correspond to the two-phase coexistence of unbound membrane and adhering membrane segments, respectively. Also one can compare the free vesicle coexistence region which is show by broken line to the adhering membrane. Similar to the free vesicle, the critical temperature of the both segments are located at the* T_c. *The four domain patterns shown in Fig. 4.6 correspond to the four starred compositions in (c). Also in these four diagram the overall area fraction of the membrane vesicle is equal to* $q = 2/3$.

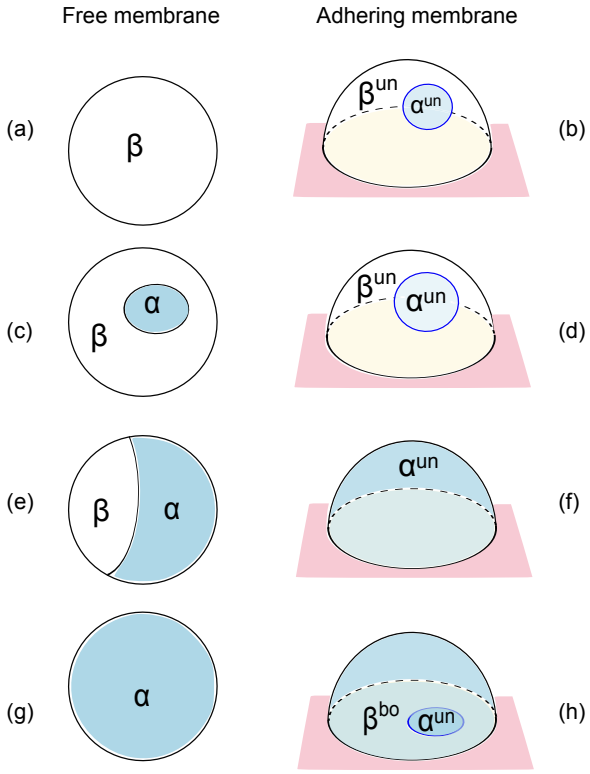

Figure 4.6 : *Free vesicles (left column) bounded by a multi-component membrane change their domain pattern when they adhere to a substrate surface (right column). The liquid-ordered and liquid-disordered phases are denoted by α and β. Each row corresponds to a different membrane composition which is shown by one star in Fig. 4.5(c) . This mole fraction increases monotonically from the top to the bottom row: (a,b) For relatively small values of X_a, the membrane of the free vesicle has uniform composition as in (a). When such a vesicle adheres to the substrate surface as in (b), the unbound membrane segment may phase separate into an $\alpha^{\rm un}$ and a $\beta^{\rm un}$ domain whereas the adhering segment has uniform composition; (c,d) For somewhat larger values of X_a, the free vesicle membrane in (c) undergoes phase separation and forms a relatively small α domain. After adhesion, see (d), only the unbound membrane segment undergoes phase separation; (e,f) As the mole fraction X_a is further increased, the membrane of the free vesicle in (e) forms an α and β domain of comparable size whereas the membrane of the adhering vesicle in (f) exhibits no phase separation at all; and (g,h) For relatively large values of X_a, the adhering membrane segment undergoes phase separation into an $\alpha^{\rm ad}$ and $\beta^{\rm ad}$ domain whereas the unbound segment has uniform composition. The situation depicted here corresponds to surface interactions that attract the a-molecules less strongly than the b-molecules, $\Delta U > 0$.*

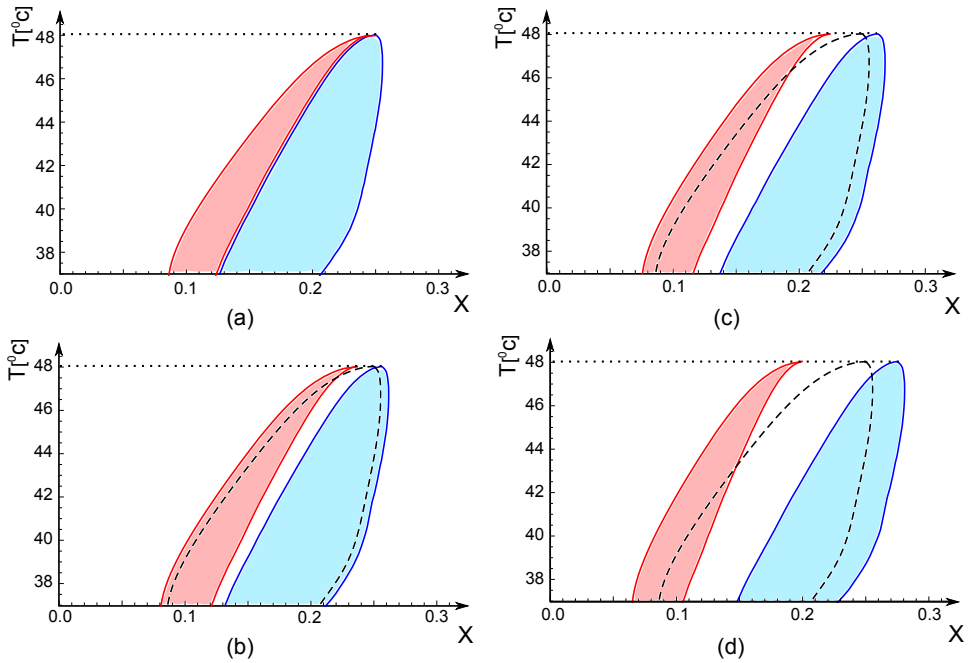

Figure 4.7 : *Phase diagram for adhering membrane in the presence of adhesive substrate surface which hes negative affinity contrast*$\Delta u = \Delta U/(k_B T) < 0$. *This phase diagram is similar to the free membrane vesicle as shown in Fig. 2.2 but with non zero affinity contrast. In this figure, the adhering membrane phase diagram for different values of affinity (a)* $\Delta u = 0^-$, *(b)* $\Delta u = -0.05$, *(c)* $\Delta u = -0.1$, *and (d)* $\Delta u = -0.2$. *The color code is similar to Fig. 4.5, red and blue represent the two phase coexistence of the adhering and unbound segments. For the same amount of negative and positive affinity contrast the coexistence regions of the adhering and unbound membrane do not change their locations similarly. The overall area fraction has the constant value* $q = 2/3$ *and also the phase diagram on a free vesicle is shown in broken line for comparison.*

5 Phase behaviour within lattice model

5.1 Mixture described by lattice model

Lattice model is an applicable model to describe order–disorder phenomena in binary mixtures with neglecting the possibility of vacancies. Thus one can discretize a flat membrane with the a and b components into a square lattice. In this model, the lattice square size is in the order of the $a - b$ component's size. Each lattice site has two occupation numbers, n_i^a and n_i^b, which both take the values 0 or 1. However, in the absence of vacancies, each site must be occupied either with an a or with a b particle and not both. This implies that

$$n_i^a + n_i^b = 1 \ . \tag{5.1}$$

Therefore, one can define occupation numbers n_i via

$$n_i \equiv n_i^a \qquad \text{and} \quad 1 - n_i = n_i^b \ . \tag{5.2}$$

Because the squares are similar in the lattice model, the molecular area of the component a is equal to the molecular area of component b

$$A_a = A_b. \tag{5.3}$$

If two sites i and j both contain the component a, the interaction between the two neighboring sites is defined as a pair-potential U_{ij}^{aa}. Likewise, one can define the pair-potentials U_{ij}^{bb} and U_{ij}^{ab}. Considering the arguments in Sec. 4.1 the chemical potential of the component a and b are related by Eq. (4.16) and (4.28). Using the relation between the molecular area of the two component, one can conclude

$$\mu_a = -\mu_b \tag{5.4}$$

In this model, the total number of component are fixed but the system can have various compositions. This condition is in agreement with the semi-grand canonical ensemble.

We start from standard grand canonical ensemble with variable concentration and try to reach the phase diagram in canonical ensemble with the fixed total number of particles and different composition. The Hamiltonian of this adhering two-component membrane

within the lattice model is

$$\mathcal{H}\{n\} = \sum_{<ij>}[U_{ij}^{aa}n_i n_j + U_{ij}^{ab}n_i(1-n_j) + U_{ij}^{ab}(1-n_i)n_j + U_{ij}^{bb}(1-n_i)(1-n_j)] + \sum_i (U_a^i - U_b^i - 2\mu_a)n_i. \quad (5.5)$$

The first sum in the above relation is over all pairs, which prevents double summation. μ^α is the chemical potential and U_i^α is the adhesion energy of the α components where $\alpha =$ a or b.
reordering the terms in configuration energy in (5.5), then the lattice model Hamiltonian is given by

$$\mathcal{H}\{n\} = \sum_{<ij>} W_{ij}n_i n_j + \sum_i (U_i - \mu)n_i. \quad (5.6)$$

In this case, the pair-potential between two particles in sites i and j, W_{ij} is defined as

$$W_{ij} = U_{ij}^{aa} - 2U_{ij}^{ab} + U_{ij}^{bb}, \quad (5.7)$$

note that in the absence of external field, the lattice gas model is independent of position;

$$\sum_j W_{ij} = 4W_0 \qquad \text{independent of } i. \quad (5.8)$$

The chemical potential, μ corresponds to

$$\mu = -2\mu_a - 2W_0 + 2\sum_j (U_{ij}^{aa} - U_{ij}^{bb}) \quad (5.9)$$

and the adhesion energy is given by

$$\begin{aligned} U^i &= U_a^i - U_b^i, \qquad \text{in adhering membrane, and} \\ U^i &= 0 \qquad\qquad\quad \text{in unbound membrane.} \end{aligned} \quad (5.10)$$

So far, a grand canonical ensemble has been used. In this ensemble, the components chemical potential, μ_a and μ_b are thermodynamic control parameters.

5.2 Mixture described by Ising spins

The lattice model is related to the Ising model if a spin variable $s_i = \pm 1$ is replaces for each lattice site. The configuration energy of the two-component membrane can be

expressed in the Ising model with a change of variables, $s_i = 2n_i - 1$:

$$n_i = \frac{1}{2}(1 + s_i) \qquad \text{and} \quad 1 - n_i = \frac{1}{2}(1 - s_i) \ . \tag{5.11}$$

producing the Hamiltonian equivalent to

$$\mathcal{H}\{s\} = -\sum_{<ij>} J_{ij} s_i s_j - \sum_i H s_i, \tag{5.12}$$

where spin interaction energy J_{ij} is given by

$$J_{ij} = -\frac{1}{4}(U_{ij}^{aa} - 2U_{ij}^{ab} + U_{ij}^{bb}). \tag{5.13}$$

H is a magnetic field which is decomposed to the fields in the unbound and adhering membrane segments H^{ub} and H^{ad}, where

$$H = H^{ub} + H^{ad}. \tag{5.14}$$

The magnetic field in the unbound membrane is,

$$H^{ub} = \mu_a + \sum_j (U_{ij}^{aa} - U_{ij}^{bb}), \tag{5.15}$$

and the field in the adhering segment has the form,

$$H^{ad} = H^{ub} + \Delta H^{ad}. \tag{5.16}$$

The excess field acting on spins in the adhering membrane ΔH^{ad} is given by

$$\Delta H^{ad} \equiv -\frac{1}{2}\Delta U, \tag{5.17}$$

where

$$\Delta U = U_a^i - U_b^i. \tag{5.18}$$

The additional magnetic field in the adhering membrane depends on the difference of the adhesion energy experienced by $a - b$ components.

5.3 Decomposition of membrane

Starting from the lattice model, one may consider different affinities of the components a and b to the wall. These differences are described by the external potentials U_a^i and

U_b^i for the a- and b-molecules within the adhering membrane segment. One can assume that component a has greater affinity to the substrate than component b.

$$U_a^i < U_b^i.$$

Since the adhesion energy does not depend on the position in the contact area,

$$\begin{aligned} U_a^i \equiv U^a \quad \text{and} \quad U_b^i \equiv U^b, \qquad & \text{in adhering membrane, and} \\ U_a^i \equiv 0 \qquad \text{and} \qquad U_b^i \equiv 0, \qquad & \text{in unbound membrane.} \end{aligned} \tag{5.19}$$

Since the membrane is composed of the unbound and adhering membrane segment, one can treat this membrane as a two lattice system in chemical potential equilibrium as seen in Fig. 5.13. The Hamiltonian of this membrane can be separated into adhering and unbound segments:

$$\mathcal{H}\{n\} = \mathcal{H}^{ub}\{n\} + \mathcal{H}^{ad}\{n\} \tag{5.20}$$

The configurational energy of the unbound segment is

$$\mathcal{H}^{ub}\{n\} = \sum_{<ij>} W_{ij} n_i n_j - \sum_i \mu_a n_i, \tag{5.21}$$

which corresponds to Hamiltonian of a simple lattice gas model. For the adhering segment, the configurational energy is equivalent to

$$\mathcal{H}^{ad}\{n\} = \sum_{<ij>} W_{ij} n_i n_j + \sum_i (-\mu_a + U) n_i, \tag{5.22}$$

where

$$U = U^a - U^b. \tag{5.23}$$

For the corresponding Ising system, the the configurational energy can be decomposed according to

$$\mathcal{H}\{s\} = \mathcal{H}^{ub}\{s\} + \mathcal{H}^{ad}\{s\} \tag{5.24}$$

where the configurational energy $\mathcal{H}^{ad}$ of the adhering membrane segment is given by

$$\mathcal{H}^{ad}\{s\} = -\sum_{<ij>} J_{ij} s_i s_j - \sum_i H^{ad} s_i, \tag{5.25}$$

and the configurational energy $\mathcal{H}^{ub}$ of the unbound segment has the form

$$\mathcal{H}^{ub}\{s\} = -\sum_{<ij>} J_{ij} s_i s_j - \sum_i H^{ub} s_i. \tag{5.26}$$

The configurational energy of the unbound membrane is similar to the usual 2-dimensional Ising model. The adhering Ising system is now decomposed to two Ising system: an unbound membrane segment with field $H = H^{ub}$ and an adhering membrane segment with field $H = H^{ad} = H^{ub} + \Delta H^{ad}$. One should note that for $U_a < U_b < 0$ the excess field ΔH^{ad} is positive.

Grand-canonical and canonical ensemble

So far, a grand-canonical ensemble has been used. In this ensemble, the chemical potential potentials μ_a and μ_b are taken to be thermodynamic control parameters. As a consequence, the "magnetic" field H, which depends on the difference $\mu_a - \mu_b$, represents an equivalent thermodynamic parameter.

In contrast, in the canonical ensemble, we do not prescribe the chemical potentials but rather the number $\mathcal{N}_a$ and $\mathcal{N}_b$ of a- and b-molecules. In the lattice representation used here, the two numbers are related by

$$\mathcal{N} = \mathcal{N}_b + \mathcal{N}_a, \tag{5.27}$$

and

$$\mathcal{N}_b = \mathcal{N} - \mathcal{N}_a = \Omega - \mathcal{N}_a \tag{5.28}$$

where Ω is the total number of lattice sites. Therefore, we need only to keep track of one of these numbers, say $\mathcal{N}_a$. The canonical ensemble is then defined by controlling the number $\mathcal{N}_a$ of a-molecules.

We now return to the adhesion geometry with two membrane segments. The two segments are in chemical (= particle-exchange) equilibrium. The population of a-molecules is then divided up into two sub-populations with molecule number $\mathcal{N}_a^{ad}$ and $\mathcal{N}_a^{ub}$, corresponding to the adhering and unbound membrane segment, respectively, with the obvious constraint

$$\mathcal{N}_a^{ad} + \mathcal{N}_a^{ub} = \mathcal{N}_a\,. \tag{5.29}$$

Physical Quantities in the Ising Model

The main advantage of the Ising representation is that it allows us to exploit the underlying particle-hole symmetry which implies that the phase transition occurs at zero field and $T < T_c$. Therefore we will use the language appropriate to the Ising model and then translate the result to the lattice model. The corresponding partition function is given by

$$Z = \sum_{\{s\}} e^{-\mathcal{H}\{s\}/k_B T} \tag{5.30}$$

and the free energy by

$$\mathcal{F}(\mathcal{S}) = -k_B T \ell n Z \ . \tag{5.31}$$

The partition function $\mathcal{Z}$ depends on these three parameters: (i) the dimensionless interaction parameter $J/k_{\mathrm{B}}T$ or the temperature, (ii) the magnetic field H and the excess field ΔH. One has to note that the external field H in Ising model contains chemical potential μ_a of the lattice binary mixture. Therefore the 2-dimensional canonical Ising model with an external field represents the 2-dimensional semi-grand canonical ensemble for lattice model.

The expectation value of the spin $\langle s_i \rangle$ at lattice site i is represented by S and is equal to

$$S = \langle s_i \rangle = \frac{1}{Z} \sum_{\{s\}} s_i e^{-\mathcal{H}/k_B T} = -(\partial \mathcal{F}(\mathcal{S})/\partial H)_T \ . \tag{5.32}$$

The expectation value S describes the local magnetization. The total magnetization can be calculated by performing a summation over the local magnetization. The effects of the boundaries can be neglected because the membrane is flat. In this case, the adhering and unbound segments either have uniform composition or separated phases. The corresponding order parameters at temperature T and the field H is the local magnetization

$$S = +S(T, H) \quad \text{for} \quad H > 0 \tag{5.33}$$

and

$$S = -S(T, |H|) \quad \text{for} \quad H < 0 \, , \tag{5.34}$$

where H is the magnetic field. One can express the order parameter of the lattice system in terms of molecular densities, N,

$$N \equiv \langle n_i \rangle = \frac{1}{2}(1 + S). \tag{5.35}$$

5.4 Phase behavior from exact solution of Ising model

From the Chapter 4 we know that each membrane segment exhibit domain formation separately. In binary mixture lattice, at $T < T_c$ the unbound sub-lattice undergoes two phase transition for zero external field $H^{\mathrm{ub}} = 0$ while adhering sub-lattice is in the spectator phase. The adhering sub-lattice also exhibit two phase coexistence at $H^{\mathrm{ad}} = H^{\mathrm{ub}} + \Delta H^{\mathrm{ad}} = 0$ with unbound sub-lattice as spectator phase.

To characterize the phase behavior of an adhering lattice the order parameter of the two sub-lattice are defined as

$$S^{\mathrm{ub}} \equiv \langle s_i \rangle^{\mathrm{ub}} \quad \text{and} \quad S^{\mathrm{ad}} \equiv \langle s_i \rangle^{\mathrm{ad}} \tag{5.36}$$

The order parameter $S^{\rm ub}$ depends on the dimensionless temperature $\bar{T}$ as

$$\bar{T} \equiv \frac{k_{\rm B}T}{J}; \tag{5.37}$$

and the dimensionless field H defined as

$$\bar{H} = \frac{H}{k_B T} \tag{5.38}$$

whereas the order parameter $S^{\rm ad}$ is a function of $\bar{T}$ and the shifted field $\bar{H} + \Delta\bar{H}$, where the dimensionless excess field has the definition as following

$$\Delta\bar{H} \equiv \frac{\Delta H}{k_{\rm B}T}. \tag{5.39}$$

One can write the equations of state for the two sub-lattices to understand the behavior of each sub-lattice as following

$$\bar{H}^{\rm ub} = h(S^{\rm ub}, \bar{T}) \tag{5.40}$$

and

$$\bar{H}^{\rm ad} = \bar{H}^{\rm ub} + \Delta\bar{H}^{\rm ad} = h(S^{\rm ad}, \bar{T})\,. \tag{5.41}$$

From thermodynamic stability the function $h(S,.)$ is a continuous, non-decreasing, and piece-wise analytic function of S. In addition, the up-down symmetry of the Ising model implies the symmetric relations

$$S^{\rm ub}(-\bar{H}^{\rm ub}, \bar{T}) = -S^{\rm ub}(\bar{H}^{\rm ub}, \bar{T}) \quad \text{and} \quad S^{\rm ad}(-\bar{H}^{\rm ad}, \bar{T}) = -S^{\rm ad}(\bar{H}^{\rm ad}, \bar{T})\,, \tag{5.42}$$

which brings the condition

$$h(-S, \bar{T}) = -h(S, \bar{T}) \quad \text{and} \quad h(0, \bar{T}) = 0\,. \tag{5.43}$$

In Fig. 5.1 One can see the qualitative form of $h(S, \bar{T})$ as a function of S for $\bar{T} < \bar{T}_c$ and $\bar{T} > \bar{T}_c$. Similar to the behavior of chemical potential as a function of mole fraction in (4.2), the function $h(s,.)$ is monotonically increasing and continuous with increasing S for $\bar{T} > \bar{T}_c$. For $\bar{T} < \bar{T}_c$ the function $h(s,.)$ has the three pieces for different order parameter zone

$$\begin{aligned} h(S, \bar{T}) &< 0 \quad \text{for } S < -\mathcal{S}_0(\bar{T}) \\ &= 0 \quad \text{for } -\mathcal{S}_0(\bar{T}) \le S \le +\mathcal{S}_0(\bar{T}) \\ &> 0 \quad \text{for } S > \mathcal{S}_0(\bar{T})\,, \end{aligned} \tag{5.44}$$

By increasing the temperature, the order parameter $\mathcal{S}_0(T)$ or spontaneous magnetization is monotonically decreasing and vanishes at $T = T_c$. The critical temperature for

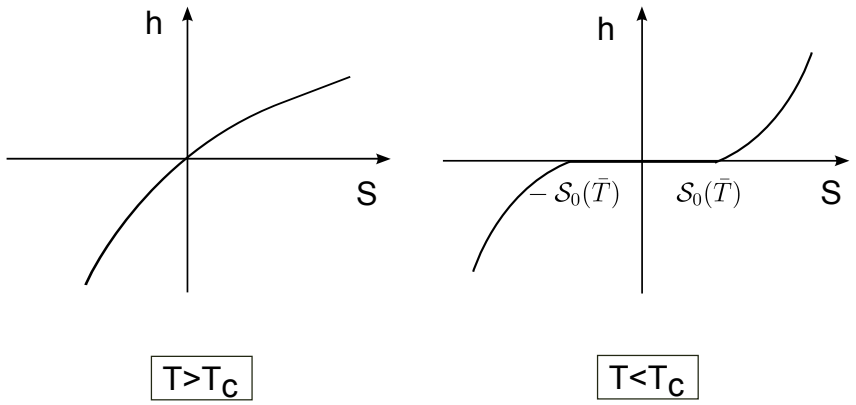

Figure 5.1 : *The qualitative form of $h(S,\bar{T})$ as a function of S for $\bar{T} > \bar{T}_c$ (a), and $\bar{T} < \bar{T}_c$ (b). For $\bar{T} > \bar{T}_c$ the function $h(s,.)$ is monotonically increasing and continuous with increasing S, (a). For $\bar{T} < \bar{T}_c$ the function $h(s,.)$ has three piece for $S < -\mathcal{S}_0(\bar{T})$, $-\mathcal{S}_0(\bar{T}) \leq S \leq +\mathcal{S}_0(\bar{T})$ and $S > \mathcal{S}_0(\bar{T})$.*

the square lattice Ising model is given by

$$\bar{T}_c = \frac{2}{\ln(1+\sqrt{2})} \simeq 2.27 \tag{5.45}$$

alsp the spontaneous order parameter has the form [40]

$$\begin{aligned} \mathcal{S}_0(\bar{T}) &= \left[1-\sinh(2/\bar{T})^{-4}\right]^{1/8} && \text{for } \bar{T} \leq \bar{T}_c \\ &= 0 && \text{for } \bar{T} \geq \bar{T}_c\,. \end{aligned} \tag{5.46}$$

5.4.1 Phase transition at $H^{\rm ub} = 0$

The unbound membrane segment undergoes phase separation at $\bar{T} < \bar{T}_c$ and $\bar{H}^{\rm ub} = 0$. If one approaches the transition line of this segment from position and negative values of $\bar{H}^{\rm ub} = 0$ the unbound order parameter reaches two different values, as

$$S_\alpha^{\rm ub} \equiv \langle s_i \rangle_\alpha^{\rm ub} = +\mathcal{S}_0(\bar{T}) \quad \text{and} \quad S_\beta^{\rm ub} \equiv \langle s_i \rangle_\beta^{\rm ub} = -\mathcal{S}_0(\bar{T}) \tag{5.47}$$

respectively following from (5.40) and (5.44). As we explained in Sec. 4.3 at the transition line of the unbound sub-lattice, the order parameter $S^{\rm ad}$ of the adhering segment plays the role of a spectator phase, thus the relation (5.41) turns in to

$$\bar{H}^{\rm ad} = +\Delta\bar{H} = h(S_*^{\rm ad}, \bar{T}) \quad \text{since } \bar{H} = 0\,. \tag{5.48}$$

It is clear now that the order parameter $S_*^{\rm ad}$ depends on only on the dimensionless $\bar{T}$ and $\Delta\bar{H}$.

From the $\Delta\bar{H}$-dependency of the $S_*^{\rm ad}$, one can conclude the following features. First of all, The sign of $\Delta\bar{H}$ determine the sign of $S_*^{\rm ad}$, i.e. , positive value of $\Delta\bar{H}$ leads to positive value of $S_*^{\rm ad}$. Secondly from the equation of state as in (5.41) and the general form of the function $h(S,.)$ as given by (5.44) one has

$$+\,\mathcal{S}_0(\bar{T}) \leq S_*^{\rm ad}(\bar{T}, \Delta\bar{H}) < 1 \quad \text{for} \quad \Delta\bar{H} \geq 0 \tag{5.49}$$

and

$$-\,1 < S_*^{\rm ad}(\bar{T}, \Delta\bar{H}) \leq -\mathcal{S}_0(\bar{T}) \quad \text{for} \quad \Delta\bar{H} \leq 0\,. \tag{5.50}$$

The spontaneous order parameter approaches $\mathcal{S}_0(0) = 1$ for low temperatures which implies that

$$S_*^{\rm ad}(\bar{T}, \Delta\bar{H}) \approx 1 \quad \text{for small } \bar{T} \text{ and } \Delta\bar{H} > 0 \tag{5.51}$$

and

$$S_*^{\rm ad}(\bar{T}, \Delta\bar{H}) \approx -1 \quad \text{for small } \bar{T} \text{ and } \Delta\bar{H} < 0\,. \tag{5.52}$$

Furthermore the relations (5.41) and (5.44) also lead to

$$S_*^{\rm ad}(\bar{T}, \Delta\bar{H}) \approx 1 \quad \text{for large, positive } \Delta\bar{H}\,, \tag{5.53}$$

$$S_*^{\rm ad}(\bar{T}, \Delta\bar{H}) \approx +\mathcal{S}_0(\bar{T}) \quad \text{for small, positive } \Delta\bar{H}\,, \tag{5.54}$$

$$S_*^{\rm ad}(\bar{T}, \Delta\bar{H}) \approx -\mathcal{S}_0(\bar{T}) \quad \text{for small, negative } \Delta\bar{H}\,, \tag{5.55}$$

and

$$S_*^{\rm ad}(\bar{T}, \Delta\bar{H}) \approx -1 \quad \text{for large, negative } \Delta\bar{H}\,. \tag{5.56}$$

5.4.2 Phase transition at $H^{\rm ad} = 0$

At the phase transition line of the adhering sub-lattice $\bar{H}^{\rm ad} = \bar{H}^{\rm ub} + \Delta\bar{H} = 0$ and $\bar{T} < \bar{T}_c$ from the positive side $\bar{H} > \Delta\bar{H}$ and negative side $\bar{H} < \Delta\bar{H}$, the order parameter $S^{\rm ad}$ attains two different values, namely

$$S_\alpha^{\rm ad} \equiv \langle s_i \rangle_\alpha^{\rm ad} = +S_0(\bar{T}) \quad \text{and} \quad S_\beta^{\rm ad} \equiv \langle s_i \rangle_\beta^{\rm ad} = -S_0(\bar{T}) \tag{5.57}$$

as follows from (5.41) and (5.44), respectively.

As we mentioned before, the order parameter $S^{\rm ub}$ in the unbound sub-lattice is now the spectator phase and has the fixed value $S^{\rm ub} = S^{\rm ub}_*$ which satisfies

$$\bar{H}^{\rm ub} = -\Delta\bar{H} = h(S^{\rm ub}_*, \bar{T}) \quad \text{since } \bar{H} = -\Delta\bar{H}\,. \tag{5.58}$$

From the symmetry we have $h(S,.) = -h(-S,.)$, then latter relation is equivalent to

$$\Delta\bar{H} = h(-S^{\rm ub}_*, \bar{T})\,, \tag{5.59}$$

and following from (5.48) one has

$$S^{\rm ub}_*(\bar{T}, \Delta\bar{H}) = -S^{\rm ad}_*(\bar{T}, \Delta\bar{H}) \tag{5.60}$$

In the limit of low temperatures, the spectator order parameter in the unbound sub-lattice behaves as

$$S^{\rm ub}_*(\bar{T}, \Delta\bar{H}) \approx -1 \quad \text{for small } \bar{T} \text{ and } \Delta\bar{H} > 0 \tag{5.61}$$

and

$$S^{\rm ub}_*(\bar{T}, \Delta\bar{H}) \approx +1 \quad \text{for small } \bar{T} \text{ and } \Delta\bar{H} < 0\,. \tag{5.62}$$

In addition the spectator order parameter $S^{\rm ub}_*(\bar{T}, \Delta\bar{H})$ is a function of the surface ordering field $\Delta\bar{H}$ and behaves like

$$S^{\rm ub}_*(\bar{T}, \Delta\bar{H}) \approx -1 \quad \text{for large, positive } \Delta\bar{H}\,, \tag{5.63}$$

$$S^{\rm ub}_*(\bar{T}, \Delta\bar{H}) \approx -\mathcal{S}_0(\bar{T}) \quad \text{for small, positive } \Delta\bar{H}\,, \tag{5.64}$$

$$S^{\rm ub}_*(\bar{T}, \Delta\bar{H}) \approx +\mathcal{S}_0(\bar{T}) \quad \text{for small, negative } \Delta\bar{H}\,, \tag{5.65}$$

and

$$S^{\rm ub}_*(\bar{T}, \Delta\bar{H}) \approx +1 \quad \text{for large, negative } \Delta\bar{H}\,. \tag{5.66}$$

Binodals for adhering and unbound sub-lattice

The unbound segment has area $\mathcal{A}^{ub}$ corresponding to Ω^{ub} lattice sites. The bound or adhering segment has area $\mathcal{A}^{ad}$ and Ω^{ad} lattice sites, and the total number of lattice sites is equal to $\Omega = \Omega^{ad} + \Omega^{ub}$. The mole fraction, X_a, defined in Eq. (2.1) can be expressed as

$$X_a = \frac{\mathcal{N}_a}{\mathcal{N}} = \frac{\mathcal{N}_a}{\Omega}, \tag{5.67}$$

where in the above equation the total number of a-particle is $\mathcal{N}_a = \mathcal{N}_a^{ad} + \mathcal{N}_a^{ub}$. One can define the area fraction in terms of the number of lattice sites,

$$\Phi^{ad} \equiv \frac{\Omega^{ad}}{\Omega} \quad \text{and} \quad \Phi^{ub} \equiv \frac{\Omega^{ub}}{\Omega}. \tag{5.68}$$

Phase separation within the adhering membrane occurs for $\bar{H}^{ad} = 0$ and $\bar{T} < \bar{T}_c$. The order parameters for the coexisting phases within this segment are then given by $S^{ad} = \pm\mathcal{S}_0(\bar{T})$ and the order parameter is $S^{ub} = S_*^{ub}$. The number of a-molecules within the unbound segment is

$$\mathcal{N}_a^{ub*} = \Omega^{ub} N_*^{ub} = \frac{1}{2}\Omega^{ub}(1 + S_*^{ub}) \tag{5.69}$$

The number of a-molecules within the adhering membrane has the form

$$\mathcal{N}_a^{ad} = \Omega^{ad} N^{ad} = \frac{\Omega^{ad}}{2}(1 \pm \mathcal{S}_0(\bar{T})). \tag{5.70}$$

Using the relations (5.69) and (5.70), the coexistence region for the adhering membrane in terms of the mole fraction satisfies the inequality

$$X_{a,\beta}^{ad} < X_a < X_{a,\alpha}^{ad} \tag{5.71}$$

with

$$X_{a,\beta}^{ad} \equiv \frac{1}{2}(1 + S_*^{ub}\Phi^{ub}) - \frac{1}{2}\mathcal{S}_0(\bar{T})\Phi^{ad} \tag{5.72}$$

and

$$X_{a,\alpha}^{ad} \equiv \frac{1}{2}(1 + S_*^{ub}\Phi^{ub}) + \frac{1}{2}\mathcal{S}_0(\bar{T})\Phi^{ad}, \tag{5.73}$$

which describes the coexistence region for the adhering membrane segment in the (X_a, T)-phase diagram. This region is centered around $X_a = \frac{1}{2}(1 + S_*^{ub}\Phi^{ub})$ and has T-dependent width $\mathcal{S}_0(\bar{T})\Phi^{ad}$. In the limit of low temperature, the order parameter $S_*^{ub} \approx -1$ and the function $\mathcal{S}_0 \approx 1$. The coexistence region, as given by Eq. (5.71), attains the simple form

$$0 < X_a < \Phi^{ad} \quad \text{for low } \bar{T}. \tag{5.74}$$

Phase separation within the unbound membrane segment occurs for $H^{ub} = 0$ and $\bar{T} < \bar{T}_c$. Similar to the adhering membrane, the order parameters for the two coexisting phases within this segment are then given by $S^{ub} = \pm\mathcal{S}_0(\bar{T})$ and the order parameter in the adhering membrane is $S^{ad} = S_*^{ad}$. The number of a-molecules within the adhering membrane segment is

$$\mathcal{N}_a^{ad*} = \Omega^{ad} N_*^{ad} = \frac{1}{2}\Omega^{ad}(1 + S_*^{ad}) \tag{5.75}$$

and within the unbound membrane it has the form

$$\mathcal{N}_a^{ub} = \Omega^{ub} N^{ub} = \frac{\Omega^{ub}}{2}(1 \pm \mathcal{S}_0(\bar{T})). \tag{5.76}$$

In terms of the mole fraction X_a, the coexisting region for the unbound membrane is defined by

$$X_{a,\beta}^{ub} < X_a < X_{a,\alpha}^{ub} \tag{5.77}$$

with

$$X_{a,\beta}^{ub} \equiv \frac{1}{2}(1 + S_*^{ad}\Phi^{ad}) - \frac{1}{2}\mathcal{S}_0(\bar{T})\Phi^{ub} \tag{5.78}$$

and

$$X_{a,\alpha}^{ub} \equiv \frac{1}{2}(1 + S_*^{ad}\Phi^{ad}) + \frac{1}{2}\mathcal{S}_0(\bar{T})\Phi^{ub}, \tag{5.79}$$

which describes the coexistence region for the unbound membrane segment in the (X_a, T)-phase diagram. This region is centered around $X_a = \frac{1}{2}(1 + |S_*^{ad}|(\bar{T})\Phi^{ad})$ and has T-dependent width $\mathcal{S}_0(\bar{T})\Phi^{ub}$, see as depicted in Fig. 5.6. For low $\bar{T}$, the order parameter is $S_*^{ad} \approx +1$ and the function $\mathcal{S}_0$ is approximately one,$\mathcal{S}_0 \approx +1$. The coexistence region, as given by Eq. (5.77), attains the simple form

$$\Phi^{ad} < X_a < 1 \quad \text{for low } \bar{T}. \tag{5.80}$$

In Fig. 5.2 the coexisting regions for unbound and adhering sub-lattice in the limit of large and small positive external field is illustrated in blue and red areas, respectively. For $\Delta H > 0$ the a-molecules prefer to stay in the unbound membrane segment. Therefore, as one increases the mole fraction X_a starting from $X_a = 0$, one first enters the blue coexistence region for the unbound segment and by increasing the X_a hits the red two phase coexistence of adhering sub-lattice. The two critical points depicted in (a) merge in the limit of vanishing ΔH. The overall area fraction has the value $\Phi^{ub} = q = 2/3$ corresponding to a semi-spherical shape of the adhering membrane vesicle.

The phase diagram of an adhering lattice system in the limit of large and small negative field is illustrated in Fig. 5.3. As in Fig. 5.2, the blue and red regions correspond the two-phase coexistence of the unbound and adhering membrane segments, respectively. Negative values of ΔH impose that the a-molecules prefer the adhering membrane sub-lattice. Therefore, as one increases the mole fraction X_a starting from $X_a = 0$, first one enters the red coexistence region for the adhering segment and then pass the unbound sub-lattice coexistence area which has the blue color. The two critical points depicted in (a) merge in the limit of zero ΔH. The overall area fraction is $\Phi^{ub} = q = 2/3$ corresponding to a semi-spherical shape of the adhering vesicle.

To summarize the discussion, one can describe the phase behavior of the coupled Ising system with two functions: the order parameter $\mathcal{S}_0(\bar{T})$ which is given by (5.46) and one

of the two spectator order parameters $S_*^{\rm ad}(\bar{T}, \Delta\bar{H})$ and $S_*^{\rm ub}(\bar{T}, \Delta\bar{H})$, which have the symmetric relation $S_*^{\rm ub} = -S_*^{\rm ad}$ and have the asymptotic $\Delta\bar{H}$-dependence as described by (5.53) - (5.56) as well as (5.63) - (5.66).

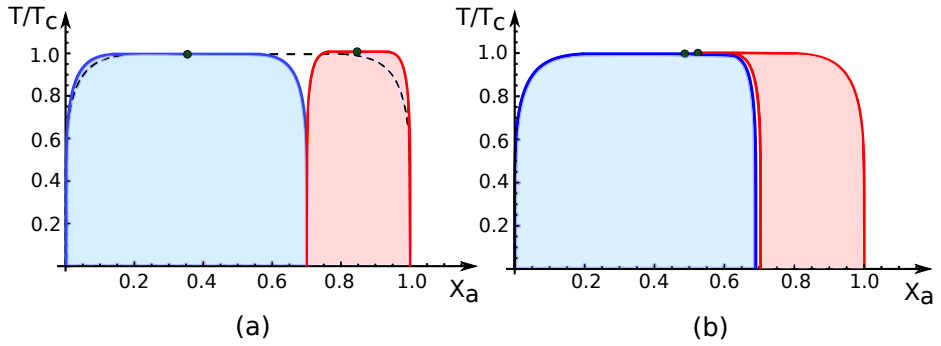

Figure 5.2 : Phase diagram of binary lattice reached by exact solution of Ising system in the presence of an adhesive substrate surface characterized by (a) small and (b) large positive values of the external field (or affinity contrast, see relation (5.17)) $\Delta H > 0$. The blue and red regions represent the two-phase coexistence regions of the unbound and adhering membrane segments, respectively. Likewise, the blue and red curves correspond to the binodal lines for these two segments. Positive values of $\Delta H > 0$ imply that the a-molecules prefer the unbound membrane segment. Therefore, one first enters the blue coexistence region for the unbound segment as one increases the mole fraction X_a starting from $X_a = 0$. The two critical points depicted in (a) merge in the limit of vanishing ΔH. The overall area fraction has the value $\Phi^{ub} = q = 2/3$ corresponding to a semi-spherical shape of the adhering vesicle.

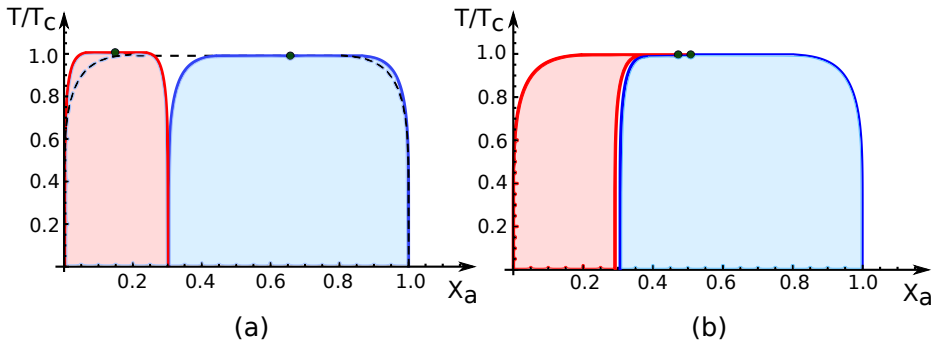

Figure 5.3 : *Phase diagrams for the same binary mixture as in Fig. 2.2 but in the presence of an adhesive substrate surface characterized by (a) small and (b) large negative values of the external field (or affinity contrast, see relation (5.17)) $\Delta H < 0$. As in Fig. 5.2, the blue and red regions represent the two-phase coexistence regions of the unbound and bound membrane segments, respectively. Negative values of ΔH imply that the a-molecules prefer the adhering membrane segment. Therefore, one first enters the red coexistence region for the adhering segment as one increases the mole fraction X_a starting from $X_a = 0$. The two critical points depicted in (a) merge in the limit of vanishing ΔH. The overall area fraction has the value $\Phi^{ub} = q = 2/3$ corresponding to a semi-spherical shape of the adhering vesicle.*

5.5 Mean field Theory

One can study the lattice model as explained by (5.1) within a simple but convenient approximation. In this approximation the couplings between the spins as in (5.12) are replaced by an effective 'mean field'

$$H_i^{\text{eff}} = \sum_j J_{ij} < s_j >= \sum_j J_{ij} S \ . \tag{5.81}$$

The local magnetization S introduced in (5.32) has the self consistent determination which is required by

$$S = \sum_{s_i=\pm 1} s_i e^{-\bar{\mathcal{H}}_i} / \sum_{s_i=\pm 1} e^{-\bar{\mathcal{H}}_i} \tag{5.82}$$

with effective mean field Hamiltonian

$$\bar{\mathcal{H}}_i \equiv (H_i^{eff} + H)s_i/k_BT \ . \tag{5.83}$$

The two relations above can be summarize to the mean field equation

$$S = \tanh([\sum_j J_{ij}S + H]/k_BT) \tag{5.84}$$

for the local magnetization S. The mean field temperature is now defined as

$$k_BT_c^{MF} \equiv \sum_j J_{ij} = zJ_0. \tag{5.85}$$

where z is the number of nearest neighbors. Using the definition above the mean field equation (5.84) becomes

$$S = \tanh([k_BT_c^{MF}S + H]/k_BT). \tag{5.86}$$

Homogeneous Phase

It is useful to rewrite the mean field equation (5.86) in terms of the generic field

$$\begin{aligned} H &= k_BT \operatorname{arctanh}(S) - k_BT_c^{MF}S \\ &= \frac{1}{2}k_BT\{\ln(1+S) - \ln(1-S)\} - k_BT_c^{MF}S \ . \end{aligned} \tag{5.87}$$

with defining the dimensionless external field $\bar{H} = \frac{H}{k_BT}$ the relation (5.87) turns into form

$$\bar{H} = \frac{1}{2}\{\ln(1+S) - \ln(1-S)\} - \frac{T_c^{MF}}{T}S. \tag{5.88}$$

One can get the free energy function,

$$\mathcal{F}(\mathcal{S}) = \mathcal{F}_{\mathrm{o}}(\mathcal{S}) - \bar{\mathcal{H}}\mathcal{S}, \tag{5.89}$$

which has the characteristic that the mean field equation (5.87) is recovered from

$$\partial\mathcal{F}/\partial\mathcal{S} \mid_{\mathcal{S}} = \partial\mathcal{F}_{\mathrm{o}}/\partial\mathcal{S} \mid_{\mathcal{S}} - \bar{\mathcal{H}} = \mathrm{o}. \tag{5.90}$$

This implies that

$$\bar{\mathcal{F}}_{\mathrm{o}}(S) = \frac{\mathcal{F}_{\mathrm{o}}}{k_BT} = \frac{1}{2}\{(1+S)\ln(1+S) + (1-S)\ln(1-S)\} - \frac{1}{2}\frac{T_c^{MF}}{T}S^2 \ . \tag{5.91}$$

The functional form of $\bar{\mathcal{F}}_{\rm o}(\rm S)$ is depicted in Fig. 5.4 for three different temperatures. Note that $\mathcal{F}_{\rm o}(-S) = \mathcal{F}_{\rm o}(S)$ reflects the up–down symmetry of the Ising model in zero external field.

For $T < T_c^{MF}$, the function $\mathcal{F}_{\rm o}(S)$ has two minima at

$$S = \pm\Upsilon_0(T) \equiv \Upsilon(T, H = 0). \tag{5.92}$$

These two minima correspond to the two coexisting phases α and β in zero magnetic field, at $H = 0$.

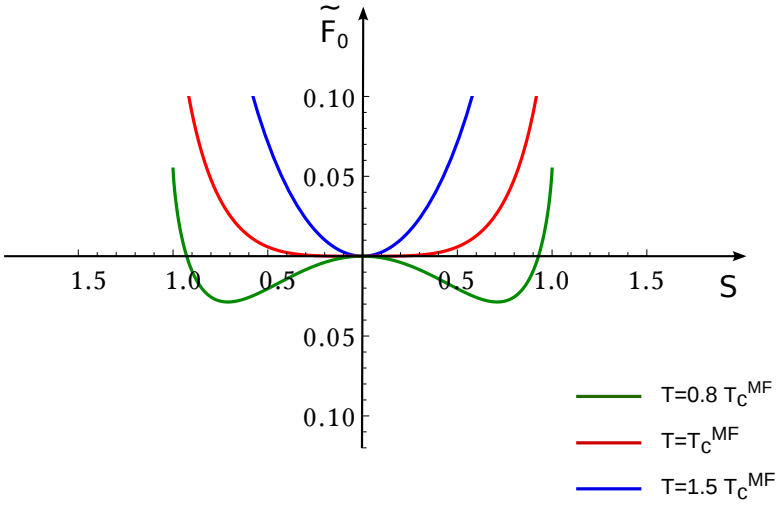

Figure 5.4 : *The functional form of $\bar{\mathcal{F}}_{\rm o}(S) = \mathcal{F}_{\rm o}/k_Bt$ for three different temperatures. For $T < T_c^{MF}$, the function $\mathcal{F}_{\prime}(\mathcal{S})$ has two minima at $S = \pm S_0$. These two minimas correspond to the two coexisting phases in zero magnetic field, at $H = 0$. Therefore, within mean field theory for the Ising model, the two coexisting phases α and β are corresponding to $S_\alpha = +\Upsilon_0(T)$ and $S_\beta = -\Upsilon_0(T)$*

5.6 Mean field Phase coexistence in adhering vesicle

In the 2-dimensional Ising model, the phase separation and the coexisting phase occurs at $H = 0$ and $T < T_c$. Starting from the Hamiltonian of the unbound membrane in Eq.

(5.26), the order parameter S^{ub} satisfies the mean field equation

$$S = \tanh([k_B T_c^{MF} S + H^{ub}]/k_B T), \tag{5.93}$$

as described by (5.86). When the unbound membrane undergoes phase separation, the mean field equation Eq. (5.93) has two different solutions corresponding to two coexisting domains α and β:

$$S_\alpha^{ub} \equiv \langle s_i \rangle_\alpha^{ub} = +\Upsilon_0(T) \quad \text{and} \quad S_\beta^{ub} \equiv \langle s_i \rangle_\beta^{ub} = -\Upsilon_0(T). \tag{5.94}$$

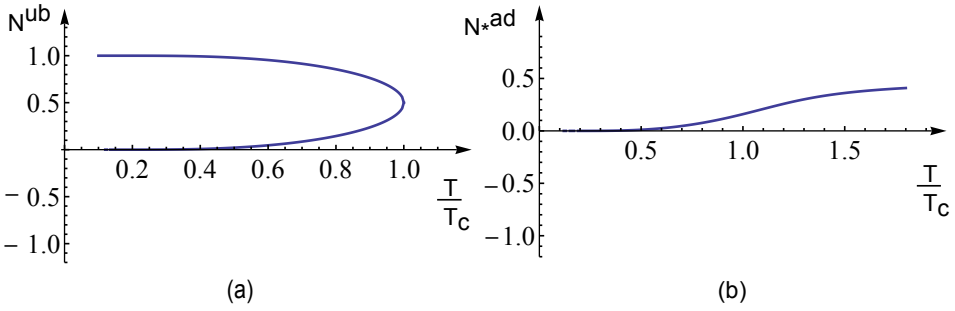

Figure 5.5 : *The density of the unbound membrane versus temperature $\frac{T}{T_c}$. At $T < T_c$ the system undergoes phase separation(a). The density of the adhering membrane versus temperature along the transition line of the unbound membrane segment(b). The $N_*^{ad}(T)$ is a monotonous function of temperature.*

In addition, along the transition line of the unbound segment, the adhering segment is exposed to the field $H^{ad} = \Delta H^{ad} > 0$ which leads to the order parameter

$$S_*^{ad} = \Upsilon(T, \Delta H^{ad}). \tag{5.95}$$

The molecular densities for a-molecules can be expressed in terms of these order parameters for the unbound membrane segment , see Fig. 5.5(a),

$$N_\alpha^{ub} \equiv \frac{1}{2}(1 + \Upsilon_0(T)) \quad \text{and} \quad N_\beta^{ub} \equiv \frac{1}{2}(1 - \Upsilon_0(T)), \tag{5.96}$$

and for the adhering membrane segment; as seen in Fig. 5.5(b),

$$N_*^{ad} = \frac{1}{2}(1 + S_*^{ad}). \tag{5.97}$$

which is a positive increasing function of temperature.
The phase transition in the adhering membrane segment occurs at $T < T_c$ and zero magnetic field,

$$H^{ad} = H^{ub} + \Delta H^{ad} = 0 \tag{5.98}$$

which denotes that $H^{ub} = -\Delta H^{ad}$. Respectively, from Eq. (5.25), the order parameter of the adhering membrane satisfies the mean field equation

$$S = \tanh([T_c^{MF} S + H^{ad}]/k_B T). \tag{5.99}$$

In the case of phase separation the mean field equation Eq. (5.99) has two different solutions which correspond to α and β domains:

$$S_\alpha^{ad} \equiv \langle s_i \rangle_\alpha^{ad} = +\Upsilon_0(T) \quad \text{and} \quad S_\beta^{ad} \equiv \langle s_i \rangle_\beta^{ad} = -\Upsilon_0(T). \tag{5.100}$$

In addition, the unbound segment is exposed to the field $H^{ub} = -\Delta H^{ad} < 0$. The order parameter for the unbound membrane segment along the phase transition line of the adhering segment has the form

$$S_*^{ub} = -\Upsilon(T, |H^{ub}| = \Delta H^{ad}) = -S_*^{ad}. \tag{5.101}$$

The corresponding densities for the phase separated adhering membrane are equivalent to

$$N_\alpha^{ad} \equiv \frac{1}{2}(1 + \Upsilon_0(T)) \quad \text{and} \quad N_\beta^{ad} \equiv \frac{1}{2}(1 - \Upsilon_0(T)), \tag{5.102}$$

and for the unbound membrane segment

$$N_*^{ub} = \frac{1}{2}(1 + S_*^{ub})\,. \tag{5.103}$$

The density function of the unbound membrane along the transition line of the adhering membrane segment is monotonously increasing function versus the temperature, similar to the Fig. 5.5(b).

Adhering and unbound binodals in mean field approximation

The order parameters for the two coexisting phases within the adhering membrane segment are given by $S^{ad} = \pm\Upsilon_0(T)$ and the order parameter is $S^{ub} = S_*^{ub}$. Using the relations (5.69) and (5.70) and replacing the $\mathcal{S}_0$ by Υ_0 the coexistence region for the adhering membrane satisfies the inequality

$$X_{a,\beta}^{ad} < X_a < X_{a,\alpha}^{ad} \tag{5.104}$$

with

$$X^{ad}_{a,\beta} \equiv \frac{1}{2}(1 + S^{ub}_{*}\Phi^{ub}) - \frac{1}{2}\Upsilon_0(T)\Phi^{ad} \tag{5.105}$$

and

$$X^{ad}_{a,\alpha} \equiv \frac{1}{2}(1 + S^{ub}_{*}\Phi^{ub}) + \frac{1}{2}\Upsilon_0(T)\Phi^{ad}, \tag{5.106}$$

which describes the coexistence region for the adhering membrane segment in the (X_a, T)-phase diagram.

Similar to the adhering membrane, the order parameters for the two coexisting phases within unbound segment are then given by $S^{ub} = \pm\Upsilon_0(T)$ and the corresponding order parameter in the adhering membrane is given by $S^{ad} = S^{ad}_{*}$. As in relations (5.77)-(5.79) the coexisting region for the unbound membrane is defined by

$$X^{ub}_{a,\beta} < X_a < X^{ub}_{a,\alpha} \tag{5.107}$$

with

$$X^{ub}_{a,\beta} \equiv \frac{1}{2}(1 + S^{ad}_{*}\Phi^{ad}) - \frac{1}{2}\Upsilon_0(T)\Phi^{ub} \tag{5.108}$$

and

$$X^{ub}_{a,\alpha} \equiv \frac{1}{2}(1 + S^{ad}_{*}\Phi^{ad}) + \frac{1}{2}\Upsilon_0(T)\Phi^{ub}, \tag{5.109}$$

in which the $\mathcal{S}_0$ in replaced by Υ_0. The relations above describe the coexistence region for the unbound membrane segment in the (X_a, T)-phase diagram. This region is centered around $X_a = \frac{1}{2}(1 + |S^{ad}_{*}|(T)\Phi^{ad})$ and has T-dependent width $\Upsilon_0(T)\Phi^{ub}$, see as depicted in Fig. 5.6.

To compare the coexistence region of free membrane vesicle reached by exact solution of Ising model as in (5.46) with the mean field binodas in relations (5.94) and Fig. 5.5(a), see Fig. 5.7. In this figure one can see that the critical temperature of the mean field approximation is higher than the exact solution [40];

5.6.1 Densities as a function of mole fraction

In the grand-canonical ensemble, the system is described by two densities or order parameters, each of which exhibits a single jump at a certain value of the chemical potential or magnetic field. In this description, the adhering and the unbound membrane segment are only related via the reservoirs for a- and b-molecules, which define the chemical potential difference $\mu_a - \mu_b$.

The canonical description introduces an additional global constraint on the total number of a-molecules in the two subsystems. Because of this global constraint, the phase diagram in the (X_a, T)-plane combines the two coexistence regions for the adhering and the unbound membrane. The behavior of the densities within these coexistence regions

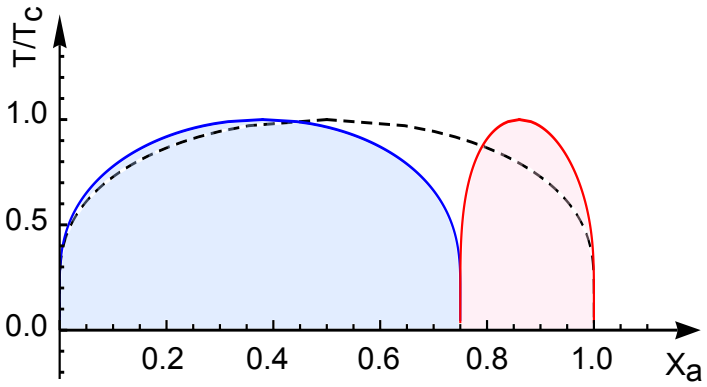

Figure 5.6 : *Canonical phase diagram of a non-adhering membrane (dashed curve) and an adhering membrane (colored curve). If we bring a uni-composition membrane in contact to a substrate, the domain forms in the contact area. The composition in the contact area changes from one-phase to two-phase coexistence. X_a is the density of the particles and T/T_c^{MF} is the reduced temperature. One can find the region under the dashed line and above the red curve, which shows no phase separation in a non-adhering membrane and phase separation in an adhering membrane in the contact area.*

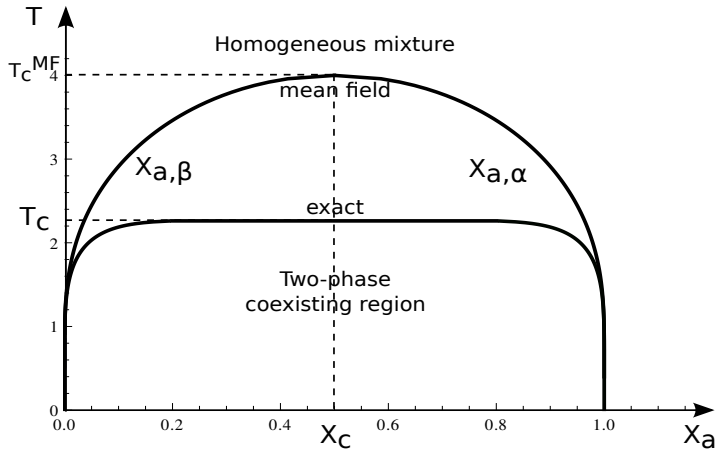

Figure 5.7 : *Two phase coexistence regions for free vesicle obtained by Ising mean field approximation (upper curve) compared with the binodals reached by exact solution of the Ising system (lower curve) and the result transform in to lattice model. the critical temperature calculated with the mean field approximation T_c^{MF} is higher than the exact solution temperature $\bar{T}_c$. The two binodals $X_{a,\beta}$ and $X_{a,\alpha}$ separate the two phase coexistence region from the homogeneous phase. The parameter X_a is the mole fraction of the a-molecules.*

and within the complementary one-phase regions is as follows.

Densities within the coexistence region of the adhering membrane

As the mole fraction X_a is varied within the coexistence region for the adhering membrane, i.e., from X_a to $X_{a,\alpha}^{ad}$ at constant temperature, compare (5.73) and (5.72), the density N^{ub} of a-molecules within the unbound membrane segment stays at the constant value $N_*^{ub} = \frac{1}{2}(1 + S_*^{ub}(T))$ with the order parameter $S_*^{ub}(T)$, as given by (5.69). Likewise, the densities in the coexisting α- and β- domains within the adhering membrane stay constant with $N_\alpha^{ad} = \frac{1}{2}(1 + \Upsilon_0(T))$ and $N_\beta^{ad} = \frac{1}{2}(1 - \Upsilon_0(T))$.

Densities within the coexistence region of unbound membrane

Likewise, as the mole fraction X_a is varied within the coexistence region for the unbound membrane, i.e., from $X_{a,\beta}^{ub}$ to $X_{a,\alpha}^{ub}$ at constant temperature, compare (5.78) and (5.79), the density N^{ad} of a-molecules within the adhering membrane segment stays at the constant value $N_*^{ad} = \frac{1}{2}(1 + S_*^{ub}(T))$ with the order parameter $S_*^{ub}(T)$ as given by (5.75). Likewise, the densities in the coexisting α and β domains within the unbound membrane stay constant with $N_\alpha^{un} = \frac{1}{2}(1 + \Upsilon_0(T))$ and $N_\beta^{un} = \frac{1}{2}(1 - \Upsilon_0(T))$.

Densities within intermediate one-phase region

For mole fractions X_a in between the two coexistence regions, both segments have a uniform composition. This region of the phase diagram is given by

$$X_{a,\alpha}^{ad} < X_a < X_{a,\beta}^{ub} \tag{5.110}$$

with $X_{a,\alpha}^{ad}$ and $X_{a,\beta}^{ub}$ as given by (5.73) and (5.78), respectively. At the left boundary of this region, the adhering order parameter is $S^{ad} = +\Upsilon_0$ and the unbound order parameter has the form $S^{ub} = -|S_*^{ub}|$. At the right boundary of this region, the order adhering parameter reaches $S^{ad} = +|S_*^{ad}|$ and the unbound order parameter is equal to $S^{ub} = -\Upsilon_0$. In between, the order parameters increase monotonically with increasing X_a and, thus, satisfy

$$+\Upsilon_0 \leq S^{ad} \leq +|S_*^{ad}| \tag{5.111}$$

and

$$-|S_*^{ub}| \leq S^{ub} \leq -\Upsilon_0\,. \tag{5.112}$$

At $T = T_c^{\rm MF}$, the function $\Upsilon_0(T)$ vanishes and the relation (5.110) becomes

$$\tfrac{1}{2}\,(1 - |S_*^{ub}|\Phi^{ub}) < X_a < \tfrac{1}{2}\,(1 + |S_*^{ad}|\Phi^{ad}), \tag{5.113}$$

which implies that the separation of the two critical points within the (X_a, T)-plane is given by $\frac{1}{2}\,(|S_*^{ub}|\Phi^{ub} + |S_*^{ad}|\Phi^{ad})$. For large ΔH^{ad} with $S_*^{ub} \approx -1$ and $S_*^{ad} \approx 1$, this separation becomes

$$\tfrac{1}{2}\,(|S_*^{ub}|\Phi^{ub} + |S_*^{ad}|\Phi^{ad}) \approx \tfrac{1}{2}\,. \tag{5.114}$$

Overall density variation

In summary, as we vary the mole fraction X_a between $X_a = 0$ and $X_a = 1$ at constant temperature, we encounter the following density variation for $T < T_c^{\rm MF}$:
(I) one-phase region with $0 \leq X_a \leq X_{a,\beta}^{ad}$:
the densities N^{ad} and N^{ub} of the a-molecules increase monotonically starting from $N^{ad} = N^{ub} = 0$ at $X_a = 0$;
(III) two-phase region with $X_{a,\beta}^{ad} < X_a < X_{a,\alpha}^{ad}$:
all three local densities N^{ub}, N_α^{ad}, and N_β^{ad} stay constant;
(IV) one-phase region with $X_{a,\alpha}^{ad} < X_a < X_{a,\beta}^{ub}$:
the densities N^{ad} and N^{ub} increase monotonically;
(V) two-phase region with $X_{a,\beta}^{ub} < X_a < X_{a,\alpha}^{ub}$:
all three local densities N_α^{ub}, N_β^{ub}, and N^{ad} stay constant; and
(VI) one-phase region with $X_{a,\alpha}^{ub} < X_a \leq 1$:
the densities N^{ad} and N^{ub} increase monotonically towards the limiting value

$N^{ad} = N^{ub} = 1$ at $X_a = 1$.

Limit of small and large adhesion energy

One way to verify the mean field phase diagram is to see its behavior in the limit of large and small adhesion energy, Fig. 5.8. In the case of large adhesion energy, the two critical temperatures stay far away from each other. By decreasing the adhesion energy, the two minima of the two membrane segments get closer together and finally, in zero adhesion energy, the two critical points meet at $X_a = 0.5$. The phase diagram of the adhering membrane in zero adhesion energy is the same as the phase diagram of the non-adhering membrane vesicle, see Fig. 5.8.

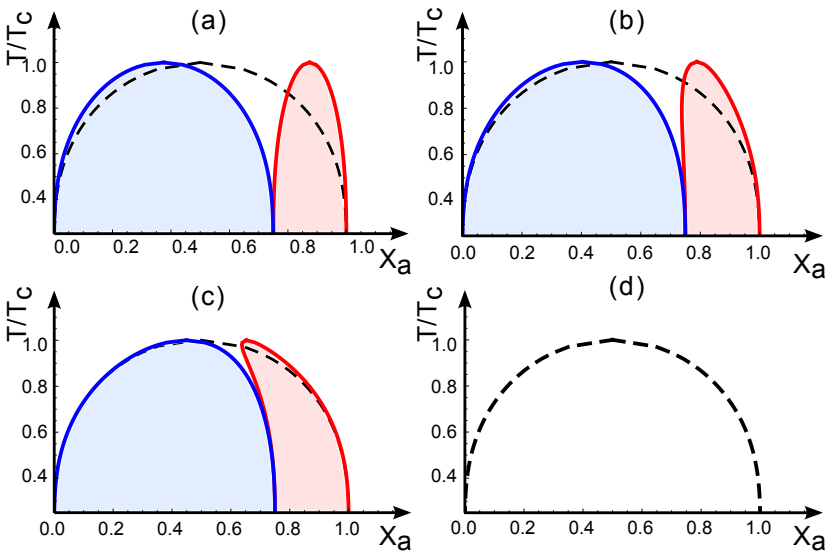

Figure 5.8 : *The phase diagram of an adhering membrane in the limit of large and small adhesion energy. When the adhesion energy is rather large, critical points of the adhering and the unbound membrane segments are far from each other (a). Decreasing the adhesion energy causes the two minima to get closer to each other (b) and (c). In the case of zero adhesion energy, the phase diagram of an adhering membrane turns into the phase diagram on a non-adhering membrane vesicle (d).*

5.7 Chemical potentials in adhering vesicle

As discussed in the Sec. 5.5, one can extract the explicit form of the magnetic field as a function of the order parameter ;

$$H = k_B T \,\mathrm{arctanh}(S) - k_B T_c^{MF} S. \tag{5.115}$$

Using the similarity between the Ising and the lattice model in Sec. 5.2, the explicit form of the chemical potential as a function of mole fraction $\mu_a = F'(X_a)$ has the form

$$\mu_a^{MF} = k_B T \,\mathrm{arctanh}(2X_a - 1) - k_B T_c^{MF}(2X_a - 1). \tag{5.116}$$

The generic form of the $\mu_a = F'(X_a)$ has been discussed in the Sec. 4.1. The unbound membrane segment is similar to the lattice system with $\mu = \mu_a^{ub}$. Compared to Fig. 4.1 in Sec. 4.1, the explicit functional form of the reduced chemical potential $\bar{\mu}$

$$\bar{\mu} = \frac{\mu^{MF}}{k_B T} = \mathrm{arctanh}(2X_a - 1) - \frac{T_c^{MF}}{T}(2X_a - 1), \tag{5.117}$$

for different temperature is shown in Fig. 5.9.

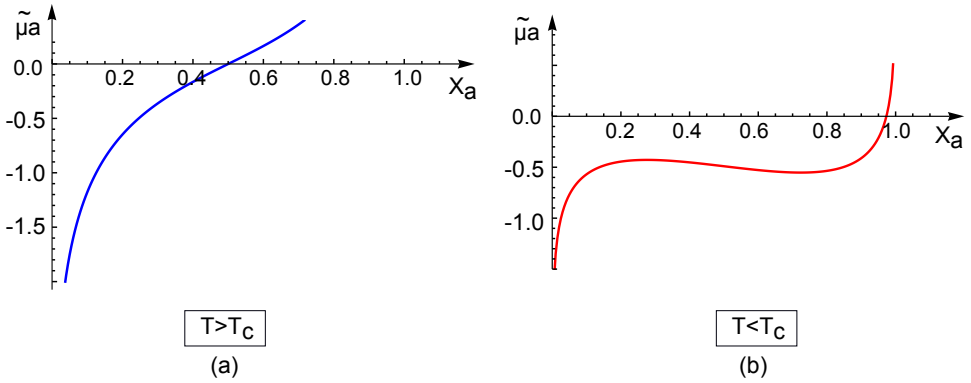

Figure 5.9 : *The explicit form of the chemical potential versus mole fraction, $\mu = F'(X_a)$ obtained in mean field approximation, see Eq. (5.116). The chemical potential is a smooth increasing function at $T > T_c^{MF}$ (a). At $T < T_c^{MF}$ the function $\mu = F'(X_a)$ does not have the convexity that is desired in thermodynamics (b). This figure is the explicit form of the Fig. 4.1 in Sec. 4.1. In this figure $\bar{\mu}_a = \mu_a^{MF}/k_B T$.*

At $T < T_c^{MF}$ the chemical potential $\bar{\mu}$ does not have the correct convexity at the phase transition zone, as required by thermodynamics, see Fig. 5.9. To reach a stable function in the coexistence regions of two-phases one can supplement the chemical potential $\mu_a^{ub} = \mu_a^{MF}$ by Maxwell construction. In the Ising representation, this construction corresponds to the following rule:

$$\begin{aligned} \mu_a^{ub} &\equiv \mu_a^{MF} \qquad \text{for} \quad X_a < X_\beta \quad \text{and} \quad X_a > X_\alpha, \\ \mu_a^{ub} &\equiv 0 \qquad\quad \text{for} \qquad\qquad X_\beta < X_a < X_\alpha. \end{aligned} \tag{5.118}$$

The function $\bar{\mu} = F'(X_a)/k_BT$ corrected by Maxwell construction is shown in Fig. 5.10. The chemical potential has the constant value $\mu_a^{ub} = 0$ for $X_\beta < X_a < X_\alpha$.

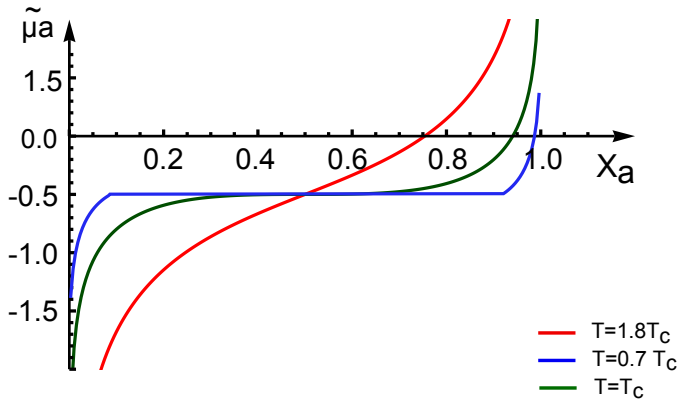

Figure 5.10 : *The chemical potential μ as a function of mole fraction X_a corrected by Maxwell construction, Eq. (5.118) $\mu = \mu_a^{MF}$. In this figure the chemical potential is shown in three different temperatures. At $T < T_c$ the Maxwell construction is used to correct the deficiency of the analytically calculated chemical potential function between the two-phase coexistence $X_{a,\alpha}$ and $X_{a,\beta}$. In this figure $\bar{\mu}_a = \mu_a^{MF}/k_BT$.*

One can get the explicit form of H^{ad} as a function of S by inverting Eq. (5.99). The explicit form of the chemical potential is again attainable from the transformation between Ising and lattice model,

$$\mu_a^{ad} = F'(X_a) + \Delta U. \tag{5.119}$$

To avoid the instability of the function $\bar{\mu}_a^{ad} = (F'(X_a) + \Delta U)/k_BT$ in the coexisting phase regions, the Maxwell construction is used , compare Fig. 5.11. This figure matches Figs. 4.3 and 4.4 in Sec. 4.3.

In agreement with the discussion in Sec. 4.3, the explicit forms of the mole fractions

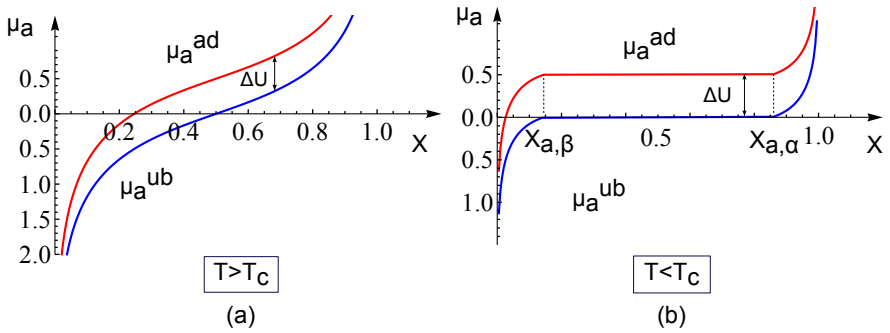

Figure 5.11 : *The adhering and the unbound chemical potentials, μ_a^{ad} (blue curve) and μ_a^{ub} (red curve) as functions of mole fraction X_a for a-molecules. The μ_a^{ad} is related to $\mu_a^{ub} = F'(X_a)$ with the adhesion affinity ΔU: $\mu_a^{ad} = F'(X_a)+\Delta U$. (a) The chemical potential is an increasing smooth function of mole fraction for $\Delta U > 0$ and $T > T_c^{MF}$ in both adhering and unbound segments. (b) At $T < T_c^{MF}$ the phase separation occurs in both segments for different value of chemical potential,see Fig. 4.2. At $T < T_c^{MF}$ the Maxwell construction is used to avoid the deficiency showed in Fig. 5.9 in the coexisting phase $X_{a,\alpha}$ and $X_{a,\beta}$. In this figure the parameter $X_{a,*}^{ub}$ and $X_{a,*}^{ad}$ represent the explicit values of the constant mole fraction at the spectator phase. In this figure $\Delta U = +0.5K_BT$ in (a) and $\Delta U = -0.5K_BT$ in (b).*

X_a^{ub} and X_a^{ad} within the unbound and adhering membrane segments are depicted as functions of the overall molecular fraction X_a, in Fig. 5.12.

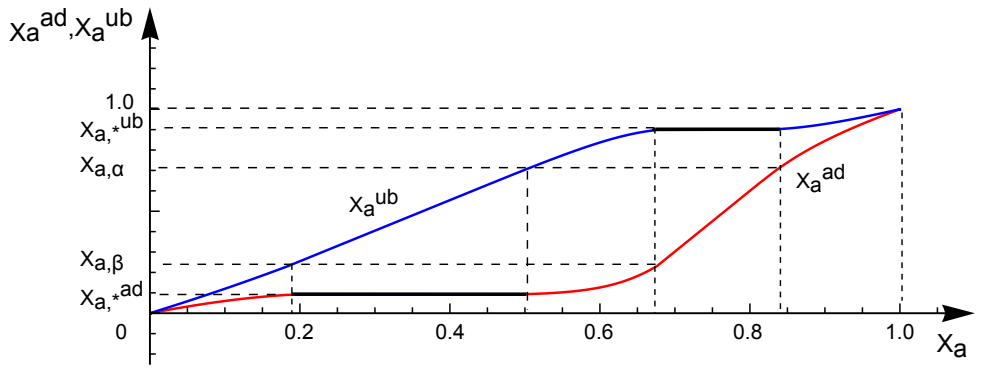

Figure 5.12 : *The explicit forms of the mole fractions X_a^{ub} and X_a^{ad} within the unbound and the adhering membrane segments as functions of the overall mole fraction X_a of the a-molecules, also see Sec. 4.3. The generic form of this figure is depicted in Fig. 4.4 In this example, the adhering vesicle has the shape of a half sphere with area ratio $q = \frac{2}{3}$ and the constant composition variables are $X_{a,*}^{ad} = X_{a,\beta}$ and $X_{a,*}^{ub} = X_{a,\alpha}$.*

The results from the mean field approximation supports the analysis of the chemical potential μ versus mole fraction X_a in Sec. 4.3. Also the variation of the mole fraction in adhering and unbound membrane segments versus the overall fraction is in accordance with the same argument on the area fraction in Sec. 4.3.

5.8 Simplified geometery and Monte Carlo simulations

In Monte Carlo (MC) simulation a flat membrane is discretized into square lattice with the occupation number 1 or 0 corresponding to the components a or b. We eliminate the vesicle volume from the description in Chapter 3 and replace the spherical cap geometry by the simplified adhesion geometry, as shown in Fig. 5.13. The simplified adhesion geometry consist of two concentric membrane segments, which are different in the adhesion energy;

$$\begin{aligned} U^i &= U_a^i - U_b^i, \qquad \text{in the adhering membrane, and} \\ U^i &= 0 \qquad\qquad\quad \text{in the unbound membrane.} \end{aligned} \tag{5.120}$$

The MC simulation is performed in canonical ensemble and the total number of a- and b- particles are fixed. The two membrane segments are in chemical equilibrium and they are allowed to exchange the particles.

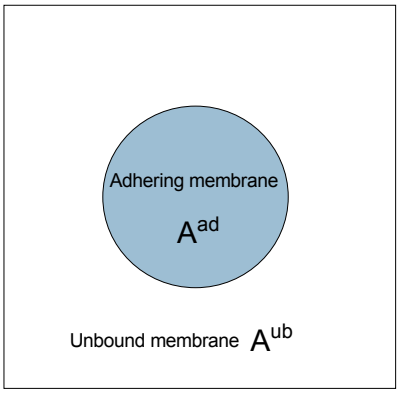

Figure 5.13 : *Simplified adhesion geometry consisting of two concentric membrane segments: the outer segment represents the unbound vesicle membrane with area $\mathcal{A}^{ub}$, the inner segment represents the adhering vesicle membrane segment with contact area $\mathcal{A}^{ad}$.*

One can pick a configuration below the coexisting line and above the critical temperature for the non-adhering membrane, see Fig. 5.14(a) . Bringing this membrane vesicle into adhesion with a substrate causes a shift in the concentration of the adhering membrane segment. This segment undergoes phase separation, and in the phase diagram the configuration moves to the two-phase coexistence region, Fig. 5.14(b). It is also interesting to study a configuration below the coexisting line of the non- adhering membrane. In this case, phase separation occurs neither in the adhering nor in the unbound membrane segment, see Fig 5.15(a). Adding the adhesion energy to this system does not drive any shift in the configuration, see Fig 5.15(b).

In the mean field phase diagram one can walk along the fixed temperature and increase the concentration of component a, Fig. 5.16(a). Starting from small concentration and increasing it, first we hit the unbound membrane section coexistence region and then the adhering membrane two-phase coexistence line. The results of the MC simulations is in accordance with the phase diagram calculation in Fig. 5.16(b). The snapshots from the MC simulation confirm the mean field phase diagram obtained by calculation. As a next step, one can reach the mean field phase diagram by MC simulation and compare the simulation results to the calculations.

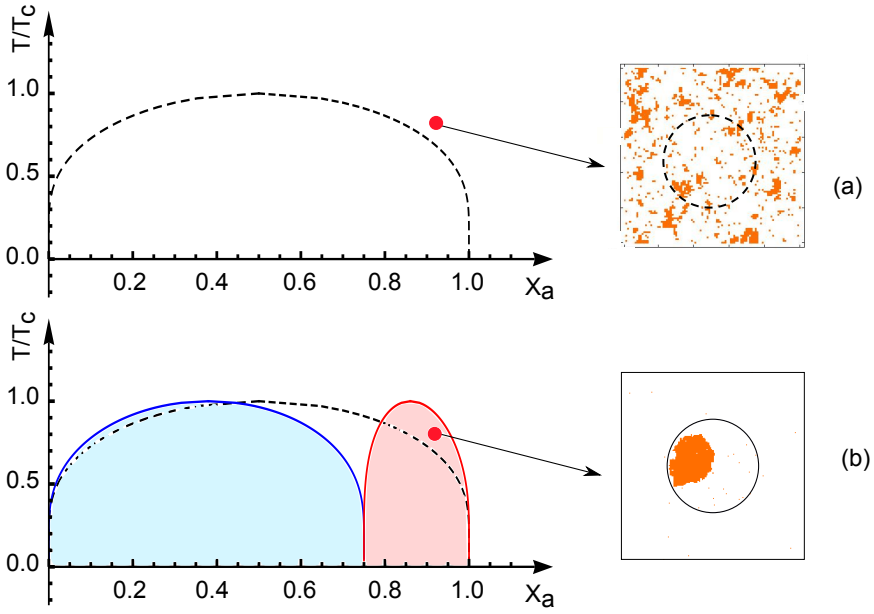

Figure 5.14 : *Consider a uniform configuration below the coexisting line of the non-adhering membrane and above the critical temperature, (a) left. The mean field phase diagram of such a membrane vesicle is shown in (a) right. If one brings this membrane in adhesion to a substrate, the domains form in the adhering membrane segment, (b) left. The chosen configuration in the phase diagram jumps into the phase coexistence region of an adhering membrane segment, (b) right. In the snapshot from MC simulation, the orange particles are represented as component a and white particles are component b. In this figure, the reduced interaction energy is equal to* $\frac{W}{k_BT} = 1.125$ *and the concentration is* $X_a = 0.15$*. The adhesion energy is equal to* $\frac{\Delta U}{k_BT} = 0$ *in (a) and* $\frac{\Delta U}{k_BT} = -0.625$ *in (b). The total number of lattice sites is 10000 in this simulation.*

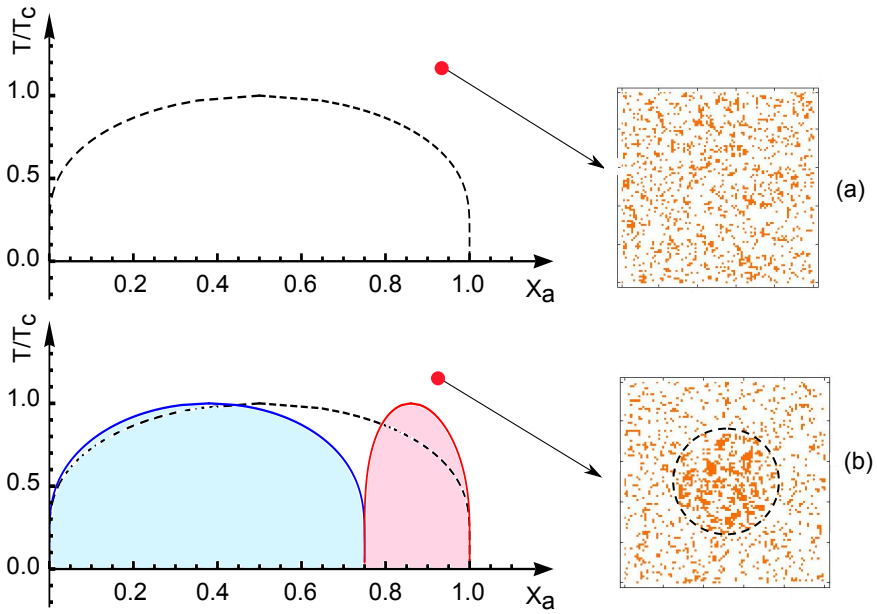

Figure 5.15 : *The MC simulation of a uniform configuration of a non-adhering membrane vesicle below the critical temperature, (a)left. The mean field phase diagram of the non-adhering membrane vesicle, (a) right. If one brings this vesicle in contact with a substrate, there will be no phase separation in the adhering segment, (b) left. and the chosen configuration remains below phase coexistence region of an adhering membrane, (b) right. In the snapshot from MC simulation, the orange particles represent component a- and white particles are component b-. In this figure, the reduced interaction energy is* $\frac{W}{k_BT} = 0.625$*, and the concentration is* $X_a = 0.15$*. The adhesion energy is equal to* $\frac{\Delta U}{k_BT} = 0$ *in (a) and to* $\frac{\Delta U}{k_BT} = -0.625$ *in (b). The total number of lattice sites are 10000 in this simulation.*

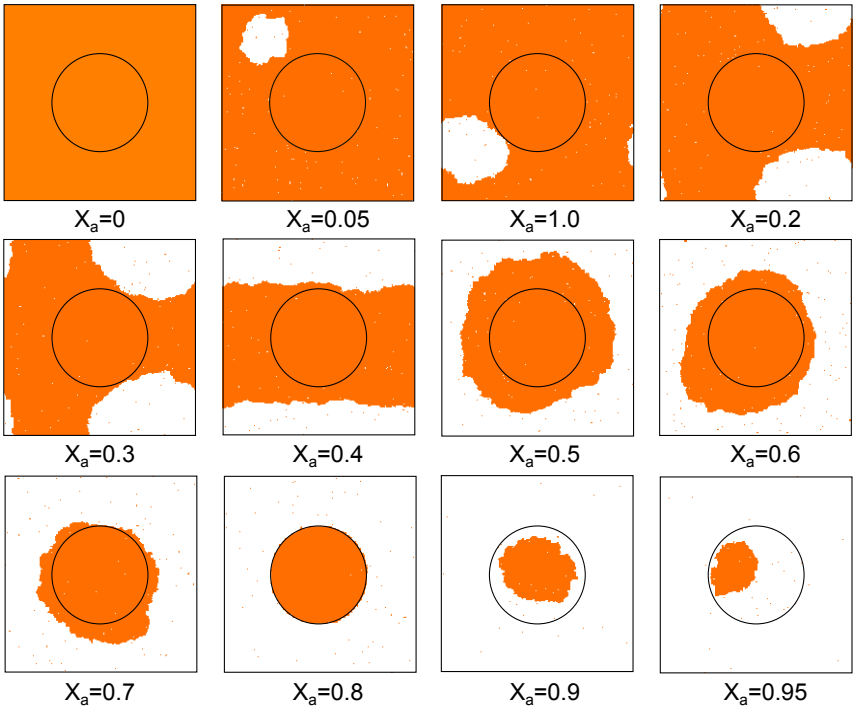

Figure 5.16 : *The MC simulation of a uniform configuration of a non-adhering membrane vesicle. Here the white particles are component a- and orange particles are component b and the total number of lattice sites is 40000. If one increases the concentration of the component a, X_a, first the phase separation occurs in the unbound membrane segment and then the adhering membrane undergoes phase separation. In the simulation, the reduced interaction energy is equal to $\frac{W}{k_BT} = 1.5$ and $\frac{\Delta U}{k_BT} = 0.625$.*

6 Summery and outlook

In this research project, the phase behavior of multi-component membrane vesicles in contact with an adhesive substrate surface has been studied theoretically using explicit calculation based on thermodynamic considerations, and also calculations using lattice binary mixture model. A simple example of multi-component membrane is provided by binary mixtures of cholesterol and a single phospholipid, which phase separate into liquid-ordered and liquid-disordered phases. When the composition of the membrane lies within the coexistence region of these two phases, large intramembrane domains are formed as has been observed by optical microscopy of giant vesicles with ternary lipid mixtures, see Fig. 2.2.

The general question that was addressed in this project is: how is the phase diagram of multi-component membrane vesicle affected by contact with a surface? The vesicle in our model system is adhere to a flat substrate surface with sufficiently large affinity contrast which provides strong adhesion regime. In the limit of strong adhesion the shape of the vesicle attains a spherical cap as in Fig. 3.2.

Using thermodynamics arguments and calculations based on lattice model, we have shown that the surface has strong effect on the phase behavior of such a system. The interaction of the membrane vesicle with the adhesive surface leads to a decomposition of the vesicle into an adhering and an unbound segment, here denoted by ad and ub, respectively. Our theory shows that such a membrane system undergoes two separate phase transitions, one within the adhering segment and a second one within the unbound segment. As the phase separation proceeds in one segment, the other segment stays in a spectator phase with fixed composition. As a consequence, intramembrane domains are predicted to form either in the adhering or in the unbound membrane segments, see Fig. 4.6.

In our calculations based on thermodynamics,we consider the adhesion of vesicle membranes that contain two molecular components, a and b. These two components differ, in general, in their affinities to the substrate surface. This affinity contrast leads to different compositions of the adhering (ad) and the unbound (ub) membrane segment, each of which can undergo a phase transition and demix into an a-poor and an a-rich phase. The compositions of the two membrane segments is expressed in terms of the area fractions X_a and X_b of the a- and b-molecules within the segments.

Furthermore, we combine the definition of the composition variables X_a, X_a^{ub}, and X_a^{ad} with the chemical equilibrium between the unbound and adhering membrane segments

in order to derive a set of two equations for the two unknown variables $X_a^{\rm ub}$ and $X_a^{\rm ad}$. We discussed a graphical solution of these two equations that depends only on the generic form of the chemical potential function as in relation (4.32) that is shown in Fig. 4.3. This graphical solution revealed generic properties of the composition variables $X_a^{\rm ub}$ and $X_a^{\rm ad}$ as explained in Sec. 4.3. Using the relations (4.32) and (4.33) as well as the free membrane binodals as in Fig. 2.2, we obtained a set of explicit solutions for the coexistence regions of the adhering membrane and thus the phase diagram of this membrane, see Fig. 4.5.

From these phase diagrams, one can conclude that for small differences between the affinity of a and b-molecules to the substrate (called affinity contrast ΔU), the phase diagram divides in to two distinct coexistence regions between liquid-ordered L_o and liquid-disordered L_d phases and also two critical points, see Fig. 4.5 for positive and Fig. 4.7 for negative affinity contrast. This division of the phase diagram implies that the adhering and unbound membrane segments can each exhibit phase separations with changes of temperature T, for a fixed mole fraction X_a of the a-molecules. As one approaches zero affinity contrast $\Delta U = 0$ then the phase diagram of the adhered system converges to the one for free vesicle, as shown in Fig. 4.5(d).

In the second part of this research project, we create a simple lattice representation of our system based of Ising model. In this model up and down spins replace the a and b-molecules. The adhesion energy is added to the lattice system as a shift in chemical potential in the contact zone. The phase diagram of adhering membrane obtained from the exact solution of the Ising system is shown in Fig. 5.2 for positive and Fig. 5.3 for negative affinity contrast. The symmetry between up and down spins simplifies the calculation of the mole fraction for positive and negative external field. Similar to the explicit calculations based on thermodynamics, duplication of the coexistence region occurs in the Ising phase diagram. Because the exact value of the spectator phase is not available in the Ising system, we are just able to calculate the phase diagram in the limit of small and large affinity contrast.

Mean field approximation is a suitable way to calculate the concentration of components within the lattice model. In contrast with the exact solution described above, the concentration of the spectator phase can be obtained by mean field approximation, see relations (5.104) and (5.107). The mean field phase diagram for the limit of small and large positive affinity contrast (or external field) is depicted in Fig. 5.8.

The results from the exact solution of the Ising model and from the mean field approximation both confirm the duplication of the phase diagram and phase separation of the two membrane segments. In all of the mentioned methods, the phase diagrams of adhering vesicles were found to depend on temperature T and mole fraction X_a as well as on a small number of additional parameters. For a binary mixture, only two additional parameters have to be taken into account: (i) the area fraction q of the unbound membrane, a purely geometric parameter and (ii) the affinity contrast ΔU between the

a- and b-molecules.

The results described in this report can be extended and generalized in several ways. One important extension is to refine the theoretical description and to include different surface potentials for the two leaflets of the adhering membrane segments. Also one can generalize these results to ternary lipid mixtures which involve two relative chemical potentials as well as two separate affinity contrasts, and should undergo duplication of coexistence regions similarly to the 2-component system investigated here.

7 Glossary

$\mathcal{A}$	total membrane area, $\mathcal{A} = \mathcal{A}^{ad} + \mathcal{A}^{ub}$
$\mathcal{A}^{ad}$	area of adhering membrane segment
$\mathcal{A}^{ub}$	area of unbound membrane segment
$\mathcal{A}^{\mathrm{do}}$	domain area of a supported membrane by a chemically patterned surface
α	intramembrane phase rich in a molecules
a	molecular species
b	molecular species
β	second intramembrane phase poor in a molecules
Φ^{ad}	area fraction of the adhering membrane
Φ^{ub}	area fraction of the unbound membrane
ΔH^{ad}	excess field acting on 'spins' in the adhering membrane segment
$\Delta\bar{H}$	dimensionless excess field which is $\Delta H/k_BT$
κ	membrane bending rigidity
θ_{eff}	The effective contact angle
DPPC	dipalmitoylphosphatidylcholine
$\mathcal{F}$	free energy
$\mathcal{F}_{\mathrm{o}}$	first order of free energy
h	equations of state$H = h(S,T)$
H	strength of magnetic field in the Ising representation
$\bar{H}$	dimensionless external field: $\Delta H/k_BT$
H^{ad}	field acting on 'spins' in the adhering membrane segment; $H^{ad} = H^{ub} + \Delta H^{ad}$
H^{ub}	field acting on 'spins' in the unbound membrane segment
H_i^{eff}	effective mean field
$\bar{\mathcal{H}}_i$	effective mean field Hamiltonian

$\mathcal{H}\{n\}$	Hamiltonian in the binary lattice model
$\mathcal{H}\{s\}$	Hamiltonian in theIsing model
$\mathcal{H}^{ad}$	Hamiltonian of the adhering membrane segment
$\mathcal{H}^{ub}$	Hamiltonian of the unbound membrane segment
i	index for lattice sites
J_{ij}	interaction parameter between lattice sites i and j in the Ising system
k_B	Boltzmann factor
μ_a	chemical potential of a molecule
μ_b	chemical potential of b molecule
μ_a^{ad}	chemical potential of a molecule in the adhering membrane segment
μ_a^{ub}	chemical potential of a molecule in the unbound membrane segment
$\Delta\mu$	difference between the chemical potential of a and b molecules
M	The curvature normal to the contact line
n_i	occupation number for lattice site i by a molecules.
N	molecular density of component a
N^{ad}	molecular density of component a in the adhering membrane
N^{ub}	molecular density of component a in the unbound membrane
N_α^{ad}	molecular density in phase separated adhering membrane
N_β^{ad}	second molecular density in phase separated adhering membrane
N_α^{ub}	molecular density in phase separated unbound membrane
N_β^{ub}	second molecular density in phase separated unbound membrane
N_*^{ad}	molecular density of the spectator phase at the coexisting area of the unbound segment
N_*^{ub}	molecular density of the spectator phase at the coexisting area of the adhering segment
$\mathcal{N}$	total number of molecules within the membrane, $\mathcal{N} = \mathcal{N}^{ad} + \mathcal{N}^{ub}$
$\mathcal{N}_a$	number of a molecules
$\mathcal{N}_b$	number of b molecules
$\mathcal{N}_a^{ad}$	number of molecules in the adhering membrane segment
$\mathcal{N}_a^{ub}$	number of molecules in the unbound membrane segment

$\mathcal{N}_{a,*}^{ad}$	number of molecules in adhering membrane segment along the coexisting area of the unbound segment
$\mathcal{N}_{a,*}^{ub}$	number of molecules the unbound membrane segment along the coexisting area of the adhering segment
Ω	total number of lattice sites
Ω^{ad}	number of lattice sites in adhering membrane
Ω^{ub}	number of lattice sites in unbound membrane
q	overall area fraction of membrane
R_{co}	contact curvature radius
R_{ve}	linear vesicle size
s_i	Ising spin at lattice site i with $s_i \equiv 2n_i - 1$.
S	order parameter in the Isisng stem; $S =< s_i >$
S^{ad}	order parameter in the adhering membrane
S_{α}^{ad}	order parameter in phase separated adhering membrane
S_{β}^{ad}	second order parameter in phase separated adhering membrane
S^{ub}	order parameter in the unbound membrane
S_{α}^{ub}	order parameter in phase separated unbound membrane
S_{β}^{ub}	second order parameter in phase separated unbound membrane
S_{*}^{ad}	order parameter of the adhering membrane along the coexisting line of the unbound segment
S_{*}^{ub}	order parameter in the unbound membrane along the coexisting line of the adhering segment
$\mathcal{S}(T)$	spontaneous order parameter
$\mathcal{S}_0(T)$	spontaneous order parameter at $H = 0$
T	temperature
$\bar{T}$	dimensionless temperature $\bar{T} = k_B T/J$
T_c	critical temperature
T_c^{MF}	critical mean field temperature
T_t	triple point temperature
U_a	strength of interaction potential between surface and a molecule
U_b	strength of interaction potential between surface and b molecule

U_a^i	strength of interaction potential between surface and a molecule in lattice site i
U_b^i	strength of interaction potential between surface and b molecule in site i
U_{ij}^{aa}	pair potential between two a components in i and j site
U_{ij}^{ab}	pair potential between two components a and b in i and j site
U_{ij}^{bb}	pair potential between two b components in i and j site
$\Upsilon(T,H)$	mean field order parameter of the Ising system in temperature T and magnetic field H
Υ_0	the order parameter of the Ising system in zero magnetic field $H=0$
v	reduced volume of the vesicle
$\mathcal{V}$	volume of the vesicle
W_{ij}	interaction between a and b components
W_0	interaction between two nearest neighbors
$X_{a,\alpha}(T)$	mole fraction of a molecules in α phase, one branch of binodal line
$X_{a,\beta}(T)$	mole fraction of a molecules in β phase, other branch of binodal line
z	nearest neighbors number
Z	partition function

Bibliography

[1] B. Alberts, D. Bray, J. Lewis, M. Raff, K. Roberts, and J. D. Watson. Molecular Biology of The Cell. Garland Publishing, Inc, second edition, 1998.

[2] I. L Weissman, L. E Hood, and W. Barry Wood. Essential concepts in immunology. Menlo Park, California, 2nd edition, 1984.

[3] B. Rozycki and M. Napiorkowski. Europhys. Lett., 66(35), 2004.

[4] J. Pietzsch. Mind the membrane. Horizon Symposia: Living Frontier. Nature Publishing Group, 2004.

[5] R. Lipowsky. The conformation of membranes. Nature, 349(475), 1991.

[6] R. Lipowsky and R. Dimova. Domains in membranes and vesicles. J. Phys.: Condens. Matter, 15:S31–S45, 2003.

[7] Y. Liu, R. Lipowsky, and R. Dimova. Concentration Dependence of the Interfacial Tension for Aqueous Two-Phase Polymer Solutions of Dextran and Polyethylene Glycol. Langmuir, 28:3831–3839, 2012.

[8] S. L. Veatch, K. Gawrisch, and S. L. Keller. Biophys. J. 90:4428–436, 2006.

[9] C. Vequi-Suplicy, K. Riske, R. Knorr, and R. Dimova. Biochim. Biophys. Acta, 1798:1338–1347, 2010.

[10] P. Uppamoochikkal, S. Tristram-Nagle, and J. F. Nagle. Langmuir, 26:17363–17368, 2010.

[11] N. Bezlyepkina. PhD thesis, University of Potsdam,, 2012.

[12] R Lipowsky. Adhesion of membranes via anchored stickers. Phys. Rev. Lett., 77(1652), 1996.

[13] R. Lipowsky. J. Bio.Phys., 28(195), 2002.

[14] T. R. Weikl. Indirect interactions of membrane-adsorbed cylinders. Eur Phys J E, 12(265-273), 2003.

[15] J. N. Israelachvili. Intermolecular and surface forces. Academic Press, London, 1992.

[16] R. Lipowsky. Generic interactions of flexible membranes. In R. Lipowsky and E. Sackmann, editors, Structure and Dynamics of Membranes, volume 1 of Handbook of Biological Physics, pages 521–602. Elsevier, Amsterdam, 1995.

[17] S. Garg, J. Rühe, K. Lüdtke, R. Jordan, and C. A. Naumann. Domain registration in raft-mimicking lipid mixtures studied using polymer-tethered lipid bilayers. Biophys. J., 92:1263–1270, 2007.

[18] T. R. Weikl, M. Asfaw, H. Krobath, B. Rózycki, and R. Lipowsky. Adhesion of membranes via receptor–ligand complexes: Domain formation, binding cooperativity, and active processes. Soft Matter, 5:3213–3224, 2009.

[19] V. D Gordon, M. Deserno, C. M. J. Andrew, S. U. Egelhaaf, and W. C. K. Poon. Adhesion promotes phase separation in mixed-lipid membranes. EPL, 84(480003), 2008.

[20] Dustin group. Science featured cover page, 1999.

[21] U. Seifert and R. Lipowsky. Adhesion of vesicles. Physical Review A, 42(8), 1990.

[22] T. Gruhn, T. Franke, R. Dimova, and R. Lipowsky. Novel Method for Measuring the Adhesion Energy of Vesicles. Langmuir, 23:5423–5429, 2007.

[23] M. D. Collins and S. L. Keller. Tuning lipid mixtures to induce or suppress domain formation across leaflets of unsupported asymmetric bilayers. PNAS, 105(1):124–128, 2008.

[24] A. Orth, L. Johannes, W. Römer, and C. Steinem. Creating and Modulating Microdomains in Pore-Spanning Membranes. ChemPhysChem, 13:108–114, 2012.

[25] A. N. Parikh. Membrane-substrate interface: Phospholipid bilayers at chemically and topographically structured surfaces. Biointerphases, 3(2), 2008.

[26] K. Tawa and K. Morigaki. In situ imaging of micropatterned phospholipid membranes by surface plasmon fluorescence microscopy. Colloids and Surfaces B: Biointerfaces, 81:447–451, 2010.

[27] D. Marsh. Liquid-ordered phases induced by cholesterol: A compendium of binary phase diagrams. Biochim. Biophys. Acta, 1798:688 – 699, 2010.

[28] M. Bloom and J. L. Thewalt. Time and distance scales of membrane domain organization. Mol. Membr. Biol., 12(9-13), 1995.

[29] D. J. Recktenwald and H. M. McConnell. Phase equilibria in binary mixtures of phosphatidylcholine and cholesterol. Biochemistry, 20(15):4505–4510, 1981.

[30] E. J. Shimshick and H. M. McConnell. Lateral phase separations in binary mixtures of cholesterol and phospholipids. Biochem. Biophys. Res. Commun., 53(2):446–451, 1973.

[31] L. M. S. Loura, A. Fedorov, and M. Prieto. Fluid-fluid membrane microheterogeneity: a fluorescence resonance energy transfer study. Biophys. J., 80(2):776–788, 2001.

[32] M. I. Colladom, F. M. Goni, A. Alonso, and D. Marsh. Domain formation in sphingomyelin/cholesterol mixed membranes studied by spin-label electron spin resonance spectroscopy. Biochemistry, 44(12):4911–4918, 2005.

[33] M. B. Sankaram and T. E. Thompson. Cholesterol-induced fluid-phase immiscibility in membranes. Proc. Natl. Acad. Sci. U. S. A., 88(19):8686–8690, 1991.

[34] J. Zhao, J. Wu, F. A. Heberle, T. T. Mills, P. Klawitter, G. Huang, G. Costanza, and G. W. Feigenson. Phase studies of model biomembranes: Complex behavior of DSPC/DOPC/Cholesterol. Biochimica et Biophysica Acta, 1768:2764–2776, 2007.

[35] L. Bagatolli and S. Kumar. Phase behavior of multicomponent membranes: Experimental and computational techniques. Soft Matter, 5:3234–3248, 2009.

[36] T. McMullen, R. Lewis, and R. McElhaney. Cholesterol-phospholipid interactions, the liquid-ordered phase and lipid rafts in model and biological membranes. Current Opinion in Colloid and Interface Science, 8:459–468, 2004.

[37] D. A. Kofke and E. D. Glandt. Monte Carlo simulation of multicomponent equilibria in a semigrand canonical ensemble. Mol Phys, 64(6):1105 – 1131, 1988.

[38] E. de Miguel, E. M. del Rio, and M. M. Telo da Gama. Liquid-liquid phase equilibria of symmetrical mixtures by simulation in the semigrand canonical ensemble. J. Chem. Phys., 103(14):6188 – 6196, 1995.

[39] C. Hofsäß, E. Lindahl, and O. Edholm. Molecular Dynamics Simulations of Phospholipid Bilayers with Cholesterol. Biophys. J., 84:2192 – 2206, 2003.

[40] B. M. McCoy and T. T. Wu. The two–dimensional Ising Model. Harward University Press, Cambridge, Massachusetts, 1973.